Theses and Dissertations

May 2013

An Optical-Fiber Based Sensor Array for the Simultaneous Analysis of Zinc and Copper in Aqueous Environments

Steven Kopitzke
University of Wisconsin-Milwaukee

AN OPTICAL-FIBER BASED SENSOR ARRAY FOR THE SIMULTANEOUS ANALYSIS OF ZINC AND COPPER IN AQUEOUS ENVIRONMENTS

by

Steven P. Kopitzke

A Dissertation Submitted in

Partial Fulfillment of the

Requirements for the Degree of

Doctor of Philosophy

in Chemistry

at

The University of Wisconsin-Milwaukee

May, 2013

ABSTRACT

AN OPTICAL-FIBER BASED SENSOR ARRAY FOR THE SIMULTANEOUS
ANALYSIS OF ZINC AND COPPER IN AQUEOUS ENVIRONMENTS

by

Steven Kopitzke

The University of Wisconsin-Milwaukee, 2013
Under the Supervision of Professor Peter Geissinger

Copper and zinc are elements commonly used in industrial applications, with many of

these processes using these elements in aqueous environments. Before the solutions can

be discharged into civil or native waterways, waste treatment processes must be

undertaken to ensure compliance with federal, state and local guidelines restricting the

concentration of ions discharged in solution. While there are methods of analysis

currently available to monitor these solutions, each method has disadvantages, be it that

they are cost prohibitive, inaccurate, and/or time-consuming. In this work, a new optical

fiber-based platform capable of providing fast and accurate results when performing

solution analysis for these metals is described. Using fluorescent compounds that exhibit

a high sensitivity and selectivity for either zinc or copper have been employed for

fabricating the sensors. These sensors demonstrated sub-part-per-million detection limits,

30-second response times, and the ability to analyze samples with an average error of

under 10%. The inclusion of a fluorescent compound acting as a reference material to

compensate for fluctuations from pulsed excitation sources has further increased the

reliability and accuracy of each sensor. Finally, after developing sensors capable of

monitoring zinc and copper individually, these sensors can be combined to form a single

optical fiber sensor array capable of simultaneously monitoring concentration changes in

zinc and copper in aqueous environments.

TABLE OF CONTENTS

LIST OF TABLES

LIST OF FIGURES

LIST OF SYMBOLS AND ABBREVIATIONS

AAS...Atomic Absorption Spectroscopy

BPO...benzoyl peroxide

C-481..Coumarin-481

cps...Counts per second

DETA...Diethylenetriamine

DDETA...Dansyldiethylenetriamine

DG..Dragon Green

DMF...N,N-dimethylformamide

DMPA...2,2-dimethoxy-2-phenylacetophenone

F...Fluorophore

FZ-1..FluoZin-1 tripotassium salt

GFAAS...Graphite Furnace Atomic Absorption Spectroscopy

GPTS..3-glycidoxypropyltrimethoxysilane

I, I_0...Intensity

ICP-MS...Inductively Coupled Plasma-Mass Spectrometry

LDR...Linear Dynamic Range

LOD..Limit of Detection

LOQ...Limit of Quantitation

LPF...Long pass filter

K_{SV}...Stern-Volmer Coefficient

mV...millivolts

NA..Numerical Aperature

Acknowledgments

If I were able to thank everyone who has helped me arrive at this point today, the length of this acknowledgement would rival that of my research. However, there are a few people who I would like to acknowledge for their support of my research and growth during my graduate school career. First, I would like to recognize my advisor, Professor Peter Geissinger. His mentoring style allowed me to develop a critical thinking process and resourcefulness which will be beneficial wherever I go. The opportunities which were offered to me extended beyond those just associated with research, allowing me to experience project leadership, travel and the ability to interact with professionals in several different fields of research.

I would also like to recognize and thank each member of my thesis committee. Dr. Bob Olsson, for asking those questions that made me stop and think; Dr. Mark Dietz, who not only served on my committee but also allowed me to serve as one of his teaching assistants for nine semesters; Dr. Kristen Murphy, who helped to show me ways to be a more efficient teacher and Dr. Jorg Woehl who would take time to answer questions I would have.

There are also several of my peers who I'd like to acknowledge. For the Geissinger research group, Paul, Hannah, John, Brad, & Ryan who've provided advice and assistance throughout the years to help me overcome hurdles with my research while helping to keep things from becoming overwhelming. To my friends in the department: Lisa, Sarah, April, Megan & Alan who I was able to work together with as teaching assistants or in classes we shared. To several staff members of the chemistry department: Carl Ferguson, for lending both last-minute chemicals and his extensive knowledge of

practical chemistry; Neil Korfhage, for constructing several apparatuses essential to my research and Michelle Koranda, who's conversations kept teaching-related issues in perspective and allowed me to find the solution to the problem.

In the end, there is one proverb I would share which every graduate student needs to take to heart in order to be successful during and after their graduate career:

"Plans fail for lack of counsel, but with many advisers they succeed"— Solomon

Steven Kopitzke

Milwaukee, WI

May 2013

This thesis is dedicated to my wife and family, who have supported me throughout

the entire process. Their understanding, encouragement and motivation

propelled me through this journey and without it,

I would not be here today.

Chapter 1

Introduction

1.1 Introductory remarks and overview

The need for water quality assurances have become a focal point of many federal, state and local regulations. Several methods have been developed to provide these assurances but there are still limitations to the current technology. Often methods must sacrifice portability for accuracy or speed for precision. The work presented here provides a means of analysis to bridge this gap, allowing for accurate and repeatable analysis with rapid measurement capability. Utilizing novel optical fiber-based technology, a sensor array capable of simultaneously analyzing solutions for zinc and copper at concentrations equal to or less than those required by governmental agencies has been developed and characterized, and this is the focus of the work presented here.

Within this chapter, several topics will be discussed. The necessity for monitoring the levels of zinc and copper is necessary will be discussed in the first section. Secondly, after establishing the need for analysis, currently used analytical methods will be examined for both strengths and weaknesses. A discussion of the theory behind optical-fiber-based sensors will follow. Specific types of sensors and designs will be examined as a means of comparison to the sensor design proposed in this work. The details relating to the sensor design described in this research will be compared against other designs to demonstrate the advantages of using the setup described within.

1.2 The need for copper and zinc analysis

Both zinc and copper are commonly occurring metals and are used in a variety of processes. Because of its ability to resist corrosion and the capacity to effectively bind with many other materials, zinc constitutes an ideal anti-corrosion material.[1] Zinc is also

commonly used in metal alloys, with brass, a mixture of copper and zinc, being the most common. Lastly, zinc can be found within medicinal components, most notably in sunscreen such as zinc oxide.

Copper is the third most commonly used metal in industrial processes. The malleability and ductility of copper, along with its ability to effectively conduct electricity, has dictated that most electrical wiring within commercial and residential structures is copper-based. It has been estimated that up to 45 kg of copper are used in the fabrication of a luxury car.[2] Copper is also one of the base metals in both brass and bronze. Most household plumbing applications that employ metal pipes are also made of copper.

With the many different applications for both of these metals, introduction of either metal into environmental settings can occur via a variety of pathways. Many different point sources have been identified as polluting species. These can include mining,[3] extraction processes used to refine the metals,[4] and industrial wastewater generated from various processes.[5] However, non-point sources can also contribute to the introduction of these species into the environment. Storm runoff or leaching from landfills can also contaminate the local waterways.[6] Because of all of these potential sources of pollution, the need for accurate and reliable means of analysis is required to assist in preventing these species from entering or containing them once introduced in regulated systems.

Copper and zinc are recognized as essential micro-nutrients required for certain biochemical processes within the human body.[7,8] Zinc is required for several metalloproteins including alcohol dehydrogenase or DNA and RNA polymerase. It is

also a key component in the preservation of nucleic acid structures within a genome. A zinc deficiency has been reported to affect several systems within the body, including slow wound healing, anorexia or a weakening of the immune system.[7] Copper also plays a role in several metalloproteins, including some involved with hemoglobin, drug metabolism, and antioxidant protection. Copper deficiencies manifest as osteoporosis; however, it has been noted that the diet of an average American provides adequate access to copper.

While both of these metals are required for physiological processes, elevated exposure to either metal has been proven to be detrimental. Short-term exposure to elevated levels of either copper or zinc has not been shown to generate any detrimental health effects. However, ingesting elevated levels (above 11 mg/kg/day) of zinc can cause serious effects on the gastrointestinal system, inducing strong nausea, vomiting or intestinal bleeding. Some studies involving animals have also produced lesions on the kidney and liver due to elevated levels of zinc, but these effects have not been observed on humans.

The daily amount of copper required (0.013 mg/kg/day) is usually obtained through a normal diet. Excess copper is most often introduced through the drinking water supply due to copper leaching from household plumbing. Exposure to elevated levels of copper is also indicated by strong gastrointestinal distress, usually vomiting or nausea. Studies have found that a concentration of 4 mg/L of copper will cause nausea, while 6 mg/L will induce vomiting.[9,10] Animal studies have also shown the liver to be target of necrosis when exposed to elevated copper levels.[8] This is also suspected to be

the case for humans, but the gastrointestinal issues will occur before this point. This usually stops the introduction of copper, and reduces the total effect on the liver.

1.3 Current methods of analysis

There are several analytical methods available to analyze aqueous solutions for both copper and zinc. The examples provided here can be divided into two categories. The first category will focus on techniques for performing on-site analysis, while the second will address laboratory-based techniques. A breakdown outlining the positive and negative aspects for each technique or technology is provided to target shortcomings of current methods that need to be addressed in the development of a better sensor.

UV-Vis absorption has been developed commercially as a means to measure zinc and copper in solution. To develop the metals for analysis, pre-treatment using complexing agents is required to form a colored metal complex in solution, which absorbs light at a wavelength within the visible spectral region. These methods are reported to measure both zinc and copper at levels below 1 mg/L, but they suffer from numerous interfering species.[11] This procedure, coupled with a portable UV-Vis spectrophotometer, allows for on-site analysis with instant feedback at a relatively low cost. However, the amount of complexing agents and sample pre-treatment required can induce error during sample preparation.

A second technique is a colorimetric technique, relying on the formation of a colored metal complex.[12] These colored solutions are then visually compared against a standard chart supplied by the manufacturer. This technique is similar to the use of pH strips allowing for rapid analysis and is useful for qualitative analysis of unknown solutions. The precision of this method suffers, as the color of the solutions are subject to human

interpretation, inducing a level of variability which is difficult to control, as each person may perceive the color differently.

The transition from on-site techniques to laboratory techniques brings about a marked improvement in the precision and accuracy of sample analysis. However, this comes at the price of portability, cost and time. On-site methods allow for instant feedback regarding the presence of metals species; analysis in a laboratory can require from hours to weeks before the sample analysis is completed due to the transportation and analysis of the samples at a laboratory. While an average colorimetric test kit can cost between \$50-\$100, most of the laboratory-based instruments have acquisition costs starting in the thousands of dollars. The ability to achieve rapid feedback with cost-efficient methods leads many facilities to use colorimetric methods as a means of internal quality control for waste treatment processes. For all public and regulatory reports, facilities must still provide samples for analysis using laboratory-based systems due to the improvement in precision, accuracy and reliability obtained using laboratory-based instruments.

The first laboratory technique is atomic-absorption spectroscopy (AAS), which is commonly used for measuring both copper and zinc in solution. The U.S. Environmental Protection Agency (EPA) recognizes this and has published methods designed for zinc and copper analysis using AAS.[13] In order to reduce the amount of sample required along with increasing the sensitivity of analysis, a transition was made from AAS to graphite furnace AAS (GFAAS).[14] These improvements are based on the fact that the graphite furnace, an electro-thermal vaporization method of sample introduction, introduces the sample more efficiently into the sample analysis chamber.[15] The gain in

sample introduction efficiency allows for a sample to be completely transferred to the analysis chamber, increasing the sensitivity. Traditional graphite furnaces are only 5 cm in length with a 1-cm diameter and require only 20-100 micro-liters of sample. This method, both with or without the graphite furnace, requires little sample preparation (a standard acid digestion process) and provides repeatable, accurate solution analysis. While the sample analysis is simpler, the AAS is a laboratory-based instrument, which prevents on-site or real-time analysis. Using the graphite furnace does improve the performance of atomic absorption spectroscopy, but the furnace chamber requires periodic replacement due to thermal degradation of the sample chamber.

Inductively Coupled Plasma Mass Spectrometry (ICP-MS) is the standard method for elemental analysis. Low detection limits, high specificity and a high degree of accuracy are the hallmarks of this technique. Several EPA methods exist where mass spectrometry is employed.[16,17] However, this instrument is not portable, severely limiting the possibility of on-site or real-time measurements. Also, the cost of the instrument, both to purchase and maintain, is much higher than any of the other methods previously described.

There are other methods available for the determination of both zinc and copper. These procedures include the use of electrochemical methods[18] or high performance liquid chromatography (HPLC).[19] However, these methods are used infrequently, as the previously described methods using AAS and ICP-MS have proven to be more efficient analytical techniques.

1.4 Optical Fiber Principles

Optical fibers were first invented in 1966 to improve long distance communications, with applications for sensing research starting in the 1970's.[20] Typical optical fibers consist of long wires of silica, forming the fiber core, encased within some type of flexible polymer cladding material (Figure 1.1). Silica-based optical fibers have excellent transmission properties over a wide range of wavelengths, including the infrared, visible and near-ultraviolet regions. However, other materials such as polymethylmetharcylate (PMMA) have been used in place of silica. These materials have not garnered as much attention due to the inability to transmit light in the IR. There has been some research focused on developing alternative material-based optical fibers for fluorescence sensing.[21] The work performed here will only focus on systems that utilize fibers with silica cores, so no further discussion of other materials is warranted.

Optical fibers owe their ability to transmit light over long distances to the phenomenon of total internal reflection (TIR).[22] This process is possible due to the nature of the materials used to create the optical fiber. By employing a core material for the fiber having a higher refractive index (η_{core}) than the cladding (η_{clad}) around the core, light propagating in the core will strike the boundary between the two surfaces and be completely reflected back into the fiber core if it exceeds a critical incident angle. The basis for TIR is described mathematically by Snell's Law (Eqn. 1.1) where $\sin \theta_1$ represents the incident angle of light propagating in the fiber on the interface with respect to the interface normal and $\sin \theta_2$ is the angle of or refraction out of the core material.

$$\left(\frac{\eta_{core}}{\eta_{clad}}\right) \sin \theta_1 = \sin \theta_2 \qquad \text{(Eqn. 1.1)}$$

To observe TIR, not only does the difference in refractive indices matter but all light entering the fiber must have an incident angle greater than the critical angle described by the formula.

$$\theta_{crit} = sin^{-1}\left(\frac{\eta_{clad}}{\eta_{core}}\right)$$ (Eqn. 1.2)

In the instances where a ray of light has an angle of incidence, which is less than the critical angle, the ray will undergo refraction and escape from the optical fiber (some of the light is still reflected; the intensities of reflected and refracted rays are described by Fresnel's equations). These relationships are displayed in Figure 1.2.

In order to successfully couple light into the optical fiber, the numerical aperture (NA) of the fiber must also be considered. This number describes the maximum angle with respect to the fiber core at which light may couple into the optical fiber and propagate in the fiber under guiding conditions.[23] The value can be calculated if the refractive indices of the core, cladding and environment (η_{env}) are known.

$$NA = \frac{1}{\eta_{env}}\sqrt{\eta_{core}^2 - \eta_{clad}^2}$$ (Eqn. 1.3)

For most cases, η_{env} will be equal to one, the approximate refractive index of air. Multi-mode fibers, the type of fibers utilized for this research, typically have numerical apertures between 0.25 and 0.4.

The mention of multi-mode fibers here requires a brief discussion about two different types of optical fibers. These types are the previously mentioned multi-mode

fibers along with single-mode fibers. To discuss the difference between these fibers, the definition of a "mode" must be given. A mode can be thought of as an individual ray of light propagating through an optical fiber.[24] The order of a mode is used to describe the path that the mode traverses through the optical fiber. For modes of a low order, number of reflections at the refractive index interface between the core and cladding are much lower (over a given length of optical fiber) and reflect off the interface with much shallower angles when compared to higher order modes. Higher order modes reflect off the interface layer more frequently and at steeper angles, sometimes resulting in the escape of a mode from the optical fiber and is referred to as a "leaky" mode (Figure 1.2). These characteristics result in the fact that low order modes will propagate in optical fibers over longer distances than higher order modes.

Multi-mode fibers, as the name suggests, are capable of transmitting multiple modes through an optical fiber.[25] The larger diameter (50 μm – 1000 μm or greater in some cases) of the silica core allows for many more modes to travel through the optical fiber. Multi-mode fibers also have a larger numerical aperture value, allowing more modes to enter the fiber and propagate under guiding conditions. Single-mode fibers, on the other hand have very small (5-10 μm) core diameters, and only support one mode. This results in a lower intensity of light propagating through the fiber but the transmission distance of the light within the fiber will be greater.

While light does undergo total internal reflection, at each point of reflection a standing electric field extending outward from the fiber core is generated. This field is often referred to as either evanescent field or evanescent wave, where the word evanescent stems from the Latin word "evanescere" which means to fade away.[26] This is

the case as the evanescent field will only exist while light is undergoing total internal reflection. Also, evanescent waves can only penetrate a short distance away from the optical fiber and decay exponentially (Figure 1.3) as the distance from the fiber is increased as seen in Equation 1.4

$$E(z) = E_0 e^{\frac{-z}{d_p}} \qquad \text{(Eqn. 1.4)}$$

where E is the energy of the field at a distance z, E_0 is the energy of the field at the interface and d_p is the distance of penetration. In order to determine the distance of penetration away from the fiber (d_p), the following equation can be employed:

$$d_p = \frac{\lambda}{4\pi\eta_{core}} (sin^2\theta - sin^2\theta_{crit})^{-\frac{1}{2}} \qquad \text{(Eqn. 1.5)}$$

Where θ describes the angle of incident light as it strikes the surface before reflection. As seen, the penetration depth will increase as the wavelength increases. For most practical applications, the evanescent field will interact with components in the environment if the components are within a distance of the order of the wavelength of the incident light. If a fluorophore can be located at a point within this distance, an interaction between the evanescent wave and the fluorophore will result. This interaction will result in the energy from the evanescent wave promoting the fluorophore from the ground state into an excited state. A fluorescence signal is then generated as the fluorophore relaxes back to the ground state. This fluorescence is then captured by guiding light modes within the fiber, allowing for transmission of the fluorescence through the optical fiber.

1.5 Types of Optical Fiber-Based Sensors

At this point, a clarification needs to be made about optical-fiber-based sensors. Thousands of papers have been published regarding development of molecules which can respond to changes in analyte concentration by undergoing some type of change of their luminescence. For a sensing device, a more stringent definition of "sensor" needs to be put forward. A definition previously published stated that a sensor must be a miniaturized device capable of providing real-time information on the presence of a specific compound or ion in a complex solution.[27] As such, sensors described forthwith will follow this new definition.

There are three main designs utilized for optical fiber-based sensors.[20] Designs that have a sensor region located at the distal tip of the optical fiber in relation to the source and detector are referred to as "point" sensors, as they can only measure at one location. Optical fibers can also be modified internally by altering the chemical composition of the silica core to provide points of analysis distributed through the entire optical fiber and are referred to as distributed sensors. This method allows for high spatial resolution as the entire fiber serves as a sensor. The last method involves replacing the fiber cladding with a compound-embedded substitute material on the optical fiber in multiple places, which will affect the luminescent properties within the optical fiber. This is the method used for analysis done within this body of work.

1.5.1 Point sensor design and application

There are several different methods of sensing when using point sensors. There are several commercially available sensors which operate by combining several fibers

into one probe.[28]   In this design, the fibers are bundled together where one fiber is surrounded by six other fibers (Figure 1.4). The six fibers serve to carry light from an excitation source and direct the light at a sample matrix. The fiber located in the middle of the bundle is used to collect either backscattered, reflected or fluorescence radiation. This can be used to analyze turbidity, dye content, and a variety of other materials for quality control purposes. A second type of sensors involves immobilizing some form of platform perpendicular and in close proximity to the end of the optical fiber. This type of platform can be used to perform both absorption and fluorescence measurements. A method of zinc sensing was developed in which fluorescently-tagged beads were trapped within a flow cell.[29] These beads had been functionalized to bind with zinc and cause a change in the fluorescence intensity. The excitation light would be directed on to the zinc recognition platform and the subsequent fluorescence would also be coupled into the optical fiber and sent to the detector. (Figure 1.5) Other types of point source probes involve the coating of the tip of an optical fiber with a fluorescent material whose fluorescence changes in the presence of an analyte.[30] In this example and in many others, including the research presented here, the cladding material is removed from the optical fiber in order to allow either the evanescent waves generated from within the fiber or direct excitation pulses for fluorophores located at the front face of the tip of the fiber to interact with the fluorescent material.

1.5.2 Distributed Sensors

Internal modification of the optical fibers as a means of sensing has also been used to study a variety of environmental changes. The most common type of fiber modification involves the creation of fiber Bragg gratings (FBG). This type of grating is

created by permanently changing the refractive index of the optical fiber using coherent UV lasers focused on the optical fiber.[31] This technique is ideal because the optical fiber can be modified while still within the cladding material and it can be selectively modified to meet the desired need for both the number of sensors desired as well as the location of the sensor regions. By changing the refractive index of the material, certain wavelengths will be reflected within the optical fiber, back towards the light source.(Figure 1.6) FBG designs have been used to monitor pressure changes over a variety of surfaces.[32] These measurements are possible due to the nature of the FBG within the fiber. As strain or pressure is introduced within the sensor region, the period of the FBG sensor will change and this change will cause a shift in the wavelength which is being reflected. This relationship has been derived in the equation below where λ_0 is original wavelength of the light source, $\Delta\lambda$ is the shift in the wavelength and ε stands for the strain exerted on the FBG.

$$\frac{\Delta\lambda}{\lambda_0} = 0.78 * \varepsilon \qquad \text{(Eqn. 1.6)}$$

A second application for FBG-based systems allows for the monitoring of changes in temperature over the length of the fiber.[33] The application relies on the principle that that refractive index of the FBG will change slightly as the temperature changes, once again causing a shift in the wavelength which is reflected. This has also been determined[34], as shown here.

$$\Delta T = \frac{1}{0.78 * \alpha_{glass} * \alpha_\eta} * \frac{\Delta\lambda}{\lambda_0} \qquad \text{(Eqn. 1.7)}$$

Since the thermal expansion of the glass (α_{glass}) is so small ($0.55*10^{-6}$/K) the change in refractive index (α_η) with relation to temperature will dominate the change in signal.

1.5.3 Quasi-distributed sensors

For chemical sensing, optical fibers with fully-distributed sensing capabilities are feasible.[35]   However, there are other instances where a fully distributed sensor is not possible. This could be due to factors related to the complicated nature of doping either the cladding or core materials. Also, for fluorescence signals in certain sensor designs, an amount of time is required so that the fluorescence generated by neighboring regions are discretely resolved by the detector such as the research performed in this work. As such, quasi-distributed optical fiber sensors have been developed.[36]   The difference between a distributed optical fiber sensor and the quasi-distributed sensor is that a distributed sensor is capable of analyte recognition at any point along the fiber as the entire fiber is homogenously doped with the analyte-recognition material. Figure 1.7 provides a comparison between the two designs.   Quasi-distributed means that not all of the fiber is capable of analyte recognition, but by integrating the fluorescent molecules at certain points along the fiber, spatially distributed methods are still feasible. While this design does not offer the same level of spatial resolution as the fully distributed optical fiber sensor, there is a greater degree of flexibility in analyte choice for which a quasi-distributed sensor may monitor.

1.6 Optical Time of Flight Measurements

For sensor designs utilizing a point sensor, one needs only be concerned about collecting one signal. However, when utilizing distributed or quasi-distributed sensors,

the need for spatial resolution requires that methods exists in order to identify and separate the signals from different sensors regions. The most efficient means of separating these signals is to measure the fluorescence signal in time. In order to perform such measurements, a pulsed source (typically, but not limited to, a laser) directs a pulse down the optical fiber. The point in time of pulse generation is considered t_0. As the pulse travels through the optical fiber, each interaction between pulse and sensor region within the optical fiber will occur at different times. The fluorescence signal is then transmitted via optical fibers to a fast-detector system, capable of nanosecond resolution. This resolution in time is required for the technique referred to as optical time-of-flight spectroscopy (OTOFS) as the pulses need to arrive and be recorded discretely and many fluorophores have fluorescence lifetimes of only a few nanoseconds.[37] . When a pulse is created, a signal is sent to the signal-processing unit. As signals from the fluorescent regions of the fiber arrive at the detector, they are arranged in relation to the time required for the signal to reach the detector after pulse generation. (Figure 1.8) The relation between the fluorescent region and time allows a user to determine where on the fiber the sensor has detected the analyte of interest. Detection systems with larger, slower timescales may result in sequential pulses overlapping, obscuring potentially small changes in a sensor's the fluorescence intensity of the sensor There are several designs allowing for OTOFS implementation. The first requires a single optical fiber.[38] (Figure 1.8) The sensor regions are located at specific intervals along the fiber. A pulse is coupled into the optical fiber after passing through a beam splitter. After fluorescence generation by each sensor, the signals travel back through the fiber and out the end through which the pulse initially entered. These signals are then reflected off of the beam

splitter to a detector. While this system is effective, spatial resolution suffers, as lengths of fiber on the order of 10 m (depending on the fluorescence lifetimes of the sensors and the desired width of the detection time window) must be placed between each sensor region. This is required so that each fluorescence pulse may arrive at the detector separately.

In order to determine the location of the fluorescence response on the fiber, the difference in time between when the pulse is generated and when the fluorescence signal is detected must be determined. At this point, the location on the fiber "l" which generated the signal can be calculated in the following manner[38]

$$\frac{c * \left(\frac{t_f - t_0}{2}\right)}{(\eta_{ex-core} + \eta_{em-core})} = l \qquad \text{(Eqn. 1.8)}$$

Where t_f describes the point in time when the fluorescence signal reaches the detector, c is the speed of light in a vacuum, and $\eta_{ex-core}$ and $\eta_{em-core}$ are the refractive indices of the fiber carrying the excitation pulse and fluorescence signal respectively.

A second design requires many optical fibers but only employs one sensor region on each fiber.[39] These fibers are coupled to one excitation source and the pulse energy divided between the fibers. (Figure 1.9) Each fiber is of differing length, providing the same spacing effect as seen with a single-fiber design. While the pulse energy for each fiber is reduced, there is a benefit as well. When utilizing a single fiber system, the pulse energy will decrease after passing through each sensor region. This is due to factors such as absorption of pulse energy by the analyte-specific compounds and scattering of light due to the changes in the refractive index from the substitute cladding material where the

fluorophore is located. These processes will occur at slightly different levels for every pulse and will have an additive effect as a pulse travels through concurrent regions. This means that sensors near the end of the array will undergo excitation with pulse intensities that have been decreased by a certain amount. This variability will in turn affect the fluorescence of the sensor, potentially providing false responses regarding analyte/fluorophore interactions. By multiple fibers, each with only one sensor region, this variability is eliminated, allowing for more accurate analysis.

Lastly, research within the Geissinger group has developed a third fiber arrangement for OTOFS.[40,41] This design utilizes two optical fibers. (Figure 1.10) The first fiber, referred to as the excitation fiber, serves as the excitation pulse conduit. The second fiber, laid orthogonal to the first fiber and referred to as the emission fiber, collects the fluorescence emission and delivers the signal to a detector. This design has proven successful for both single and multiple analyte-sensitive regions. A positive feature of this design is that the spatial resolution of the complete sensor region can be significantly improved. The analyte-specific regions located on the excitation fiber can be placed much closer to each other than previous designs, on the order of centimeters apart. This is allowed as the emission fiber can have loops of fiber in between each sensor region, providing the spatial delay required to separate each of the fluorescence signals in time.

1.7 Sensor attachment schemes

To this point, different methods of sensor distribution along optical fibers have been discussed. However, the means for introducing analyte-responsive compounds must

also be described. These techniques can range from the doping of the cladding or core material, substitution of the cladding material, or removal of the cladding with subsequent modification of the optical fiber with an analyte-specific compound.

Doping of the cladding or core material is the first technique to be discussed. The benefits to this design are that the fiber system requires no substitute cladding or removal of the cladding, which would require measures to maintain propagation of light in the fiber under TIR conditions. Doping of either cladding or core avoids this issue. With regard to doping of the core material itself, often rare earth elements are used and this technique has successfully been used to develop optical fiber sensors capable of studying high temperatures ranges (900-1500 °C) or measurements of CO_2 gas.[20] Both of these sensors relied on changes in the fluorescence intensity to describe changes occurring with the environment of interest. Doping of the cladding material was employed for oxygen analysis.[41] In this case, an excitation source was directed at the cladding material and the subsequent fluorescence was coupled into the fiber core.

Removal of the original cladding material followed by substitution with a replacement material doped with fluorescent molecules is commonly employed.[42-45] There are several factor that must be taken into account when working with these materials. First, to maintain the transmission capability of the optical fiber, the refractive index of the replacement cladding needs to be smaller than or equal to the refractive index of the original cladding. Secondly, the polymer must be of sufficient porosity to allow analyte access to the analyte-specific fluorophores. There are numerous sensors which have been developed with this approach, including research performed within the Geissinger group, utilizing a number of different polymers to serve as replacement

cladding materials.[40,41]   The polymers have been doped with compounds capable of measuring both pH and oxygen concentration or partial pressure. A majority of the research performed within this body of work will also utilize this technique.

The last technique for integrating analyte-specific fluorophores involves the removal of the cladding material, followed by the covalent attachment of a fluorophore to the optical fiber surface. This approach is often utilized for biological or biochemistry purposes. The hydroxide group located at the source of most silica-based fibers provides for the ability to attach various biosensors to the optical fiber. Sensors have been developed to measure bacteria such as *E. Coli*, used proteins as pH sensors, and measured concentrations of certain DNA strands.[46-48]

1.8 Heavy Metal Fluorescence Sensors

As the body of this work is designed for the quantitation of heavy metal ions using optical-fiber-based fluorescent sensors, a brief review of other sensors developed for heavy metal sensing is appropriate. Several different luminescence approaches are used during these analyses, but most focus on using either the absorption or fluorescence generated upon binding of a metal to a specific chromophore.

Although current literature has many examples of fluorophores which show an affinity and a change in the fluorescence signal for a certain metals, most of these compounds are not capable of being integrated within an optical fiber platform, as most of them suffer from one of three limitations. The first is that the excitation wavelength is in the UV range, where excitation light is strongly attenuated by the optical fiber core. Secondly, the specificity for a given metal of many of these compounds is inadequate for

quantitative analysis due to competitive binding by other metals in solution. Conversely, promotion of a high degree of specificity often requires the binding or strong electrostatic interaction of the metal to the fluorophore. This often means that upon binding, the metal cannot be easily removed from the fluorescent compound. This lack of reversibility would render the fluorophore a single-use sensor, which is an undesirable feature.

However, several sensors have been created that are capable of monitoring heavy metals in solution. Although this field is expanding, research to this point has focused on a few metals of particular environmental concern. Sensors capable of zinc analysis have been developed. An approach favored by some utilizes proteins as a means of recognizing and binding with zinc.[49,50] Both absorption and fluorescence methods were used during the development of these sensors for zinc Cadmium is a second element that has received a significant amount of research and development. Several sensors have been developed that utilize either a change in the fluorescence or change in the absorption profile of the metal-sensitive dye.[51-53] All of the sensors are adsorbed or entrapped within some type of polymer matrix and show reversible binding of the metal to the chromophore. Lastly, copper-specific sensors have also received attention.[54,55] Many of these sensors employ the quenching of fluorescence by copper to measure the copper concentrations.

The research presented herein will detail the development of a quasi-distributed sensor platform capable of simultaneous zinc and copper determination utilizing covalently linked and replacement cladding-integrated means of analyte-specific fluorophore integration to the optical fiber. Unlike other quasi-distributed systems that have required long lengths of fiber to collect measurements, the designs described here

will significantly reduce the sensor size based on a unique design utilizing two optical fibers. While other sensors have be developed for the analysis of metals, the speed, sensitivity and precision of the analysis, coupled with the ease of reversibility for the sensor designs provide a new avenue for metal sensing. Lastly, while the ability to successfully perform multi-analyte analysis using optical fibers has been accomplished, prior research has focused on non-metallic species. The work performed here expands the boundary of multi-analyte sensors by investigating and proving that a multi-metal sensor platform, with specificity for each metal, is possible.

Figure 1.1 A depiction of the cross section of an optical fiber. The light grey area (1) denotes the silica or plastic core material with the refractive index, η_{core}. The dark grey region (2) is a cladding material with a lower refractive index (η_{clad}), in order to cause total internal reflection. The black section (3) denotes an outer layer designed to protect the inner sections from physical stress.
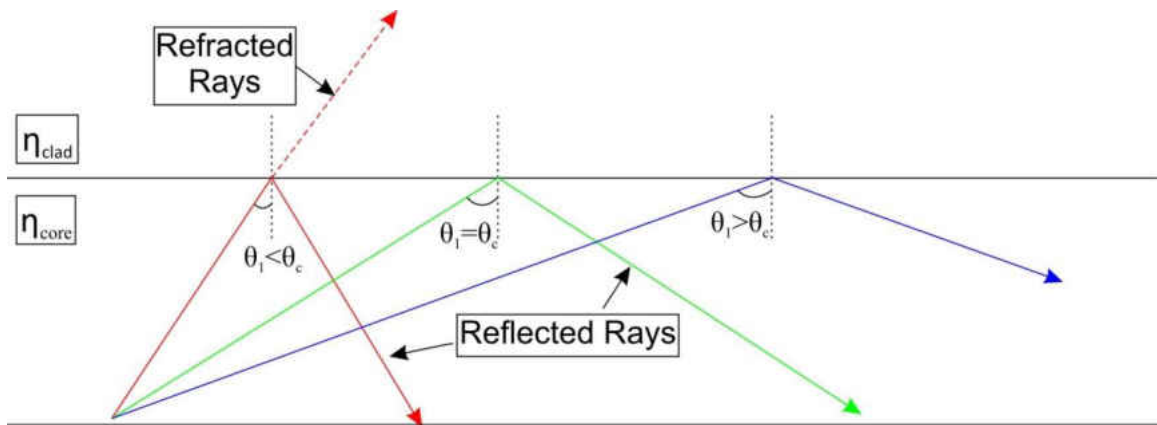
Figure 1.2 In order to undergo total internal reflection, light must strike the core/cladding interface at an angle equal or greater than the critical angle. Light incident at angles less than the critical angle will be partially refracted. The green line, reflecting at a steeper angle than the blue line, is considered to be a higher mode than the blue mode. The red line, with some of the radiation escaping out of the fiber, is referred to as a leaky mode.

$$d_p = \frac{\lambda}{4\pi\eta_{core}}(\sin^2\theta - \sin^2\theta_{crit})^{-1/2}$$
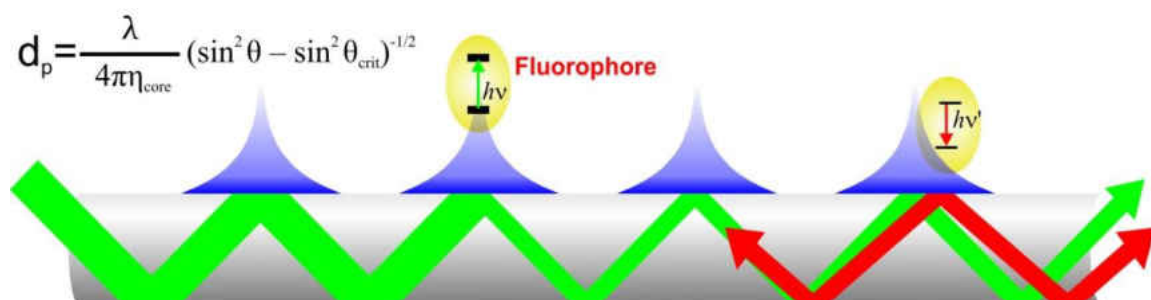
Figure 1.3 When a fluorescent molecule located in the evanescent field (blue regions), the energy from the field can be utilized to interrogate the fluorophore. The penetration depth of the evanescent field is wavelength dependent. The fluorescence generated by the fluorophore is coupled back into the fiber and transmitted to a detector. (Figure adapted from Ref. 56.)

1.4a   **1.4b**
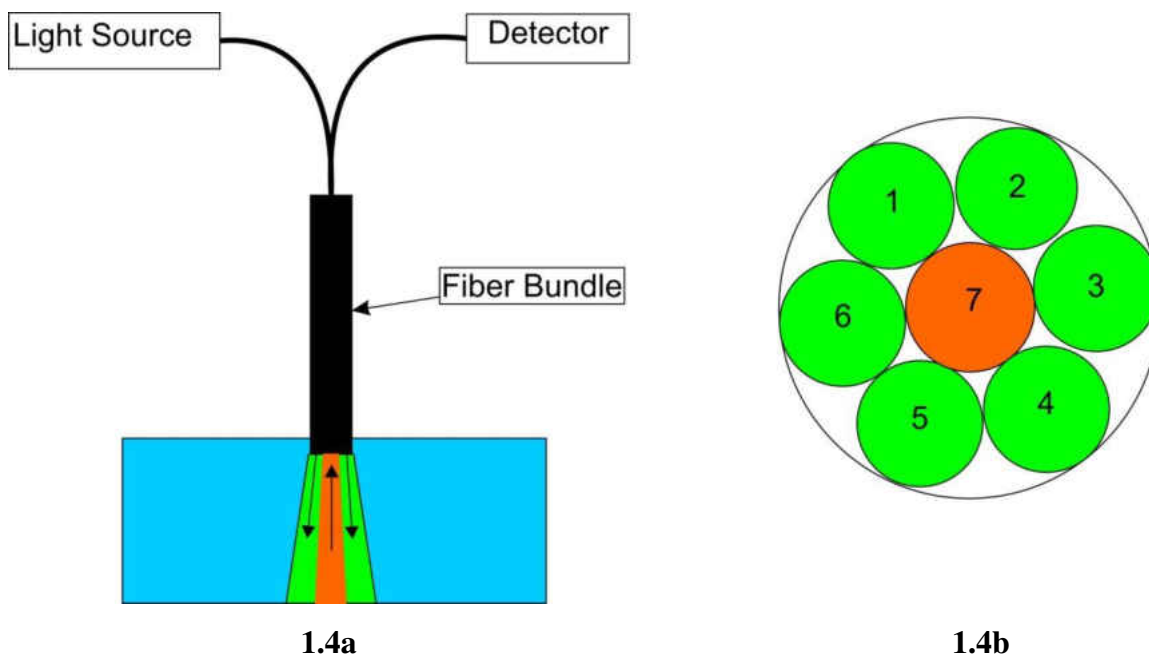
Figure 1.4 Optical fibers are often bundled together to increase either the amount of excitation light projected or to increase the signal collection capability. In this case, in 1.4a the fiber bundle is immersed in a solution containing a fluorescent compound. Light from the source (in green) induces fluorescence from the analyte of interest. This fluorescence (orange) is then coupled into the fiber bundle and transmitted to the detector. For this particular fiber bundle (1.4b) fibers 1-6 transmit excitation light, while fiber number 7 is used to collect the fluorescence. Figure adapted from ref. 28
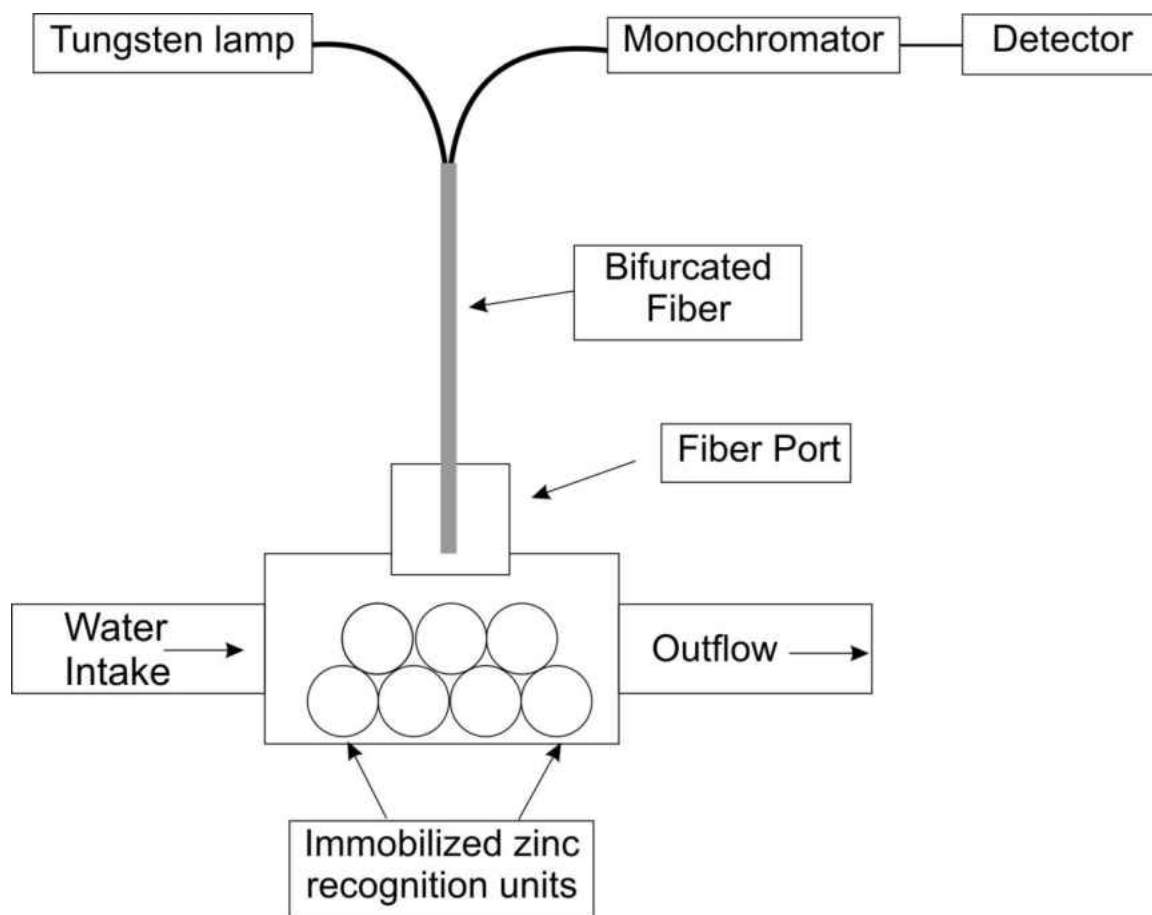
Figure 1.5 A sensor developed for the determination of zinc in water used functionalized polymer beads to bind with zinc. A tungsten lamp coupled to an optical fiber directs full spectrum light onto the beads. Light reflected off of the sensor beads is coupled back into the bifurcated fiber and the reflectance spectrum is collected. Changes in the reflectance profile allowed for the quantitation of zinc in solution. Figure adapted from ref. 29
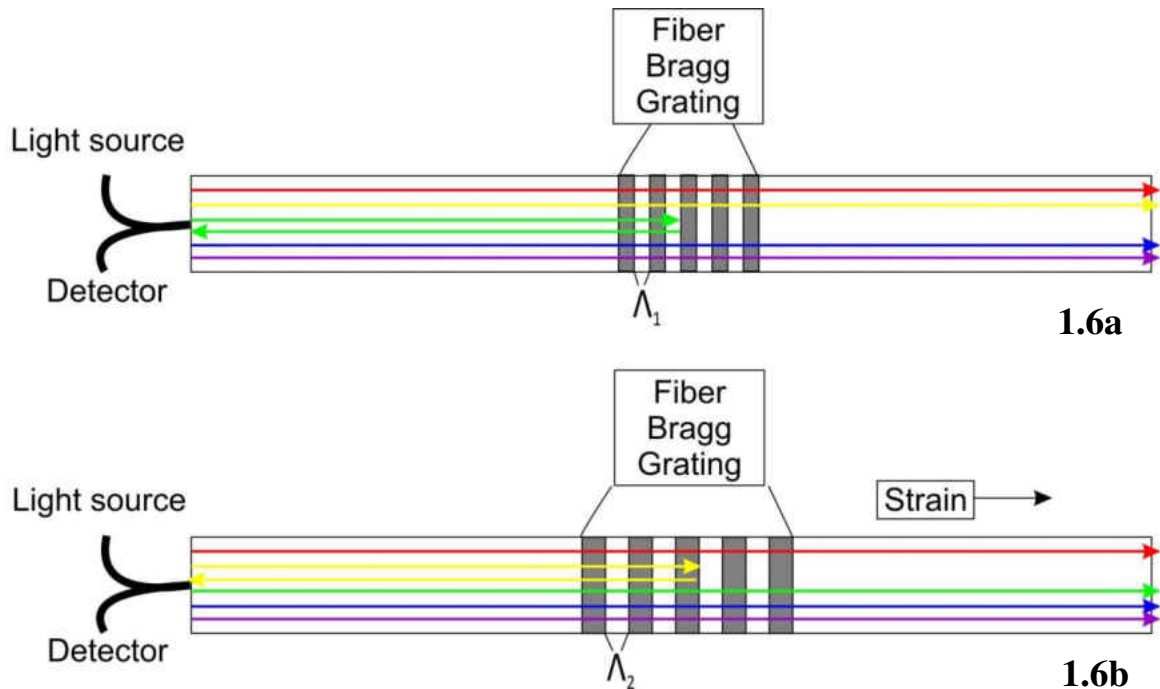
Figure 1.6 By creating areas within the optical fiber of different refractive indices (dark grey), FBG sensors can be used to selectively reflect specific wavelengths. This is not only dependent on the refractive index difference but also on the spacing, or period (Λ), of the grating. In Figure 1.6a, the fiber exists in an unperturbed state. However, in Figure 1.6b the fiber undergoes strain; in this case one end of the fiber is being pulled. The introduction of strain will induce a change in the period of the grating which will change the wavelength of light reflected.
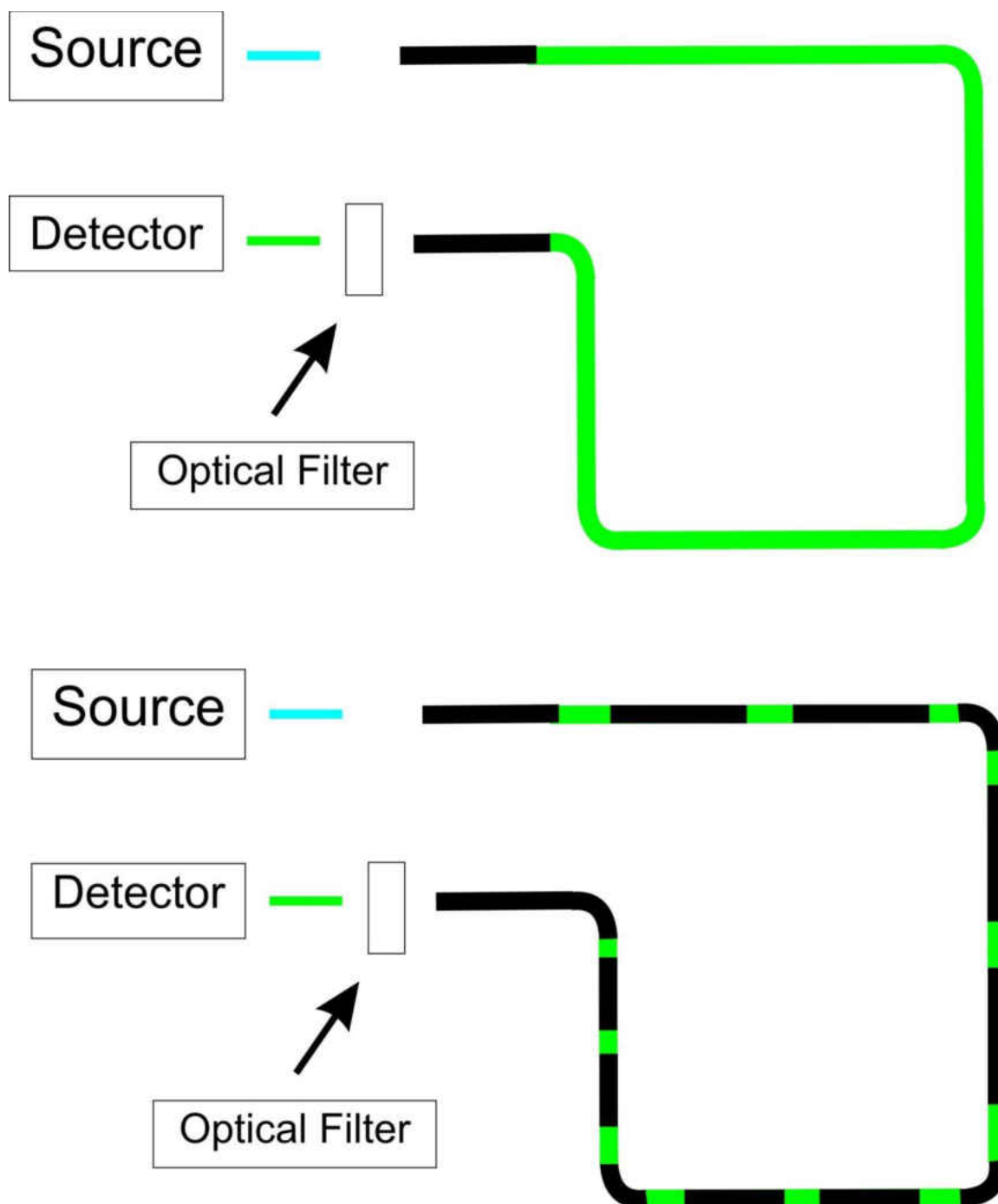
Figure 1.7 A comparison between a fully distributed sensor array (top) and a quasi-distributed sensor array (bottom). The green areas indicate the sections of the optical fiber that are doped with an analyte-specific fluorophore. As seen in the top figures, a fully distributed array consists of a fiber completely doped with the analyte-specific fluorophore. In contrast, the quasi-distributed sensor has specific sections of the fiber doped with the fluorophore. (Figure adapted from ref. 38)
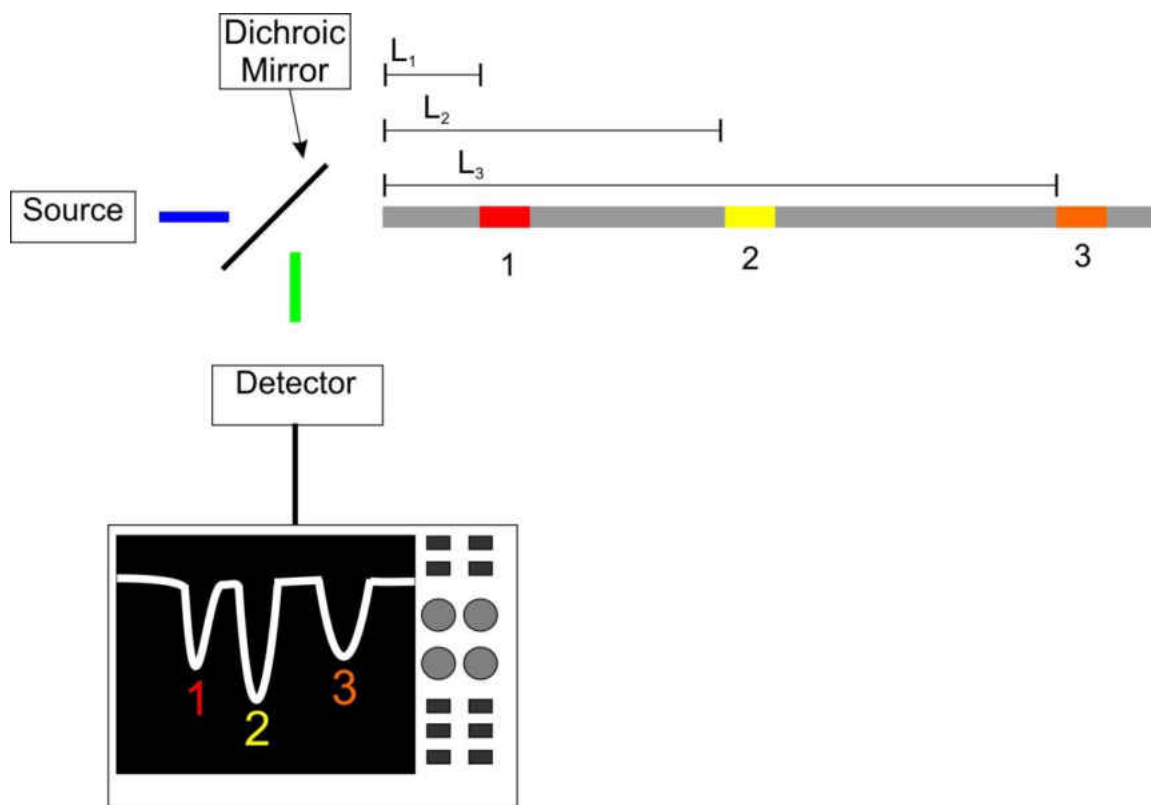
Figure 1.8 Optical Time of Flight Spectroscopy (OTOFS) is possible using a single optical fiber. As a pulse from the source, after passing through a dichroic mirror, travels through the optical fiber, the evanescent wave interacts with sensor regions one, two and three. The fluorescence from each sensor region is coupled into the fiber and travels back through the fiber. The fluorescence is then reflected off the mirror and measured by the detector. To discretely resolve each fluorescence signal however, approximately 10 m of fiber is required between each sensor region. (Figure adapted from ref. 38.)
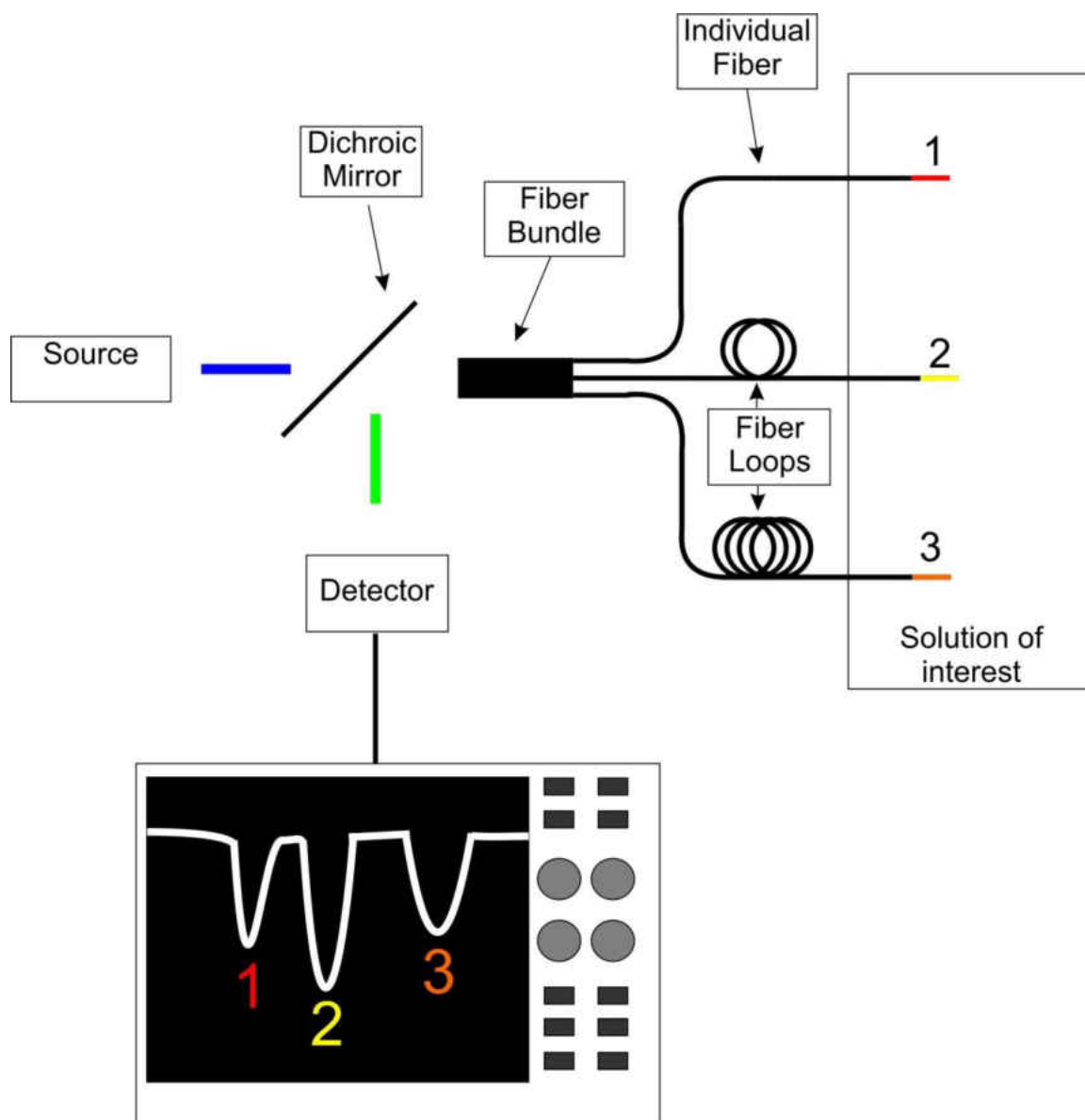
Figure 1.9 A second scheme using OTOFS employs several fibers bundled together where the excitation pulse energy is divided between the fibers. The fibers are of differing lengths and each fiber only contains one sensor region, located at the tip of the fiber. Separations in time of the fluorescence signals occur as in a similar manner as was observed in Fig. 1.8. Figure adapted from ref. 39.
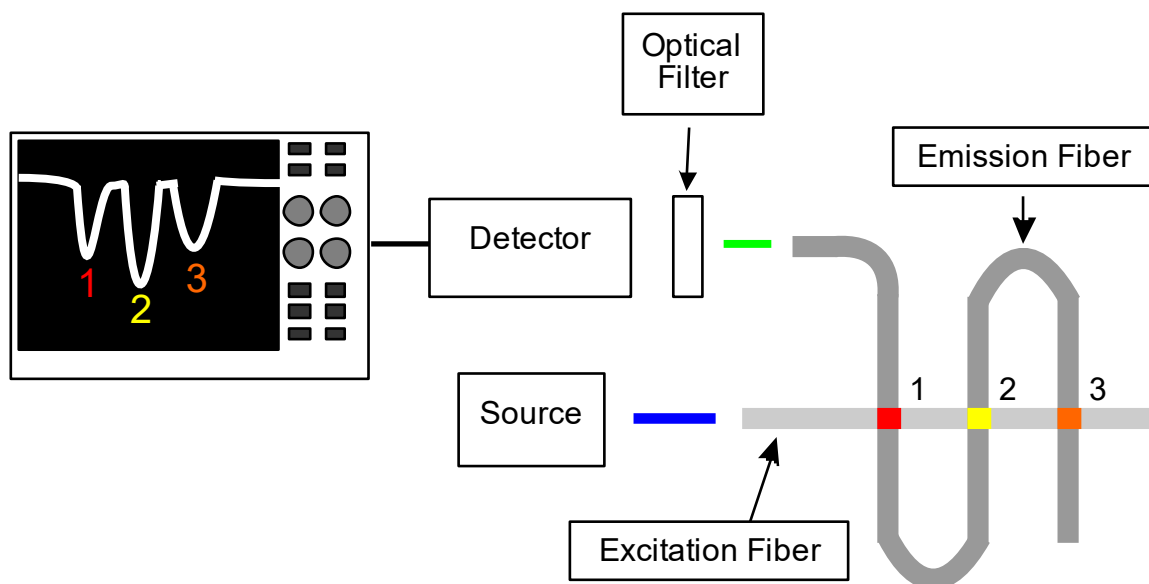
Figure 1.10 The crossed-fiber sensor design will be the basis of the research performed in this work. Two fibers, laid perpendicular to each other, serve to direct the excitation pules to and the fluorescence signals away from the sensor region. This design allows for the reduction of space required between sensor regions and significantly reduces the amount of scattered excitation light reaching the detector. (Figure adapted from ref. 56.)

References

1. U.S. Geological Survey *Zinc – The Key to Preventing Corrosion*; Fact Sheet 2011-3016; US Department of the Interior: 2011

2. U.S. Geological Survey *Copper – A Metal for the Ages*; Fact Sheet 2009-3031; US Department of the Interior: 2009

3. Safe Drinking Water Foundation. Mining and Water Pollution. http://www.safewater.org/PDFS/resourcesknowthefacts/Mining+and+Water+Pollution.pdf (Accessed March 14th, 2013)

4. Spurgeon, D., Hopkin, S., Jones, D. Effects of cadmium, copper, lead and zinc on growth, reproduction and survival of the earthworm *Eisenia fetida* (Savigny): Assesing the environmental impact of point source metal contamination in terrestrial ecosystems. *Environ. Pollut.* **1992**, *84,* 123-130

5. Dahab, M., Montag, D., Parr, J. Pollution prevention and waste minimization at a galvanizing and electroplating facility. *Wat. Sci. Tech.* **1994**, *30(5)*, 243-250

6. Davis, A., Shokouhian, M., Ni, S., Loading estimates of lead, copper, cadmium and zinc in urban runoff from specific sources. *Chemosphere* **2001**, *44*, 997-1009

7. Agency for Toxic Substances and Disease Registry *Toxicological Profile for Zinc* U.S. Dept. of Health and Human Service: 2005

8. Agency for Toxic Substances and Disease Registry *Toxicological Profile for Copper* U.S. Dept. of Health and Human Service: 2004

9. Araya M, McGoldrick MC, Klevay LM, Strain, J., Johnson, L., Robson, P., Nielsen, F., Olivares, M., Pizarro, F., Poirier, K. Determination of an acute no-observed-adverse-effect level (NOAEL) for copper in water. *Regul Toxicol Pharmacol* **2001**, *34(2)*, 137-148.

10. Araya M, Chen B, Klevay LM, Strain, J., Johnson, L., Robson, P., Shi, W., Nielsen, F., Zhu, H., Olivares, M., Pizarro, F., Haber, L. Confirmation of an acute no-observed-adverse-effect and low-observed-adverse-effect level for copper in bottled drinking water in a multi-site international study. *Reg Tox Pharmacol* **2003**, *38*, 389-399

11. Hach. DR 2800 Spectrophotometer Procedures Manual http://www.hach.com/quick.search-quick.search.jsa?keywords=DOC022.53.00725 (Accessed March 10th, 2013)

12. Cole-Parmer. CHEMets Colorimetric Copper Test Kit. http://www.coleparmer.com/Product/CHEMets_Colorimetric_Copper_Test_Kit/EW-00290-50 (Accessed March 14th, 2013)

13. U.S. Environmental Protection Agency *Method 700B:Flame Atomic Absorption Spectrophotometry*; 1996

14. U.S. Environmental Protection Agency *Method 1639:Determination of Trace Elements in Ambient Waters by Stabilized Temperature Graphite Furnace Atomic Absorption*; 1996

15. Skoog, D., Holler, F., Crouch, S. *Principles of Instrumental Analysis*; Thomson Brooks/Cole, Belmont, 2007

16. U.S. Environmental Protection Agency *Determination of Trace Elements in Waters and Wastes by Inductively Coupled Plasma – Mass Spectrometry*; Method 200.8; 1996

17. U.S. Environmental Protection Agency *Determination of Metals and Trace Elements in Waters and Wastes by Inductively Coupled Plasma – Atomic Emission Spectrometry*; Method 200.7; 1994

18. Jagner, D., Aren, K. Potentiometric stripping analysis for zinc, cadmium, lead and copper in sea water. *Anal. Chim. Acta* **1979**, *107(6)*, 29-35

19. Ichinoki, S., Sasai, S., Sugai, H., Fujii, H. Determination of Copper Ion in River Water by Solvent Extraction with 2-Mercaptobenzothiazole Followed by Reverse Phase HPLC. *J. Liq. Chromatogr. Relat. Technol.* **2009**, *32*, 3066-3076

20. Grattan, K., Sun, T. Fiber optic sensor technology: an overview *Sens. Actuators* **2000**, *82*, 40-61

21. Zubia, J., Arrue, J. Plastic Optical Fibers: An Introduction to Their Technological Processes and Applications. *Opt. Fiber Technol.* **2001**, *7*, 101-140

22. Anderson, G., Taitt, C. Evanescent Wave Fiber Optic Biosensors, 2nd ed; Ligler, F., Taitt, C.; Elsevier: 2008; pp 83-138

23. RP Photonics. Encyclopedia of Laser Physics and Technology. http://www.rp-photonics.com/numerical_aperture.html (Accessed March 13th, 2013)

24. Alwayn, V. *Optical Network Design and Implementation*; Cisco Press 2004

25. RP Photonics. Encyclopedia of Laser Physics and Technology. http://www.rp-photonics.com/multimode_fibers.html (Accessed April 6th, 2013)

26. Kramer, M. Evanescent Waves in Microscopy *Photonik* **2004**, *2*, 42-44

27. McDonagh, C., Burke, C., MacCraith, B. Optical Chemical Sensors Chem. Rev. 2008, 108(2), 400-422

28. Ocean Optics. Reflection/Backscattering Probes. http://www.oceanoptics.com/Products/reflectionprobesstandard.asp (Accessed March 13th, 2013)

29. Vaughan, A., Narayanaswamy, R. Optical Fibre Reflectance sensors for the detection of heavy metal ions based on immobilized Br-PADAP *Sens. Actuators, B* **1998**, *51*, 368

30. Jorge, P., Caldas, P., Rosa, C., Oliva, A., Santos, J. Optical fiber probes for fluorescence based oxygen sensing *Sens. Actuators, B* **2004**, *103*, 290-299

31. Hill, K., Meltz, G. Fiber Bragg Grating Technology Fundamentals and Overview *J. Lightwave Technol.* **1997**, *15(8)*, 1263-1276

32. Zhang, Y., Feng, D., Liu, Z., Guo, Z., Dong, X., Chiang, K., Chu, B. High-Sensitivity Pressure Sensor Using a Shielded Polymer-Coated Fibre Bragg Grating *IEEE Photonics Technol. Lett.* **2001**, *13(6)*, 618- 619

33. Kreuzer, M. Strain Measurements with Fiber Bragg Grating Sensors. http://www.hbm.com/fileadmin/mediapool/techarticles/2007/FBGS_StrainMeasurement_en.pdf (Accessed March 10th, 2013)

34. Jung, J., Nam, H., Lee, B., Byun, J., Kim, N. Fiber Bragg grating temperature sensor with controllable sensitivity. *Appl. Opt.* **1999**, *38(13)*, 2752-2754

35. Cordero, S., Beshay, M., Low, A., Mukamal, H., Ruiz, D., Lieberman, R. A distributed fiber optic chemical sensor for hydrogen cyanide detection. *Proc. SPIE* **2005**, *5993*, 599302-1–599302-8

36. Henning, P. E., Benko, A., Schwabacher, A., Geissinger, P., Olsson, R., Apparatus and methods for optical time-of-flight discrimination in combinatorial library analysis *Rev. Sci. Instr.* **2005**, *76*, 062220

37. Valuer, B., *Molecular Fluorescence Principles and Applications*. Wiley-VCH: New York, 2002

38. Potyrailo, R., Hieftje, G. Optical Time-of-Flight Chemical Detection: Spatially Resolved Analyte Mapping with Extended-Length Continuous Chemically Modified Optical Fibers *Anal. Chem.* **1998**, *70*, 1453-1461

39. Potyrailo, R., Hieftje, G. Spatially resolved analyte mapping with time-of-flight optical sensors *TrAC, Trends Anal. Chem.* **1998**, *17(10)*, 593-604

40. Henning, P. E.; Geissinger, P. Application of time-correlated single photon counting and stroboscopic detection methods with an evanescent-wave fibre-optic sensor for fluorescence-lifetime-based pH measurements. *Meas. Sci. Technol*. **2012**, *23*, 045104

41. Rigo, M.V., Plasmonic Optical Fiber Sensor for Oxygen Measurement. Ph.D. Thesis, University of Wisconsin-Milwaukee, Milwaukee, WI, May 2009

42. Lieberman, R., Blyler, L., Cohen, L. A Distributed Fiber Optic Sensor Based on Cladding Fluorescence *J. Lightwave Technol.* **1990**, *8(7)*, 212-220

43. White, J., Kauer, T., Dickinson, A., Walk, D.R. Rapid Analyte Recognition in a Device Based on Optical Sensors and the Olfactory System. *Anal. Chem.* **1996**, *68*, 2191-2202

44. Baldini, G.E., Grattan, K.T.V., Tseung, A.C.C. Impregnation of a pH-sensitive dye into sol-gels for fiber optic chemical sensors. *Analyst*, **1995**, *120*, 1549-1554

45. Ferguson, J., Healey, B., Bronk, K., Barnard, S., Walt, D. Simultaneous monitoring of pH, CO_2 and O_2 using an optical imaging fiber. *Anal. Chim. Acta* **1997**, *340(1-3)*, 123-131

46. Tripathi, S., Bock, W., Mikulic, P., Chinnappan, R., Ng, A., Tolba, M., Zourob M. Long period grating based biosensor for the detection of *Escherichia coli* bacteria *Biosens. Bioelectron.* **2012**, *35*, 308-312

47. Veselov, A., Thür, C., Efimov, A., Guina, M., Lemmetyinen, H., Tkachenko, N. Acidity sensor based on porphyrin self-assembled monolayers covalently attached to the surfaces of tapered fibers *Meas. Sci. Technol*. **2010**, *21,* 115205

48. Epstein, J., Lee, M., Walt, D., High-Density Fiber-Optic Genosensor Microsphere Array Capable of Zeptomole Detection Limits *Anal. Chem.* **2002**, *74*, 1836-1840

49. Thompson, R., Jones, R. Enzyme-Based Fiber Optic Zinc Biosensor *Anal. Chem.* **1993**, *65*, 740-734

50. Wang, K., Seiler, K., Rusterholz, B., Simon, W., Characterisation of an optode membrane for Zn(II) incorporating a lipophilized analogue of the dye 4-(2-pyridylazo) rescorcinol *Analyst* **1992**, *117,* 57-60

51. Lu, J., Zhang, Z., Optical fibre fluorosensor for cadmium with diethylaminoethyl-sephadex as a substrate *Analyst*, **1995**, *120*, 453-455

52. Czolk, R., Reichert, J., Ache, H. An optical sensor for the determination of cadmium (II) ion *Sens. Actuators A* **1991**, *25-27*, 439-441

53. Compano, R., Ferrer, R., Guiteras, J., Prat, D., Spectroflourimetric detection of zinc and cadmium with 8-(Benzenesulfonamido)-quinoline immobilized on a polymeric matrix *Analyst* **1994**, *119*, 1225-1228

54. Mahendra, N., Gangaiya, P., Sotheeswaran, S., Narayanaswarmy R. Investigation of an optical fibre Cu(II) sensor using Fast Sulphon Black F (FSBF) immobilized onto XAD-7 *Sens. Actuators B*, **2002**, *81*, 196-201

55. Mahendra, N., Gangaiya, P., Sotheeswaran, S., Narayanaswarmy R. Investigation of an optical fibre copper based on immobilized α-benzoinoxime (cupron) *Sens. Actuators B* **2003**, *90*, 118-123

56. Prince. B., Schwabacher, A., Geissinger, P. A Readout Scheme Providing High Spatial Resolution for Distributed Fluorescent Sensors on Optical Fibers *Anal. Chem.* **2001**, *73*, 1007-1015

Chapter 2

Experimental Methods and Materials

2.1 Introductory remarks

This chapter explains all experimental procedures involved in optical-fiber-based sensor research. The chapter will start with a description of the general instrumentation used. General sensor procedures will also be described here, with specific sensors being described later in the chapter. Several supporting projects, not directly using optical-fiber-based sensors, are also described. Finally, calculations that are applicable to the development of both sensors will be described in the last section. Much of this work is based on earlier research done within the research group.[1,2]

2.2 Software employed

Raw data files collected using spectroscopic instrumentation were saved as text files, while raw data collected from the oscilloscope were collected as ASCII files. Initial peak integration was done using Origin ver. 7.0 (Northampton, MA), but later data integration was performed using a program written in LabView ver. 7.1 (Austin, TX). This program was written by Dr. Paul Henning, a member of the Geissinger group. All data plots were done in Origin. Calculations and statistical analyses were performed using Microsoft Excel 2003 and Excel 2010 (Redmond, WA).

2.3 Spectroscopy Instrumentation

Absorption measurements were performed with two different instruments. For qualitative absorption profiles of filters, an Agilent 8453 UV-Visible Spectrophotometer system (Santa Clara, CA) was used. The instrument consisted of a deuterium/tungsten lamp set with a 1024 element photodiode array detector. The instrument is interfaced to a PC using the Chemstation software (Rev.A 10.01) provided with the instrument.

Absorption measurements were performed with a resolution of 1.0 nm with an integration time of 1.0 second. Data was saved in .txt file format.

All absorption measurements pertaining to solutions were performed using a Perkin-Elmer (Waltham, MA) Lambda 650 UV/Vis Spectrophotometer. Instrumental components consisted of tungsten and deuterium lamps, with signal collection using a 1440 lines/mm Littrow grating and an R9555 photomultiplier tube. Signal processing on a PC was performed using the PerkinElmer ver. 6.3 UV Winlab software. Data was collected with a resolution of 1.0 nm and 1.0 second integration time. Absorption data was saved as .txt files and then plotted in Origin.

Fluorescence measurements were recorded using a Fluorolog-3 FL-22 flourimeter made by Horiba Scientific (Ann Arbor, MI). The instrument utilizes a 450 W xenon lamp. Fluorescent signals were collected using a 1.0 mm excitation slit width and 2.0 mm emission slit width with a resolution of 1.0 nm and an integration time of either 1.0 or 0.5 s. Signals were collected using an R928P photomultiplier tube (PMT) made by Hamamatsu (Hamamatsu City, Japan), with data processing performed with an attached SpectACQ unit. The SpectACQ unit was also responsible for all data averaging and statistical analysis within the software. Data was displayed using the DataMax ver. 2.2 software system. The raw data collected were saved as .txt files and plotted in Origin.

2.4 General Supplies

2.4.1 General Chemicals

2,2-dimethoxy-2-phenylacetophenone (DMPA), trimethylolpropane triacrylate (TPT), poly(ethylene glycol) diacrylate (PEG-DA) (MW 575), 1,4-paradioxane, polyacrylonitrile (PAN), sodium dodecyl sulfate (SDS) and 1000 mg/L Zn AA standards

were purchased from Sigma-Aldrich (Milwaukee, WI). 1000 mg/L AA standards for Al, Ca, Fe, K, Mg, Na, Ni, Pb, and Sn were obtained from J.T. Baker (Phillipsburg, PA). 1000 mg/L AA standard for Cd, ACS grade acetone, absolute ethanol, and ACS grade acetonitrile were purchased from VWR (Radnor, PA). ACS grade nitric acid, sodium sulfite, sodium nitrate, sodium dodecyl sulfate (SDS) and disodium hydrogen phosphate were purchased from Fisher Scientific (Pittsburg, PA). 6.5-μm diameter polymethylmethacrylate (PMMA) microspheres were purchased from Bangs Laboratory (Fisher, IN) and glacial acetic acid was purchased from Mallinckrodt (St. Louis, MO). Laser dyes used to generate the excitation pulses consisted of analytical research grade Coumarin-481(C-481), 2,5-diphenyl-oxazole (PPO) and Rhodamine-110 (Rh-110) were purchased from Exciton (Dayton, OH). ACS grade dichloromethane, ACS grade toluene, N,N-dimethylformamide (99.8%) and citric acid monohydrate were purchased from Alfa Aesar (Ward Hill, MA). Ultrapure water with a resistivity of 18 MOhm•cm was prepared using a Thermo-Scientific Nanopure Ultrapure Water Purification System (Waltham, MA).

2.4.2 Zinc sensor specific chemicals

FluoZin-1 tripotassium salt (FZ-1), purchased from Invitrogen (Carlsbad, CA) was stored at -20 °C in solid form. To prepare the solid for sensors applications, FZ-1 was dissolved in 2 mL of ultrapure water, providing a stock concentration of 4.17×10^{-4} M. The solutions were stored at 3 °C in the dark. A proprietary compound, Dragon Green (DG), was the reference material paired with the zinc sensor. Dragon Green is a commercial product consisting of dyed polymer microspheres (average diameter of 7.32

μm) from Bangs Laboratory chosen to match the spectral properties of FZ-1. Stock solutions of 1% microspheres suspended in water were stored at 3 °C.

2.4.3 Copper sensor specific chemicals

Dansyl chloride (≥99.0%), diethylenetriamine (DETA) (99%), quinine sulfate monohydrate and 3-glycidoxypropyltrimethoxysilane (GPTS) (≥98 %) were purchased from Sigma-Aldrich. All reagents were used without further purification.

2.4.4 Polystyrene microsphere specific chemicals

Styrene (≥99%), benzoyl peroxide (BPO) (purum, ≥97.0%), and poly(acrylic acid) (PAA) (MW ~450,000) were purchased from Sigma-Aldrich. γ-alumina (99.97%) was purchased from Alfa Aesar.

2.4.5 General lab equipment

Solutions were mixed using a VWR VM-3000 vortex mixer. All experiments requiring heating, temperature control or stirring utilized a Fisher Scientific Isotemp Digital Stirring Hotplates. pH values were measured using a VWR sympHony SB80PC pH meter with a gel Ag/AgCl electrode. The meter was calibrated prior to each set of measurements using a 3 point calibration curve with pH values of 4, 7, and 10. For all UV curing procedures, a Spectroline (Westbury, NY) ENF-260C handheld UV lamp with emissions centered on 365 nm was used. All glassware was doubly rinsed with ultrapure water before being immersed in a 2% nitric acid bath for 48 hours, then rinsed three times with ultrapure water before use.

2.5 Optical time of flight experimental setup

The optical time-of-flight system (depicted in Figure 2.1) consists of three components: an excitation source, the chemical sensors, and detection equipment. Each of the components will be discussed in further detail below.

2.5.1 Excitation Source

A Photon Technology International (PTI) PL-3300 nitrogen laser was used to pump a PL-201 tunable dye laser (Birmingham, NJ). The zinc sensor required a different excitation (λ_{ex}=495 nm) wavelength than the copper sensor (λ_{ex}=365 nm). For laser emission at 495 nm, the dye C-481 dissolved in 1,4-dioxane at a concentration of 1.0×10^{-2} M was employed. For lasing at 365 nm, the dye PPO was dissolved in toluene to a final concentration of 6.0×10^{-3} M. The nitrogen used to supply the PL-3300 laser was either high-purity grade from Airgas (West Chicago, IL) or 4.8 grade from Praxair (Danbury, CT). The emitted pulses from the dye laser were passed through a focusing lens and coupled into a FT-1000-UMT, high OH optical fiber (NA=0.39) from Thorlabs (Newton, NJ).

To monitor pulse intensities from the laser, a Thorlabs DET10A fast photodiode, with a rise time of 1 ns, was used to record emitted pulses. Signals measured by this photodiode were obtained from the light that was back-reflected from the optical fiber coupling system. This detector also served as a timing trigger for all optical time-of-flight measurements. Signals were measured using a LeCroy LC564DL digitizing oscilloscope with a 1-GHz sampling rate (Chestnut Ridge, NY). The oscilloscope was set to internally average the same number of pulses as was averaged for the sensor signal.

Data, as an averaged single trace, was transferred to the PC and displayed in ScopeExplorer ver. 2.25. Each trace was saved as an ASCII file. The area under each curve was integrated initially using Origin but later data analysis was done using the same LabView program as for the fluorimetry data.

2.5.2 Fiber sensor construction

All optical fibers and connectors were purchased from ThorLabs. Sensors were constructed using FT-200-UMT fiber with a core-diameter of 200 μm and a numerical aperture (NA) of 0.39. These fibers were chosen because of their high OH content, allowing for better signal transmission at shorter wavelengths. Lab space allocation required that the laser be located in a different room than the sensor systems and as such, the experimental setup dictated that approximately 30 m of FT-1000-UMT optical fiber was used to transmit the excitation pulses from the source to the sensor unit. This high OH-fiber also had a numerical aperture (NA) of 0.39 but with a 1000-μm core diameter. The ends of the connector cable were fitted with SMA-905 terminators and polished following manufacturers specifications.[3] Two lenses within a one-inch-long tube were used to couple the light between the two fibers. The 200-μm diameter fiber was cleaved with a razor blade to approximately 1-m lengths for both excitation and emission fibers. Because of the high turnover of these sensors, the fibers were cleaved but not polished and utilized a temporary SMA connector from ThorLabs. Optical fiber ends not coupled to either excitation or emission terminals were immersed in glycerol to prevent back reflections within the fibers.

A Bunsen burner was employed to remove the outer layers (cladding and inner jacket) of the optical fibers, leaving only the glass cores. In order to selectively remove these materials, a metal sheet with 7.5 mm holes acted as a template to remove only the desired sections of cladding. The fibers were exposed long enough to remove the cladding, but short of heating the glass cores to a glowing red color. It was found that heating the cores for too long caused the fibers to become more brittle. After removal of the cladding, the fibers were wiped with a Kimwipe containing acetone to remove any residues or soot. Before beginning sensor-specific processes the fibers were cleaned by soaking in 1.0-M ACS grade nitric acid for one hour, then rinsed with 18MOhm•cm (ultrapure) water.

2.5.3 Sensor support and sample analysis chamber development

All sensors were inherently fragile due to the inflexibility and brittleness of the glass core. To provide structural support for the sensor, two polypropylene blocks, each having dimensions of 1" x 1" x 0.5", were employed to hold the optical fibers in place. (Figure 2.2) Shallow grooves were cut into a face of the block to provide a channel in which the fibers could sit . Once the fibers were seated and secured with transparent cellophane tape in the grooves of the first block, the second block was placed on top of the fibers, effectively sandwiching the fibers and locking them in place. A 0.5-inch hole was drilled through the middle of both blocks to allow analyte access to the sensor. Four 1/8" holes were drilled into each corner of both blocks and served to house bolts used to hold the polypropylene blocks together. Initial sensor development used galvanized screws. However, immersion of these screws in solution induced leaching of zinc from

the screws into solution and caused the fluorescent response of the sensor to increase over time. Plastic screws were subsequently employed to eliminate this issue.

Early experiments used shallow containers in which the block sensors were immersed in the sample environments. However, transferring the sensor to different containers resulted in changes of the fiber alignment causing changes in signal intensity not related to changes in concentrations. A sample container (Figure 2.3) was fabricated in the UW-Milwaukee glassblowing shop to eliminate this source of interference. A long-stem funnel capable of containing approximately 300 mL was modified to allow the sensor to remain in a fixed position while individual solutions could be introduced and flushed from the container. The stem was modified to house a stopcock. A ledge was added to the main funnel body with a one-inch hole about two inches below the lip of the funnel. This provided a shelf on which the fiber array could rest . Four small notches were cut into the funnel for the optical fibers to sit in to keep the sensor from twisting or sliding within the chamber.

2.5.4 Multi-Sensor Array Construction

Single sensors were housed within the previously mentioned polymer blocks. However, for sensor arrays containing more than one sensor, a plastic slab drilled with 0.5 inch holes arranged in a 5 x 5 array was employed. The fibers were locked in place using cellophane tape placed on all sides of a fiber junction. These pieces of tape served as a replacement for placing individual sensor regions in between two polymer blocks. The metal sheet used to selectively remove cladding from the sensor was drilled with a series of holes to match the spacing of the holes in the plastic slab.

A two-sensor array was arranged following the design shown in Figure 2.4. Two optical fibers were used, one acting as the excitation fiber and one as the emission fiber. The emission fiber contained 10 m of fiber between the two sensors as a means of separating the fluorescence signals from each sensor before arriving at the detector. The reference sensor is excited first followed by the sensor designed for analyte recognition.

The final portion with regard to sensor development involved creating a four sensor array (Figure 2.5). The fiber section for the copper sensor was stripped first, and then underwent synthesis to produce the copper sensor. The remaining three sections were stripped after the synthesis was complete. This was done because the copper synthesis requires bending of the optical fibers and stripping the cladding renders the fibers fragile and incapable of being bent. For the three sensors that utilize the PEG-DA polymer, the bare fibers were placed on the slab first, and then the polymer mixtures were applied. The slab was too large to fit in the previously described sensor container, so a 9" x 13" Pyrex baking dish was used.

One excitation fiber was used to excite each of the sensors. However, four different emission fibers of varying lengths were used to allow for temporal separation of each of the signals. In Figure 2.5 where the first fiber had a length of approximately 0.5 m, with the remaining fibers having lengths of 15 m, 25 m, and 35 m respectively. All of the fibers were bundled together through a temporary SMA connection and coupled to the detector.

2.5.5 Detection and Signal Processing

Fluorescent emissions from the sensors were passed through a filter specific to the sensor of interest. For the zinc sensor, a FL514.5-10 515 narrow bandpass filter was used, while for the copper sensor a B52-544 500 nm longpass filter was employed (Figures 2.6 and 2.7). Both filters were purchased from Edmund Optics (Barrington, NJ) and were employed to remove any scattered excitation signals. Signal collection was performed using a Peltier-cooled Burle C31034A photomultiplier tube with an applied voltage of 1.8 kV. Power was supplied to the unit with a RQE-3001 regulated power supply made by Northwest Scientific Corp (Acton, MA). Data collection was performed using the LeCroy LC 564 DL 1-GHz oscilloscope. The oscilloscope internally averaged between 100-300 individual pulses and displayed one signal trace. The signal trace from the oscilloscope was transferred to a PC using ScopeExplorer ver. 2.25 made by LeCroy. The data was converted to an ASCII file format and uploaded in Origin. For each trace, the area under the curve was integrated. Initial data integration was performed using Origin but for later measurements, integration was performed using the same LabView program as for the fluorimeter data.

2.6 Individual sensor fabrication

While all of the optical fibers underwent the same pre-treatment process in preparation for the addition of the sensors, each sensor region contains a unique set of reagents used to build the sensor.

2.6.1 Zinc sensor

10 mg of DMPA (a photo-initiator) were mixed into 1 mL of PEG-DA. The mixture was left for 24 hours to allow the DMPA to dissolve. After complete dissolution, 300 µL of the PEG-DA/DMPA solution, 50 µL of TPT (a cross-linking agent), 100 µL of ultrapure water, 50 µL of stock FZ-1 solution and 75 mg of PMMA (6.5-µm diameter) microspheres were mixed together in a vortexer. This yielded a final concentration of 4.16×10^{-5} M for FZ-1. After the crossed-fiber setup had been constructed, 10 µL of the polymer mixture was added to the crossing point of two fibers, such that a small drop (about 1 mm in diameter) encapsulated the two fibers. The liquid polymer was cured using 365 nm light. In order to dissolve the microspheres, the polymer sensor on the crossed-fibers was immersed in acetone for 24 hours. When exposed to water, the polymer exhibits a certain degree of swelling which will affect the fluorescence signal. To account for this, the crossed fiber sensor was left in ultrapure water for 24 hours to allow the polymer to reach equilibrium in solution.

2.6.2 Reference for zinc sensor

The steps for preparing the Dragon Green reference sensor are very similar to the zinc sensor. The only difference is that the reference sensor does not undergo the microtemplating process and, therefore, does not contain any PMMA microspheres. This is important, because the analyte has to be prevented from reaching Dragon Green to avoid any possibility of causing a change in its luminescence; Dragon Green's function is to report the intensity of the excitation pulse. A mixture of 300 µL of the PEG-DA/DMPA solution, 50 µL of TPT, 100 µL of ultrapure water, and 50 µL of stock

Dragon Green were combined to form the reference sensor. A 10-µL droplet was added to a crossed-fiber system and cured with 365 nm light in the same manner as the zinc sensor; however the sensor was not immersed in acetone but was immediately submerged in ultrapure water for 24 hours to reach equilibrium in solution.

2.6.3 Zinc reference sensor utilizing Rh-110

The purpose of a reference is to monitor changes in the intensity of the pulses generated by the source. As such, any reference material must be protected from other factors that will influence the fluorescence of the reference. The previously mentioned reference material, Dragon Green, is sold where the fluorescent dye is already protected within an impermeable polymer. However, Rhodamine-110 was used as a reference material during the initial validation of the two-sensor array design. To provide Rh-110 protection from environmental factors (dissolved oxygen, pH, etc.) which would change the fluorescent signal, an impermeable shell was synthesized around Rh-110. For the development of the Rh-110 reference, polyacrylonitrile (PAN) was used to encapsulate the Rh-110 dye. The process was outlined in the literature.[4] 120 mg of PAN and 3 mg Rh-110 were added to 25 mL of N,N-dimethylformamide (DMF). The solution was gently heated in order to speed up the dissolution of the PAN. Separately, 60 mg of SDS was dissolved in 125 mL of ultrapure water. A slight change in the stated method was employed at this point. The literature method stated that the PAN solution was removed from the heat before addition of the SDS solution. Empirical evidence collected from a separate project within the Geissinger group demonstrated that leaving the DMF solution on the hot plate while adding the first 7 mL of SDS solution provided for a more reliable encapsulation process. While the DMF solution was still warm, the SDS solution was

added dropwise using a burette. After the addition of approximately 7 mL, the DMF solution became cloudy with the formation of nanospheres. After the SDS solution was completely added, the mixture was centrifuged at 3500 rpm for 5 minutes. The solution was decanted and the solid was washed with ultrapure water. The resulting solutions were centrifuged and washed two more times. Finally, the nanospheres were washed and centrifuged with acetone. After decanting the acetone, the nanospheres were stored in acetone in the dark at room temperature.

In order to verify that total encapsulation had occurred, approximately 100 mg of Rh-110 was suspended in various solvents such as toluene, water, acetone and ether. When Rh-110 was added to each of the solutions as a free dye, the maximum emission wavelength for the dye would vary by 20-30 nm, depending on the solution. If the dye was fully encapsulated within the PAN nanospheres, the wavelength dependency of the dye would be significantly reduced. Fluorescence measurements of the solutions confirmed total encapsulation. Figure 2.8 shows that for solvents of differing polarity, only a one to two nm shift in the emission maximum was observed. This small shift in the maximum emission was considered acceptable. This reasoning for this acceptance was due to the fact that empirical observations during several other fluorescence studies had shown fluorescent dyes to have emission maximum shifts of one to two nm between spectral scans even while exposed to identical environments.

After confirming total encapsulation of Rh-110, the encapsulated dye was incorporated onto a crossed-fiber sensor following the same ratio (10 % (v/v)) as previously described sensors.

2.6.4 Copper Sensor

The copper sensor fabrication followed a published procedure,[5] which allows for the sensor to be covalently attached to the glass core of the optical fiber. The composition of the sensor consists of two parts. The first part is a spacer unit between the copper-sensitive portion and the glass core. This spacer unit is partially responsible for the large Stokes shift (130 nm) between the excitation and emission wavelengths and serves as the anchor point of the sensor to the optical fiber. The copper sensitive portion was combined with the spacer component following a published method.[6] 5.85 mL of diethylenetriamine (DETA) was cooled on an ice bath. Simultaneously, 1.50 g of dansyl chloride was added to 170 mL of acetonitrile. Once DETA had fully cooled, the acetonitrile/dansyl chloride mixture was added. A light green precipitate instantly formed but the solution was stirred vigorously for 24 hours to allow the reaction to go to completion. Once the reaction was finished, the acetonitrile was evaporated, leaving a light green solid, referred to as DDETA. Figure 2.9 depicts the synthesis procedure.

While the reaction between DETA and dansyl chloride was underway, the optical fibers were prepared in the manner previously described. After the acid wash was complete, the optical fibers were immersed in 0.6% solution of 3-glycidoxypropyltrimethoxysilane (GPTS) in 250 mL of toluene. This process functionalized the optical fibers to allow bonding of DDETA to the optical fiber. The solution was heated to 50 °C and left to react for 24 hours. The fibers were removed from the solution and washed three times with both toluene and dichloromethane. The DDETA solid was dissolved in 150 mL of dichloromethane and the fibers were immersed for 48-72 hours. Finally, the fibers were washed three times with dichloromethane then

water and acetone. Figure 2.10 describes the complete synthesis procedure. The fibers were mounted within the sensor block as previously described. Sensors were stored in open air and not in water, because water causes hydrolysis of the spacer unit, which degraded the sensor more quickly over time.

2.6.5 Reference for copper sensor

Quinine sulfate (QS) was chosen as the reference material for the copper sensor. Once again, to prevent the sensor from interfering species, the PAN encapsulation process was employed. However, because no published method existed for encapsulation of QS, the method used for Rh-110 was employed. The amount of QS used in the PAN encapsulation process is important. The original method used in literature was designed so that PAN was in excess in order to ensure that the dye of interest would be fully encapsulated. For this method, too much QS could consume all of the PAN in a scheme where many QS molecules would be partially encapsulated but only a few would be fully encapsulated. Having lower amounts of QS would allow for complete encapsulation but would sacrifice fluorescence intensity in the process. During the initial testing, different amounts of QS were added to the PAN solution in order to strike a balance between the ability to completely encapsulate the dye and signal strength of the sensor. As a baseline, the percent change in signal was measured for QS free in solution when exposed to a clean solution and exposed to a 2 ppm Cu solution. The encapsulated QS underwent the same test and the amount of QS in PAN, which yielded the smallest change in signal, was chosen as the optimal amount. The PAN encapsulated QS was then integrated into the PEG-DA polymer at a 10% (v/v) concentration.

2.7 Polymer Film Study

To determine the longevity of the zinc sensors, polymer films were created and fixed to UV-grade methacrylate disposable cuvettes (Sigma-Aldrich). PEG-DA is a natural cross-linking polymer; however, the amount of the additional cross-linker, TPT, was varied between the polymer films to determine if dye leaching was affected by the amount of TPT present.

2.7.1 Film creation

Polymers consisting of PEG-DA, TPT, water and the FZ-1 solution were mixed in different ratios. All the polymers contained 60% PEG-DA and 10% FZ-1 solution; only the water and TPT levels were altered. The total volume of each liquid polymer was 1 mL. The first solution contained 5% TPT, the second 20% TPT, and the third contained 25% TPT. The volume of each solution was brought to 1 mL using ultrapure water.

In order to create the polymer films, Spectrosil Far UV Quartz 0.2 mm demountable cuvettes, manufactured by Starna (Atascadero, CA), served as a mold into which the liquid polymer was poured. To cure the polymer, the solution was exposed to the UV light. Upon curing, the film detached from the glass slide without any assistance. Using a plastic microspatula, the film was transferred to a polymethylmethacrylate cuvette with a 1-cm pathlength. Before the film was added, a layer of Norland (Cranbury, NJ) optical adhesive 61 was spread onto one face of the cuvette. The polymer film was placed on top of the layer of adhesive. The film and adhesive were exposed to 365-nm light, causing the adhesive to cure, locking the film in place.

2.7.2 Film study measurements

Before discussing the film study performed, a discussion of the method to analyze the film studies is warranted. Front-face fluorimetry is a type of fluorescence spectroscopy often used to analyze solid samples or thin films like the ones created in this study. Traditional fluorimetry is orientated so that the fluorescence signals are collected at a 90° angle with respect to the excitation source. This is done to limit the amount of scattered light reaching the detector. This method works well for solutions as the excitation radiation can fully penetrate the solution and generate significant fluorescence in all directions. However, for thin films and solids, the cross section is significantly smaller when observing the fluorescence at a right angle. Instead, a detector is located at a 22° angle with respect to the source. This allows a much larger cross section of the sample to generate fluorescence. Internally, the instrument software processes the signal differently to compensate for the increase in the scattered excitation light reaching the detector. Instead of only processing and reporting the signal from the fluorescence intensity observed by the detector as done for traditional 90° fluorimetry, a ratio between the fluorescence intensity and the source intensity is used when performing front-face fluorimetry. Figure 2.11 demonstrates the difference between traditional and front-face fluorimetry by depicting the different instrumental orientations.

Each film was immersed in pH 5.5 acetic acid/sodium acetate buffer. The buffer was changed before each day of measurement to remove all dye that was not retained within the polymer. Front-face fluorescence measurements were performed daily for the first 25 days to track the change in fluorescence intensity. The excitation wavelength was shifted from 495 nm to 475 nm in order to prevent the excitation signal from

overpowering the fluorescence signal at 515 nm. All other fluorescence parameters remained at the same values as in previous measurements. After 25 days, the frequency of fluorescence measurements was reduced to every 2 or 3 days for a 90-day period. To account for fluctuations with the lamp intensity, two solutions of 5 mM Rh-110 were analyzed before every day of analysis. Every data point is a ratio of the integrated intensity of the film and the integrated intensity of the Rh-110 signal.

2.8 General data treatment for sensors

It was determined that integrating the area under the curve was a more reliable method and reduced the standard deviation of each measurement set when compared to using the peak value of the curve. data sets that relied on values describing intensities underwent integration.

Determination of the limit of detection (LOD) and limit of quantitation (LOQ) followed published methods.[7] The base equation is:

$$X_L = X_{bl} + k s_{bl} \qquad \text{(Eqn 2.1)}$$

Where X_L is the calculated value of the limit, X_{bl} is the average of 10 blank values, k is a factor used to describe either LOD (k=3) or LOQ (k=10), and s_{bl} is the standard deviation of 10 blank values. After collecting the 10 blank values, a calibration curve must be performed. Using the equation generated by the linear regression analysis of the calibration curve, the LOD and LOQ can be calculated with the following relationship:

$$X_L = m[M^{+2}] + b \qquad\qquad \text{(Eqn 2.2)}$$

Where $[M^{+2}]$ is the concentration of the metal species of interest.
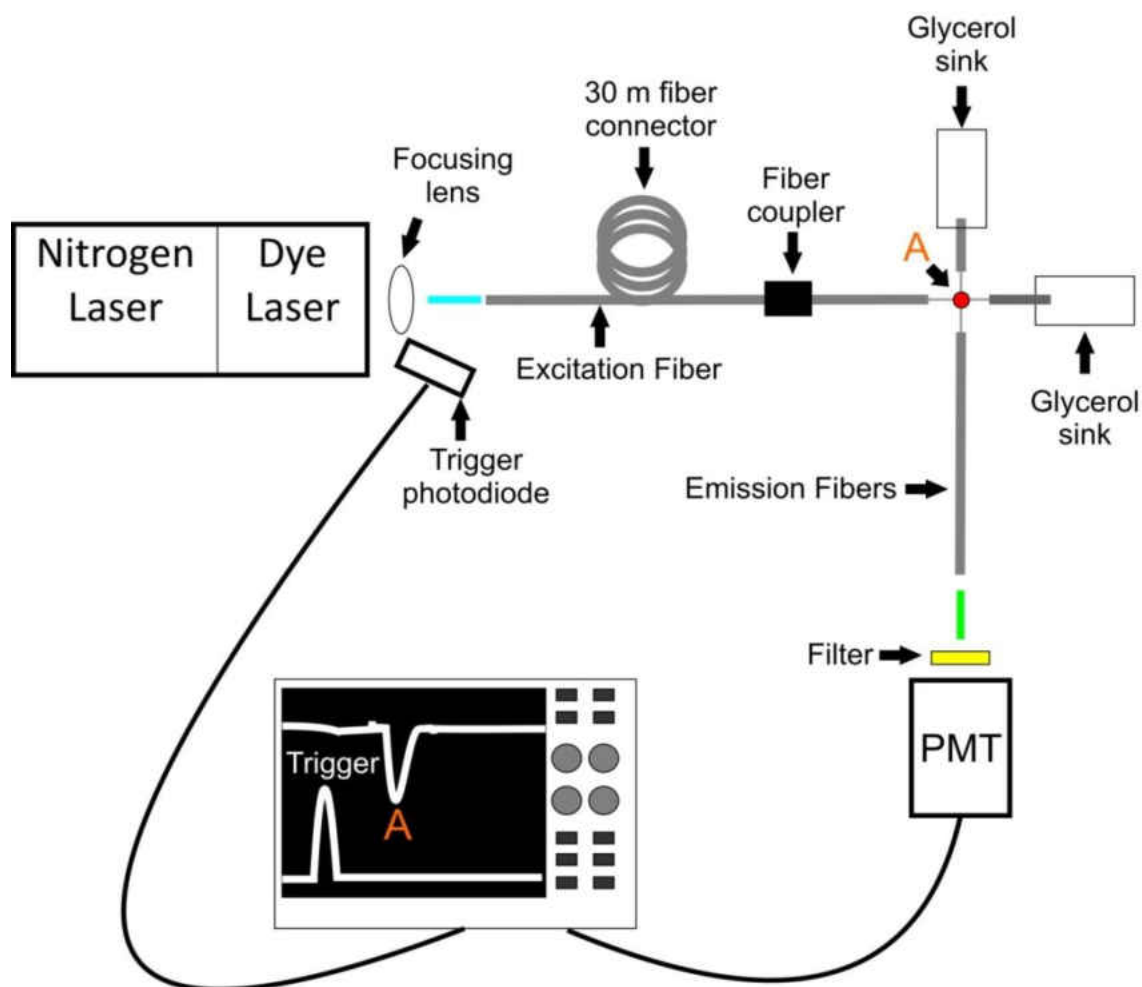
Figure 2.1 A schematic representing a single optical fiber sensor experimental design
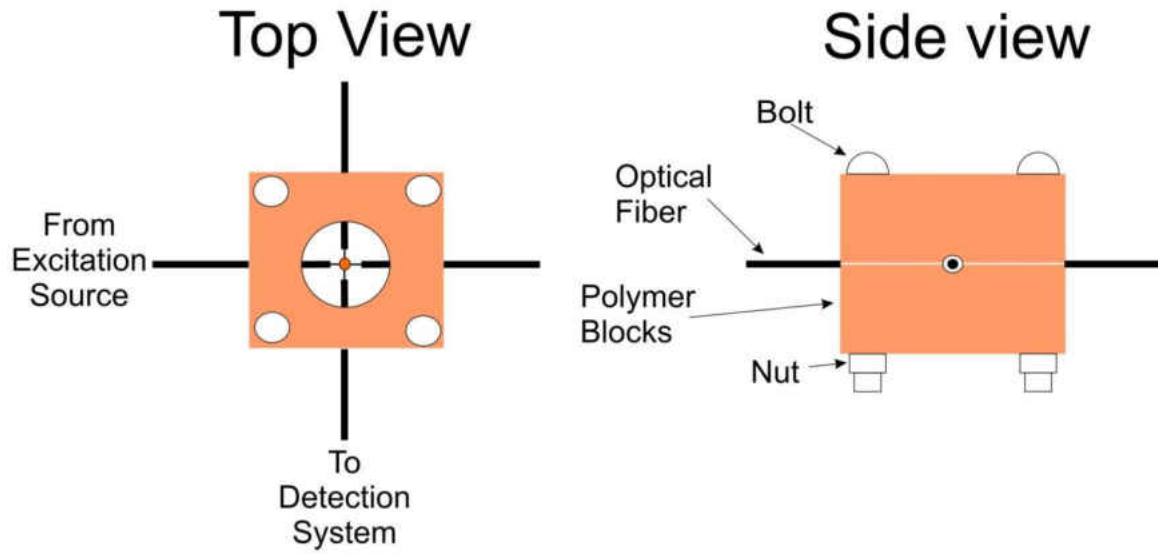
Figure 2.2 The polymer block support structure for a single optical fiber sensor
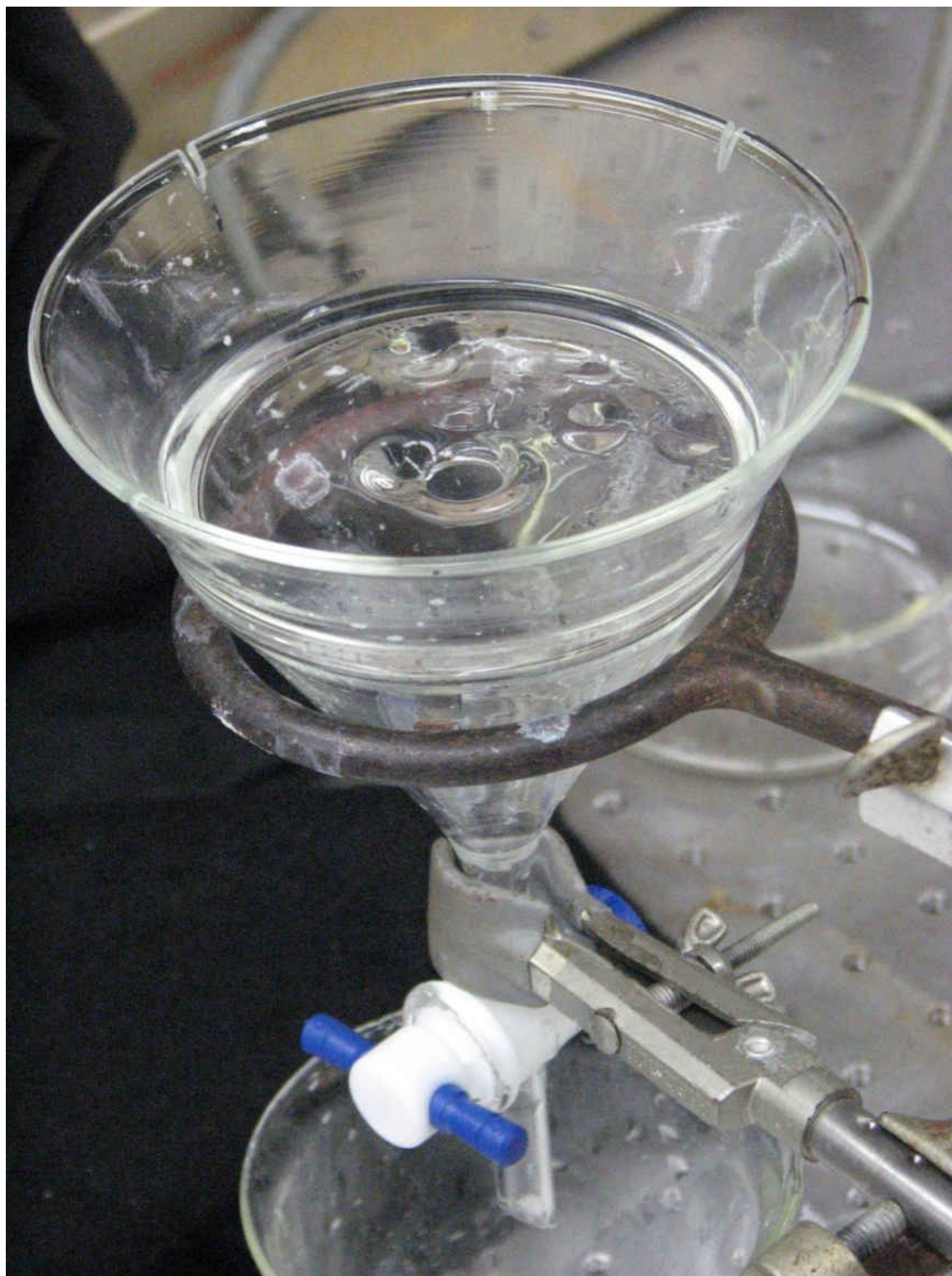
Figure 2.3 The housing chamber for a single optical fiber sensor contained within the polymer block setup.
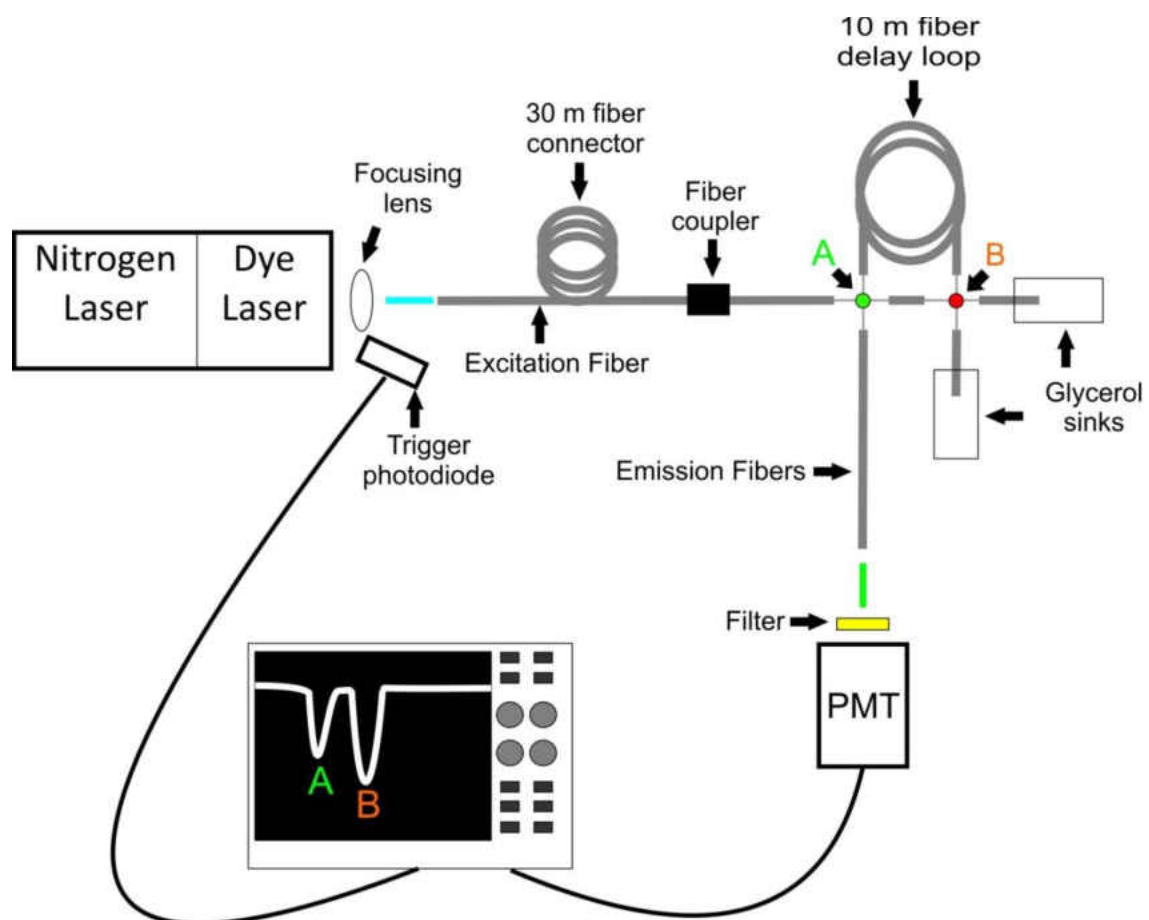
Figure 2.4 A schematic of a sensor array utilizing two sensor regions, where sensor "A" is the reference dye and sensor "B" is the metal-specific dye.
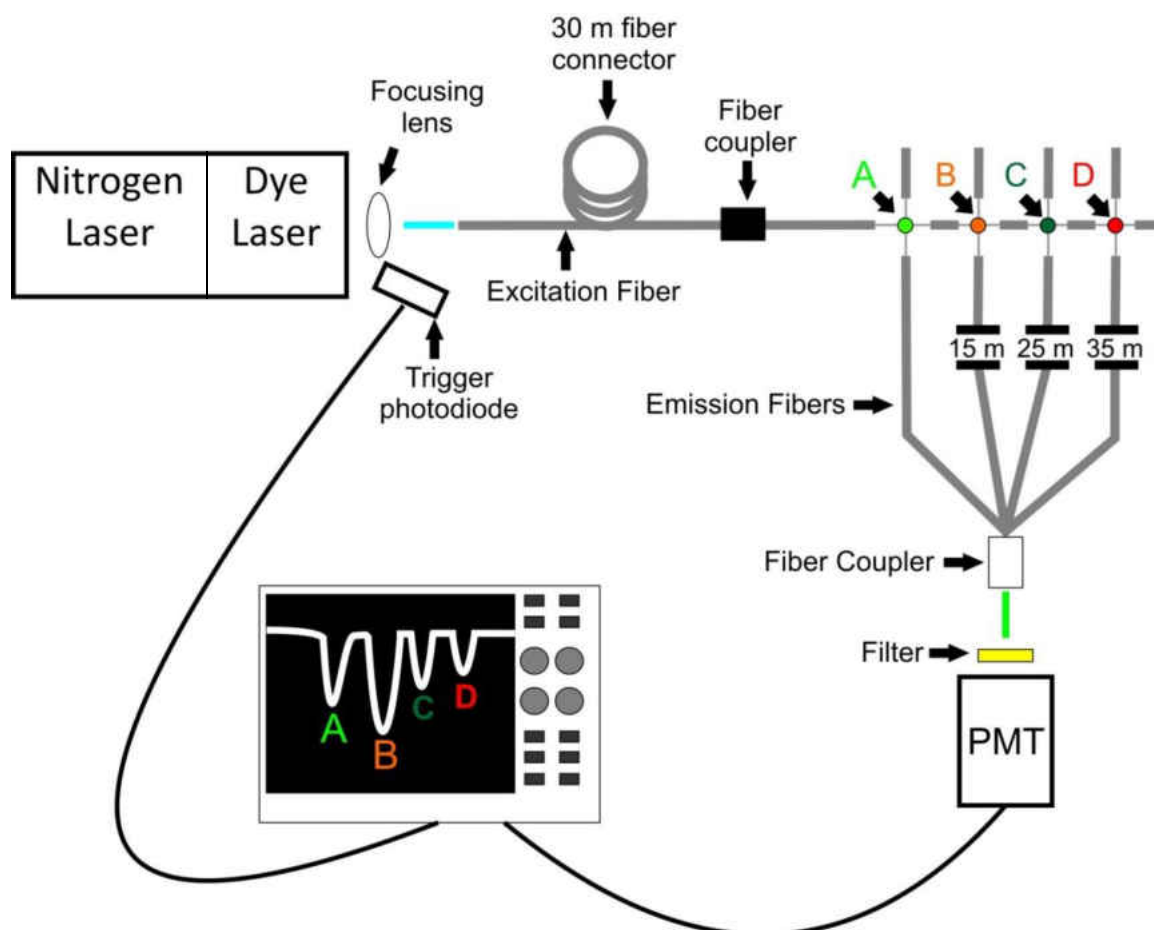
Figure 2.5 A schematic depicting the arrangement of a four sensor array.
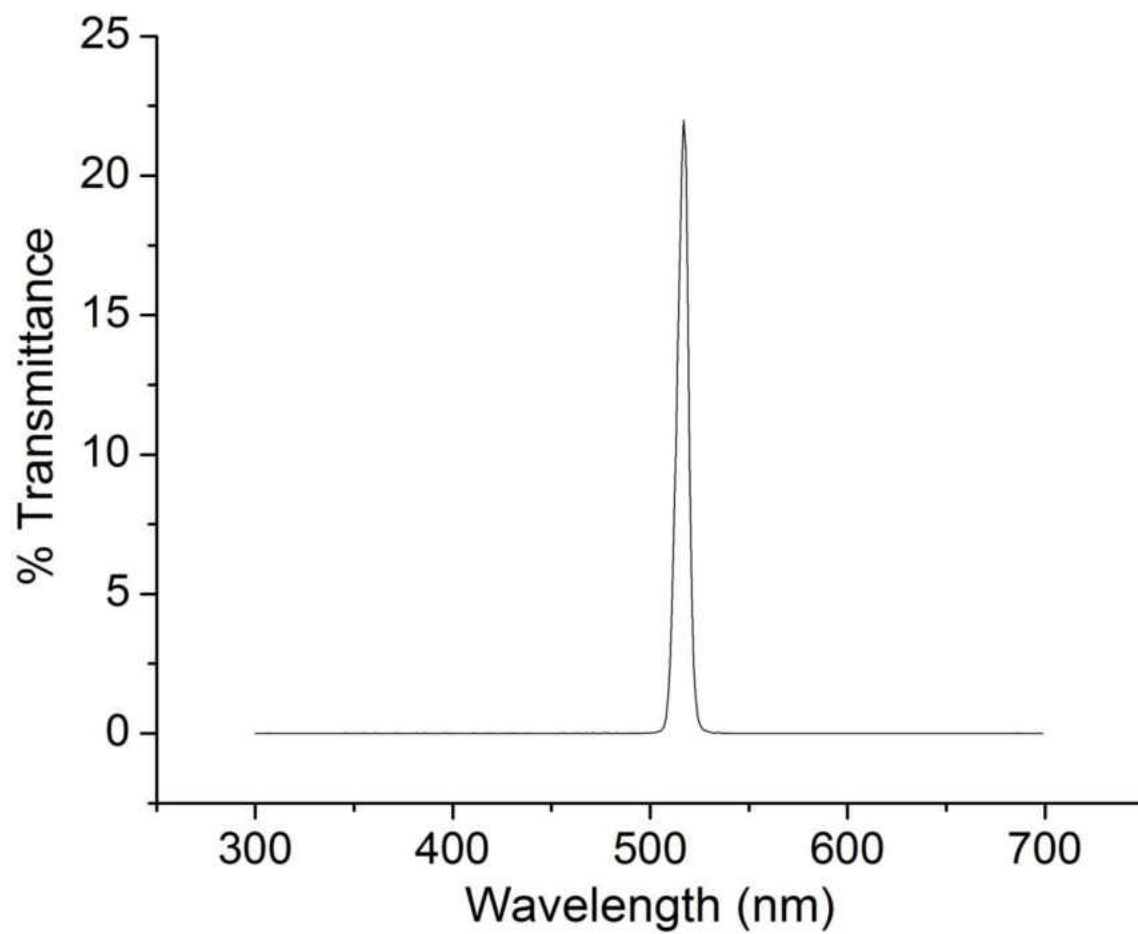
Figure 2.6 Transmittance profile for the FL514.5-10 narrow bandpass filter
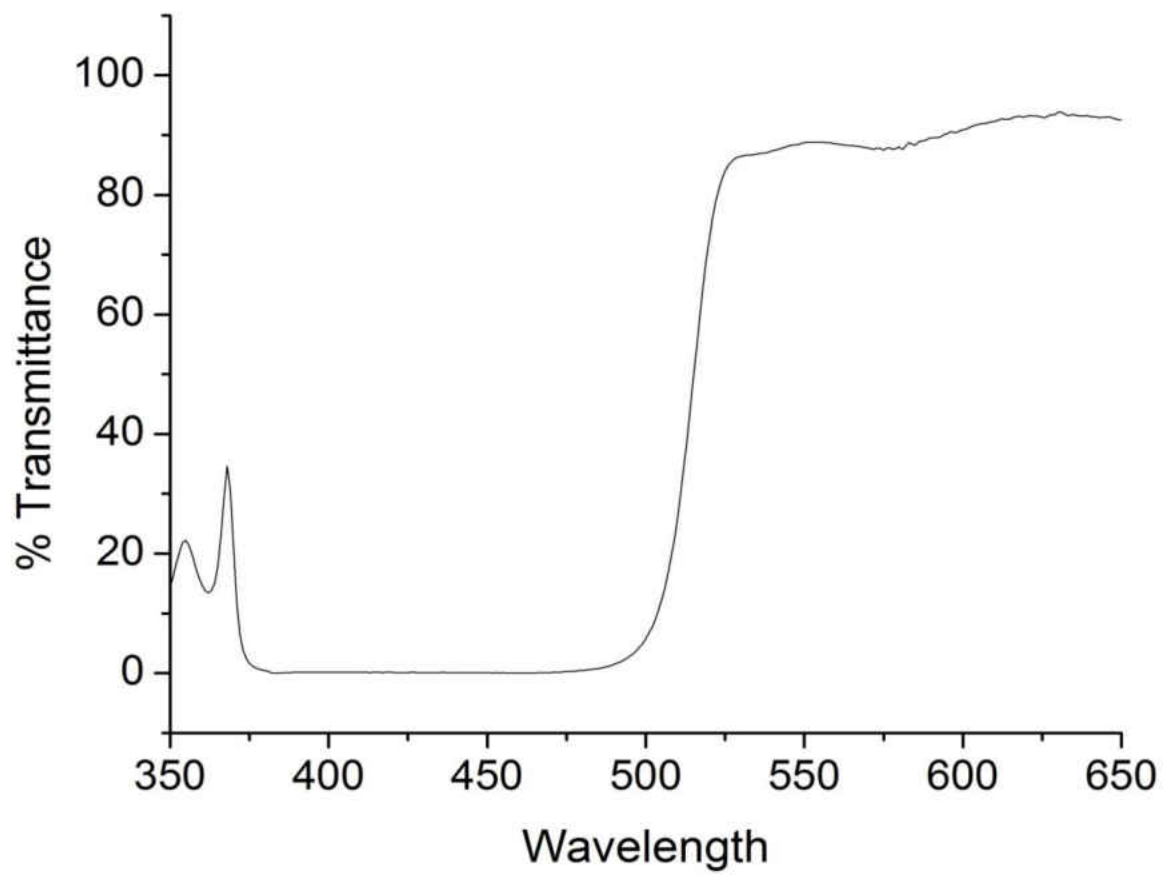
Figure 2.7 Transmittance profile for the B52-544 500 nm longpass filter
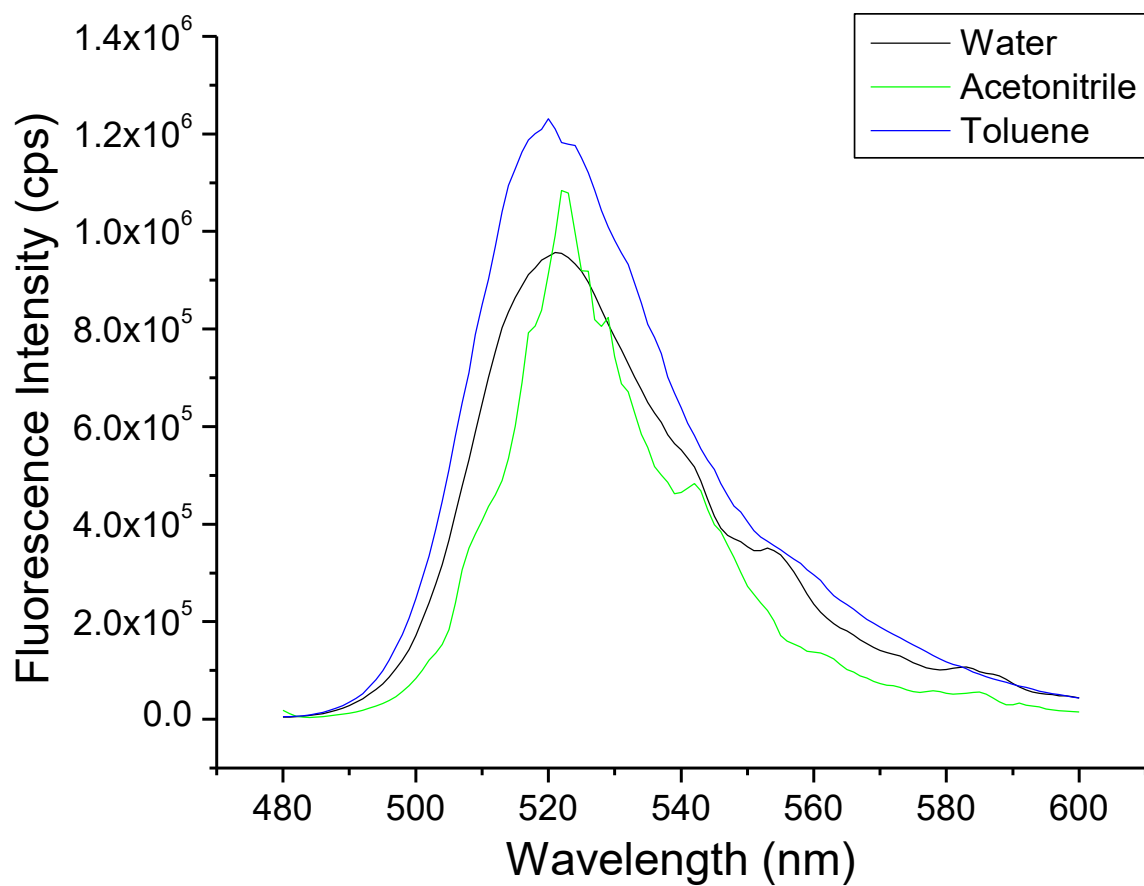
Figure 2.8 Confirmation of encapsulation of Rh-110 in PAN by mixing PAN with various solvents.
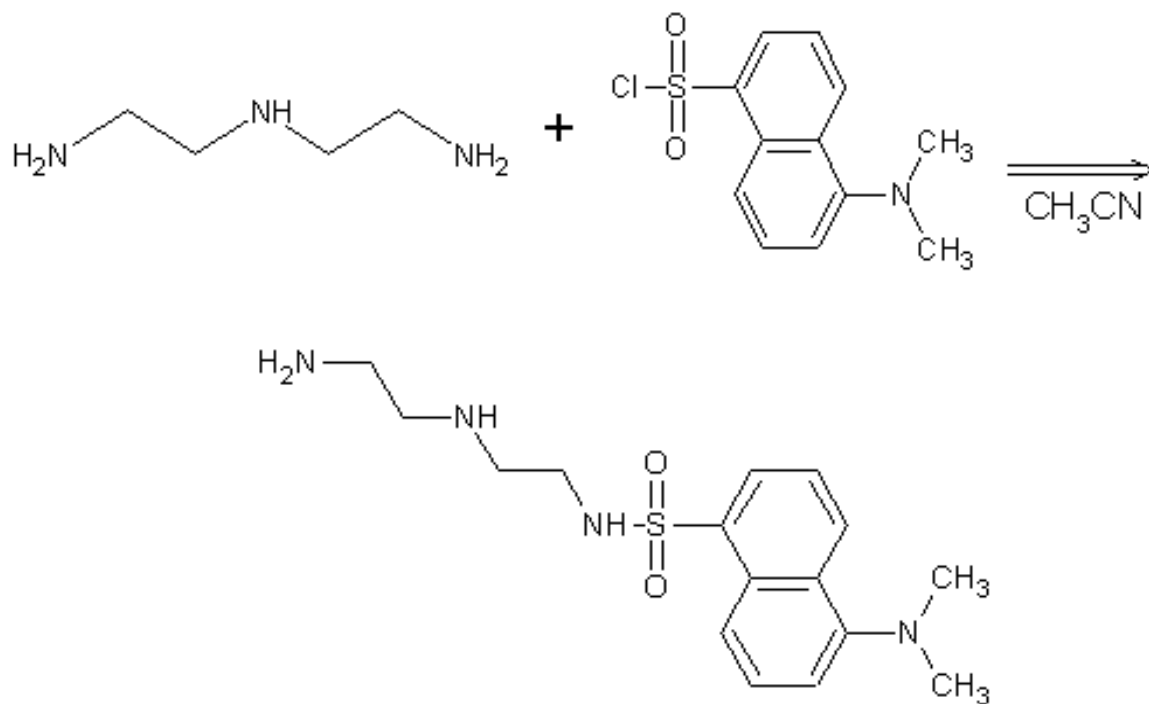
Figure 2.9 The synthesis procedure yielding the copper recognition component of the copper sensor, referred to as DDETA
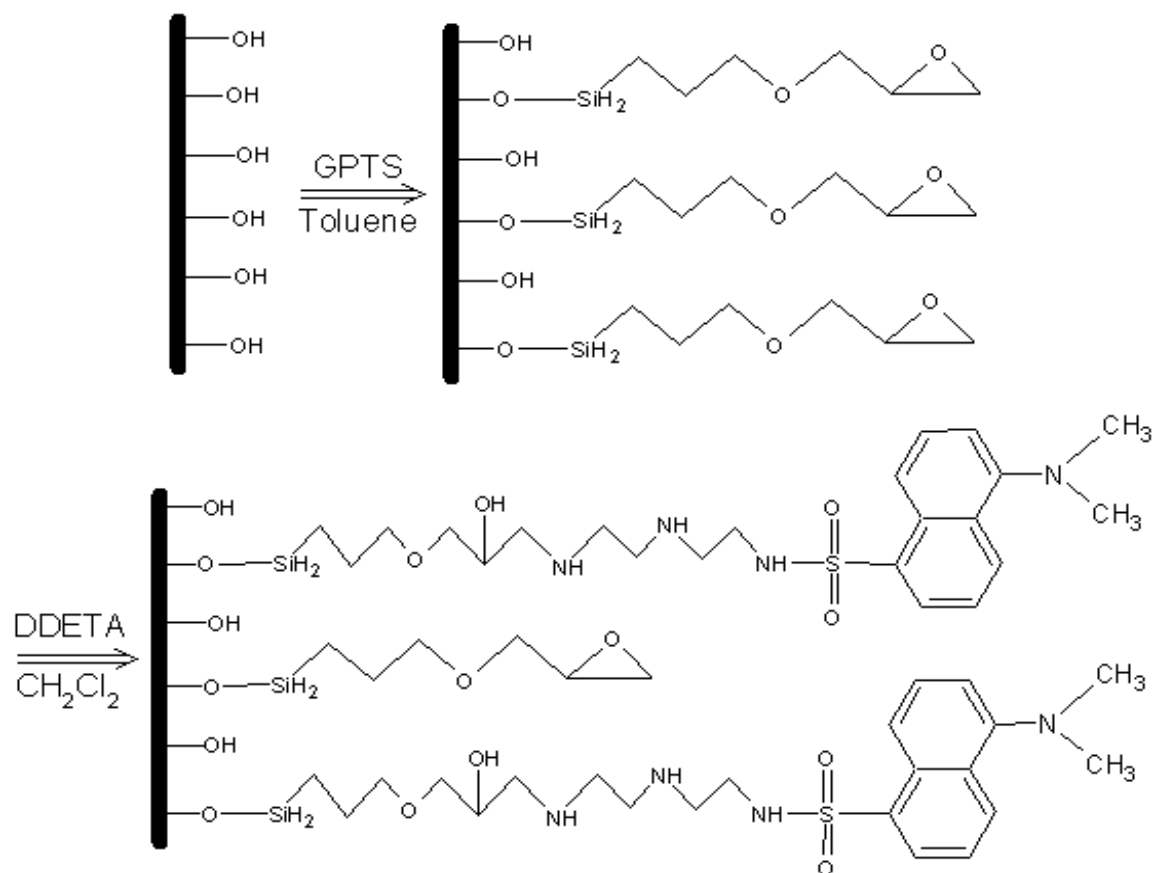
Figure 2.10 The synthesis procedure for covalently attaching the copper sensor to the optical fiber surface.
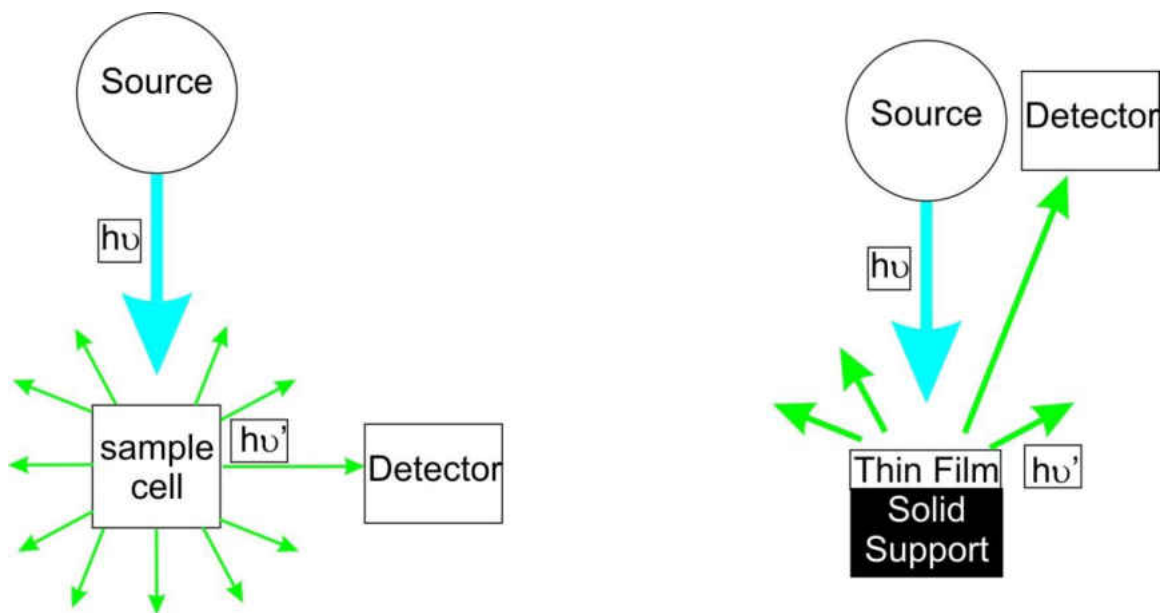
Figure 2.11 A comparison between right-angle (traditional) fluorimetry and front-face fluorimetry. As seen in the figure on the left, when the excitation radiation in blue is directed at a liquid sample, the fluorescence, in green, from the solution is generated in all directions. This allows for a detector to be placed at a 90° angle with reference to the source. For thin film studies, most of the samples are located on some type of solid support. This support blocks much of the fluorescence and the surface area of the thin film facing in the direction of a right angle detector is much smaller than a traditional sample cuvette, limiting the fluorescence intensity that will be measured by the detector. Therefore, a detector placed at a 22° angle with respect to the source will more efficiently collect the fluorescence signal generated by a thin film.

References

1. Rigo, M. V. Plasmonic Optical Fiber Sensor for Oxygen Measurement. Ph.D. Thesis, University of Wisconsin-Milwaukee, Milwaukee, WI, 2009

2. Henning, P. E. Application of Advanced Time-Resolved Fluorescence Detection Techniques for Remote pH Sensing with Optical Fibers. Ph.D. Thesis, University of Wisconsin-Milwaukee, Milwaukee, WI, 2009

3. *Guide to Connecterization and Polishing Optical Fibers*; ThorLabs, Inc. 2012

4. Kurner, J. M., I. Klimant, Krause, C., Preu, H., Kunz, W., Wolfbeis, O. Inert Phosphorescent Nanospheres as Markers for Optical Assays. *Bioconjugate Chem.* **2001,** *12*, 883-889.

5. Ding, L. Sensing Performance Enhancement via Chelating Effect: A Novel Fluorescent Film Chemosensor for Copper Ions. *J. Photochem. Photobiol., A.* **2007**, 1*86*, 143

6. Corradini, R., Dossena, A., Galaverna, G., Marchelli, R., Panagia, A., Sartor, G. Fluorescent Chemosensor for Organic Guests and Copper (II) Ion Based on Dansyldiethylenetriamine-Modified Cyclodextrin. *J. Org. Chem.* **1997**, *62,* 6283

7. Thomsen, V., Schatzlein D., Mercuso, D. Limit of Detection in Spectroscopy. *Spectroscopy* **2003**, *18,* 11

Chapter 3

Zinc Sensor Development and Characterization

3.1 Introductory Remarks

The work described in this chapter will focus on the development of a zinc sensor. This work will be centered on four milestones. The first portion of the research is focused on characterizing the zinc-specific fluorophore in solution. Secondly, the behavior of the fluorophore within a polymer matrix was investigated. Thirdly, incorporation of the fluorophore within the crossed-fiber sensor platform and subsequent performance characteristics were determined. Lastly, after incorporating a second crossed-fiber sensor to serve as a reference, validation of the sensor array was confirmed by successful sample analysis.

3.2 Basic properties of the zinc-specific fluorophore

The sensor chosen for the measurement of zinc concentrations is a commercially available dye called FluoZin-1 (FZ-1). There are two different forms of FZ-1. The first is the water soluble tri-potassium salt version shown in Figure 3.1a. The other is a water-insoluble version, in which each of the potassium ions from the previous molecule is replaced by an ester functionality (Figure 3.1b). This modification allows for FZ-1 to become cell permeable.[1] For all experiments described here the tri-potassium salt was used.

The dye FZ-1 has been shown to exhibit preferential recognition of zinc and, up to this point, has been employed mainly to measure zinc in biochemical or biological settings.[2,3] FZ-1 is naturally fluorescent, stemming from a structure analogous to 2',7'-difluorofluorescein, which is a substructure of FZ-1. Zinc is recognized by FZ-1 as a +2 cation. This is due to the coordination between the two negatively charged carboxylic

acid segments with Zn^{2+}. Upon binding of zinc, the overall fluorescence of the sensor will increase due to the inhibition of the photo-induced electron transfer (PET) mechanism occurring within the molecule.[1,4] The lone pair located on the nitrogen atom acts as a stabilizing agent for the xanthene ring upon excitation. The process provides a non-radiative pathway by which the energy absorbed from the excitation radiation can be dispersed.[5] However, upon binding of zinc, the lone pair of electrons located on the nitrogen cannot be transferred due to their interaction with Zn^{+2}. This leads to more of the excess energy being released as fluorescence, which will cause an increase in the fluorescence intensity observed for FZ-1.

3.3 FluoZin-1 characterization in solution

The overall goal of this work is to develop an optical-fiber sensor for zinc. Before testing within the optical-fiber platform, verification that FlouZin-1 is a viable fluorescent sensor candidate was required. These initial validation trials were conducted in solution instead of within the optical fiber array. Invitrogen, the manufacturer of FZ-1, states that the excitation wavelength is centered about λ_{ex} = 495 nm, whereas the emission is centered about λ_{em}=515 nm.[6] It has also been demonstrated that the fluorescence of 2',7'-difluorofluorescein, a molecule similar to FluoZin-1, is strongly pH dependent, due to the protonation or deprotonation of the hydroxyl group located on the xanthene ring.[7] The pKa value of the hydroxyl group was previously calculated to be 4.68 by absorption spectroscopy.[7] To verify this, absorption and fluorescence spectra of FZ-1 were collected at different pH levels. In a solution of 5×10^{-7} M FZ-1, the pH was varied using a series of McIllvaine buffers ranging between pH units of 2-8. When visually inspecting the solutions, the usual orange color of the dye was found to fade for pH values below 4.

The absorption profile of the dye (Figure 3.2) corroborates this observation, as there is a change in the absorption profile when the pH level is below 4. While FZ-1 strongly absorbs when the pH is below the pKa, the fluorescence emission is significantly decreased (Fig. 3.3), for previously described reasons. It should also be noted that the carboxylic acids groups at the binding site of FZ-1 will experience protonation around pH 4.5. This protonation will result in competitive binding between H^+ and Zn^{+2} ions, reducing the sensor efficiency. Based on these results, to prevent interference of the binding sites, the pH will be buffered to 5.5. Initial buffering of the solutions was done using a McIllvaine buffer. However, zinc forms an insoluble compound with phosphate,[8] eliminating the ability for FZ-1 to bind with Zn in solution. To avoid this, a buffer containing 0.2 M sodium acetate and 0.2 M acetic acid producing a pH at 5.5 was utilized. Lastly, a set of absorbance profiles at constant pH with increasing amounts of FZ-1 were collected. Using Beer's Law and the measured absorbance value at 495 nm, the molar absorptivity (ε) of the compound was calculated, yielding a value of 66,800 ($\pm$ 1300) $cm^{-1}M^{-1}$, a previously unpublished value. In comparison, 2',7'-difluorofluorescein, the compound mentioned earlier, has a molar absorptivity of 86,400 ($\pm$800) $cm^{-1}M^{-1}$.[7]

The vendor states that FluoZin-1 is able to measure zinc levels between 0.5-50 μM.[1] However, because EPA regulatory limits are listed as mg/L, measurements for all analytes will be listed as mg/L or ppm in this body of work. Therefore, the previous Zn concentration range converts to 0.04 - 3.27 mg/L. This is an ideal range as the EPA states that an average of 1.48 mg/L of Zn may be discharged per day from municipal water treatment systems into the environment over a 30 day period.[9] The FZ-1 fluorescence signals for varying concentrations of zinc (shown in Figure 3.4) support the

claim made by Invitrogen. Low-concentration measurements will be discussed in detail later in the chapter.

While the manufacturer has tested FZ-1 against most divalent cations[6], the interferences were kept at constant molar concentrations.   In accordance with the statements regarding all concentrations being in mg/L, the interference panel was retested.   By changing the units from molarity to mg/L, the interferents will have different concentrations than what was already stated in literature. Most notably, both lead and cadmium will decrease in concentration, reducing the effect these metals will have on zinc analysis. This is important because cadmium has been recognized as a principal interfering species due to the fact that cadmium shares many chemical properties with zinc, allowing cadmium to be recognized by FZ-1.[10] As shown in Figure 3.5 nickel has now become the principal interfering species at identical concentration levels. To ensure that FZ-1 is still capable of measuring zinc in the presence of the top three interfering species (Cd, Ni, and Pb), identical calibration curves of zinc were measured in the presence of increasing levels of each interferent. (Figures 3.6 − 3.8) After the data was collected, it was noted that the sensitivity (i.e., the slope of each calibration curve) for every calibration curve decreased slightly as the concentration of the interferent was increased. In Figure 3.9, the decrease in the sensitivity was expressed as a percentage. The percent change was determined by first measuring the slope of a zinc calibration curve when no interfering species were present and using this slope as the initial value. As the interfering metal concentration was increased and the calibration curve repeated for each concentration increase a new slope was obtained. The slope from each of these lines was compared against the original slope (with no interferences

present) and the percent change was calculated. The baseline value for the slope was calculated for each interfering species present as the sampling was done over multiple days. It is also noted that the baseline for each calibration curve shifted upwards as the interferent was increased. The baseline value, represented by the y-intercept value of each calibration curve, is the fluorescence of FluoZin-1 with no zinc present; however, interfering metals were present in some solutions. In an identical manner as stated for the change in sensitivity, the percent change in the baseline as the concentration of the interfering species was increased was plotted. In Figure 3.10 the baseline fluorescence of FZ-1 increases as the amount of the interfering metal species increases. This is expected as these metals have already been shown to cause an increase in the fluorescence of FZ-1.

Lastly, the effect of reducing and oxidizing environments was examined. Three types of solutions were created for this study. For all three types, a pair of analyses was done. The first test investigated how the fluorescence of FZ-1 alone in solution changed based on to what type of environment the dye was exposed. The second examined whether or not the different environments affected the interaction between FZ-1 and Zn, at a concentration of 1 mg/L. The first pair of solutions used only the pH-5.5 acetate buffer, which was present to eliminate changes in pH from affecting the fluorescence, and served as the baseline for comparison. The second pair of solutions also used the acetate buffer but included an oxidizing agent, in this case a 0.2 M $NaNO_3$ solution. The third set of solutions contained 0.2 M $NaSO_3$, a reducing agent, along with the acetate buffer. As seen in Figure 3.11 there is a significant reduction in the amount of fluorescence when exposed to reducing environment. This is to be expected as the hydroxyl group would undergo protonation during this reduction process, once again

preventing the fluorescence from occurring. It should also be noted that the sensor was unable to detect zinc in a reducing environment due to the fact that Zn was reduced from the +2 state to its neutral state. The decrease in the change of the fluorescence between the clean solution and the zinc solution while exposed to the oxidizing solution may be attributed to the oxidation of the carboxylic receptor sites. Under oxidizing environments, some of the –COOH groups will be converted to esters, eliminating the sensing ability of FZ-1.

3.4 Polymer basic properties and FZ-1 integration

The development of a functional optical-fiber sensor requires that the sensor be held at a constant distance with respect to the optical fibers. Ideally, a sensor capable of covalent attachment directly to the optical fiber would be desired. However, there is no cost-effective manner by which covalent attachment is possible, because potential schemes for covalent attachment were predicted to only be 30-40% effective and would require several grams to achieve a sufficient number of attached dyes. With 0.5 milligrams of FZ-1 costing \$200, the cost to synthesize one sensor could quickly become prohibitive. Therefore some other means of dye inclusion within the fiber sensor platform is required. Earlier work within the Geissinger research group has determined that an efficient polymer for this application is a PEG-DA based polymer, which is classified as a hydrogel due to its hydrophilic nature.[11] The polymer, in a liquid state, consists of three components: a principal polymer, a photo initiator, and an additional cross-linker. The principal polymer for all sensors used in this work is polyethylene glycol diacrylate (MW≈575). For each polymer mixture that was created, 60% (v/v) of the hydrogel was PEG-DA.

The photo initiator serves as a curing agent, causing the polymer to solidify. 2,2-dimethoxy-2-phenylacetophenone (DMPA) was added to the polymer mixture at a ratio of 10 mg DMPA per 1 mL of polymer mixture. To induce dissolution and ensure thorough mixing of the polymer, the solution was vortexed for 1-2 min, stored in the dark for 24 hours, then vortexed for 30 seconds immediately before use. After mixing, curing of the polymer was induced by exposing the solution to 365-nm light. Upon exposure, the UV light caused the DMPA to dissociate into methyl and benzaldehyde radicals. These radicals react with the terminal acrylate bonds of PEG-DA causing polymerization of the PEG-DA molecules.[12]

3.5 FZ-1 integration within the polymer matrix

While PEG-DA has the capacity to act as a cross-linking polymer, an additional cross-linking agent, trimethylolpropane triacrylate (TPT), was employed to provide additional structural support. The amount of TPT contained with each polymer varied between 0-25% (v/v) but for most sensors a 5% (v/v) amount was used. Varying the amount of TPT constituted a trade off in polymer capabilities. Increasing the amount of TPT would create stronger, more rigid polymers while reducing the amount of dye leaching. However, higher levels of TPT would also increase the refractive index of the polymer and would increase the amount of light scattered by the polymer. While not a concern for the film study, this is an issue that must be addressed during the optical fiber sensor development. Leaching of FZ-1 from the polymer mixture was observed for every sensor. Observations with early versions of the FZ-1 sensor had shown an apparent relationship between the amount of TPT and the rate of dye leaching. It was informally observed that higher levels of TPT slowed the rate of dye leaching. Formal analysis of

this behavior was accomplished by creating hydrogel films with varying amounts of TPT (5%, 20%, and 25%). Each of these films contained 10% FZ-1 dissolved in 18-MΩ•cm water. The films were formed by adding the liquid polymer to a demountable cuvette well, followed by UV curing. After curing, the polymer would be peeled from the cuvette. To one inner face of a polymethylmethacrylate (PMMA) cuvette, an optically transparent adhesive was applied. The film was placed on the top of the adhesive making sure the film was flat against the adhesive. The adhesive was UV cured, locking the film against the cuvette wall, and the cuvette was filled with the pH-5.5 sodium acetate/acetic acid buffer. The first test consisted of five films containing 20% TPT and five films containing 5% TPT. Front-face fluorescence measurements were performed for each of the films immediately after creation to determine the initial fluorescence intensity. Before every measurement, the buffer was replaced with a fresh buffer solution. This was done to remove any dye, which had leached from the polymer into solution. Fluorescence spectra were then measured every day for 30 days. During the entire course of all film studies, two 5-μM solutions of Rh-110 were used to correct for day-to-day excitation source fluctuations. After 30 days, it was apparent that dye leaching had ceased. While the films were still fluorescent after 30 days, the fluorescence was significantly weaker. This low level of fluorescence after 10 days indicates that as a zinc sensor, the period over which a sensor can be used will most likely be approximately 10 days. Examination of the data revealed that the rate of dye leaching was slower for the 20% TPT polymer, although equilibrium occurred for both polymers around 10 days. (Figure 3.12) The readings were then continued at 2-3 day intervals to also investigate the lifetime of the polymer. One polymer film from each TPT batch detached from the

adhesive early on in the experiment and was discarded, leaving four trials for each TPT level. At the 96-day mark, all polymer films were found to have no appreciable fluorescence signal, indicating a polymer lifetime of approximately three months. Based on the above findings, it is apparent that the practical lifetime of a zinc sensor in solution will be approximately 10 days, which is limited by the rate of dye leaching, and not the stability of the hydrogel, which required approximately three months before decomposing in solution. The four films used for each part of the study illustrated another feature about the dye/polymer relationship. While all the dye-containing polymer solutions were taken from the same batch, which had been well mixed, the fluorescence intensity varied between individual films, having an average relative standard deviation of 30% between same day data points. This indicates that daily calibration will be required for each sensor constructed in order to account for this variation.

A second experiment was undertaken to determine if FZ-1 experiences a different rate of dye leaching or increased level of photodecomposition when exposed to solutions containing zinc. It was theorized that the presence of zinc may put greater strain on the molecule, inducing photodecomposition not seen previously, or that zinc ions may assist in removing or retaining the dye within the polymer into solution. One polymer solution, this time containing 25% TPT, was used to create ten films in a method identical to the previous experiment. For five of the films, the same pH-5.5 buffer contained 0 mg/L of zinc. For the other five, the buffer contained 1 mg/L of zinc. These solutions were also changed immediately before collecting every day's front-face fluorescence data. This experiment was only conducted for 30 days, as it had become apparent that dye leaching had stopped. In order to compare the two types of films, the fluorescent intensities of

both sensors for the first day were normalized to one. The subsequent fluorescent readings for both films were then normalized against the respective first day value. Figure 3.13 provides more support to the claim that increasing the amount of TPT will slow the rate of dye leaching. However, leaching was still observed and after about 16 days, the fluorescence of the films had dropped to a low level, a similar behavior as observed for the 5% and 20% films. It should also be noted that it took about three days for the zinc in solution to fully penetrate the polymer and interact with the sensor. This is why the fluorescence intensity of the films exposed to the zinc solutions increased over the first few days, providing values greater than one. The length of time required for Zn to fully interact with the polymer-entrapped dye is a concern for future sensor development and will be discussed further in a later section. While fluorescence intensities were higher for the solutions containing zinc, the trend was identical for both sets. On approximately days 16 through 17, the fluorescence for both sets of films had stabilized, supporting the idea that dye leaching will be the limiting factor for crossed-fiber sensor lifetime. This claim is supported by the behavior of the hydrogel film over the 30 day period. Visual inspection of the hydrogel at the end of this study (30 days) showed no signs of degradation (i.e. curling away from the cuvette wall, holes in the film, pitting, etc.) indicating that the structural integrity of the polymer was maintained. The previously mentioned data leads to the conclusion that the presence of zinc does not affect the rate of either dye leaching or photodecomposition of FZ-1 while in PEG-DA.

3.6 Optical fiber sensor creation

Crossed-fiber sensors have already been created for monitoring both pH and dissolved oxygen.[11,12] The work performed here follows many of the procedures

established for creating the optical-fiber sensors. The polymer used the same components as were employed for the film studies. While the overall goal of this body of work is to develop a multi-sensor array, initial characterization was done by creating single sensor regions to test figures of merit for the sensor. Development of the zinc sensor can be divided into four steps. First, the response time and reversibility of the sensor was investigated, followed by determining parameters such as limit of detection (LOD), limit of quantitation (LOQ), and linear dynamic range (LDR). Third, an optical fiber-based intensity reference was developed, and fourth, a simulated sample analysis was carried out.

The limit of detection (LOD), according to the IUPAC definition, is the lowest concentration that can be measured assuring that the signal recorded is greater than the background noise of the instrument.[13] As stated in Chapter 2, the level measured needs to be three times greater than the standard deviation of 10 blank measurements.[14] The limit of quantitation (LOQ) follows a similar definition for the limit of detection. It is generally accepted that a signal which is ten times the standard deviation stronger than the blank will give a reliable LOQ. The linear dynamic range (LDR) dictates the range over which the relationship between concentration and signal strength is directly proportional. The lower limit of the LDR is traditionally defined as the LOQ. The upper limit is traditionally defined as when the linear relationship deviates by more than 5% from a linear relationship.[15]

Initial sensor design utilized a polymer recipe identical to the polymer matrix used for the film study. The exact ratio for sensor testing initially was 60 % (v/v) PEG-DA, 25 % (v/v) TPT, 1% (w/v) DMPA, 10% (v/v) FZ-1, and 5 % (v/v) ultrapure H_2O. This

resulted in a final concentration of FZ-1 being 4.17×10^{-5} M. The concentration of the dye was much higher than used for studies in solution, but this was done as a way to account for dye leaching. The first tests investigated the response time of the sensor. Signal stabilization required at least 90 minutes when using a sensor with the above-mentioned polymer matrix. This response time was considered too long for this application as other conventional methods, such as atomic absorption spectroscopy, are capable of performing sample analyses on the order of one to two minutes. Data collected during the earlier film study demonstrated that the PEG-DA films doped with FZ-1 required three days for equilibration. Clearly, the 90-minute equilibration time observed for the crossed-fiber sensor was much faster. This difference is attributed to the difference in the volume of the FZ-1-doped PEG-DA polymer used in the two methods. For the film study, approximately 100 μL were used to make a film while the crossed-fiber design used only 2-3 μL. The smaller size would result in fewer FZ-1 molecules contained in the polymer, reducing the time required for all of the FZ-1 to form complexes with zinc.

To reduce the response times further, a modification of the polymer matrix was required. For this, a technique referred to as micro-templating was employed.[16-18] This procedure allows for the creation of a micro- and nanoscale channel network within the polymer matrix. The microspheres, in solid form, are added to the polymer in its liquid precursor form. The polymer is cured, converting the liquid into a solid. The microspheres are trapped within the polymer. Subsequently, a dissolving agent is used to remove the microspheres. Once the microspheres are dissolved, holes remain within the polymer where the microspheres used to be. (Figure 3.14) By having a sufficient

concentration of microspheres the holes become connected, creating a porous network. The concentration of microspheres is important for the dissolution process as well. Enough microspheres must exist within the polymer so that the microspheres are in contact with each other. The contact points between spheres will allow the dissolving solution to permeate through the polymer and effectively dissolve all of the microspheres. The results of this procedure were confirmed with SEM imaging in earlier research within the Geissinger group.[19] This network allows for the rapid transit of the analyte to the sensor molecules, greatly reducing the response times of the sensor. However, the size of the microspheres and the concentration of the microspheres needed to be limited. Having microspheres too large in diameter can either change the refractive index of the polymer, due to an increase in the amount of water present within the polymer, or it can cause the polymer to become structurally unstable. Having a high concentration of microspheres will cause the same issues, hence both parameters must be controlled.

When applied to the crossed-fiber sensor, solid polymer microspheres with a diameter of 7 – 10 μm were added to the polymer mixture. These spheres were added to the polymer matrix at a ratio of 10% (w/v). Microspheres of two different materials were used. Initially, microspheres consisting of polystyrene were used. After the polymer mixture containing FZ-1 was cured onto the crossed fiber setup, the entire fiber sensor was immersed in toluene for three days. A switch to microspheres made of polymethylmethyacrylate (PMMA) was made about halfway through the sensor development for two reasons. First, the new material was dissolvable with acetone, a less toxic chemical. Secondly, the amount of time required to dissolve the same concentration of microspheres was reduced from 3 days down to 1 day.

After the micro-templating procedure was completed, the sensor was exposed to solutions containing zinc concentrations of 0 mg/L or 0.66 mg/L. The first test determined how quickly the sensor would equilibrate after exposure to a 0.66 mg/L zinc solution. Figure 3.15 demonstrates that the sensor deployed on the crossed-fiber-sensor platform equilibrates after a change in zinc concentration in less than 1 minute. Secondly, the reversibility of the sensor was examined. FluoZin-1 is marketed as a binding dye, irreversibly binding zinc in solution. However, these applications are designed for solution monitoring where the dye is not recovered. Having the sensor encapsulated within the polymer changes this property. The sensor was exposed to a 0.66 mg/L solution, allowed to reach equilibrium and then transferred to an ultrapure (18 Mohm•cm) water bath. The lack of ions in the ultrapure water served to pull the zinc from the FZ-1 binding sites in order to re-establish equilibrium with the water bath. Initially, water treated by reverse osmosis was used for the washing process, but it was found that the ultrapure water more efficiently removed the zinc from the sensor region. As seen in Figure 3.16 the sensor shows rapid and repeatable changes in signal intensity when exposed alternatively to zinc solutions and ultrapure water. This is an essential parameter for designing sensors capable of remote deployment.

Four separate sensors were created with identical concentrations of FZ-1. Ten data points from a solution with no zinc were collected for each sensor, which was followed by measurement of a calibration curve. After calculating the standard deviation, the values were analyzed with a linear regression equation obtained from the calibration curve. Table 3.1 lists the LOD and LOQ determined for each sensor and the average value for each. As seen in the table the average LOD was 0.010 (±0.006) mg/L while the

average LOQ was 0.040 (±0.008) mg/L. These values are well below the maximum limit established by the EPA, allowing a user the ability to effectively monitor systems even at low levels, not just at levels of regulatory concern.

Previous work investigating FluoZin-1 has demonstrated that at low levels of zinc (≤ 0.05 mg/L) the sensor exhibits a non-linear behavior.[20] This was confirmed in our experiments, as shown in Figure 3.17. It was also theorized that the linear dynamic range could be modified by changing the amount of FZ-1 in the polymer. A higher concentration of FZ-1 results in a larger number of sensor molecules being available for binding of zinc.   Consequently, there is a higher probability for zinc binding, which in turn implies that measureable signal changes can occur for lower zinc concentrations. As seen in Figure 3.18 there is a strong relationship between the FZ-1 concentration and the response to changes in zinc concentration. This is useful as it provides a versatile platform capable of being deployed in many different environments. An initial concentration of FZ-1 of 4.17×10^{-5} M was chosen as this provided a range which encompassed the EPA regulatory value for the maximum average concentration of zinc discharged over a 30-day period,1.48 mg/L.

As a continuation of interference testing, the sensor was exposed to solutions simultaneously containing 0.25 mg/L Zn and 0.25 mg/L of a competing species to see if the sensor would still be resistant to chemical interferences. Figure 3.19 shows that small amounts of signal change were observed in the presence of interfering species. This contradicts the data obtained from Figures 3.6-8, where the presence of interfering species caused an increase of fluorescence. The three species identified as the principal interfering components (Ni, Cd, Pb) generated little to no difference in the fluorescence

intensity of the sensor when compared to the solution that contained only zinc. There are two possible reasons for this deviation from the behavior in solution. First, the available FZ-1 molecules may have been saturated with zinc, so no fluorophores would be available for other metal species. However, the concentration level chosen (0.25 mg/L) was specifically selected to avoid such an issue. The second possibility is that the PEG-DA polymer impedes the transport of the interferent species and prevents it from reaching the fluorophore. An exact mechanism is not known but the difference in size of the ions may play a role in the diffusions of the ion within the polymer. While the micro-templating procedure allows for rapid diffusion of the analyte, the fluorophore is still entrapped within the polymer matrix. Any fluorophore existing in one of the micro-channels would quickly diffuse into solution.

While this data is promising, further investigation is required before these interfering metal species can be conclusively eliminated as a source of error during zinc analysis. All of these solutions to this point were analyzed as static solutions. For remote deployment, a sensor may be exposed to moving solutions. These moving solutions may contain levels of zinc or an interfering species which are not constant throughout the measurement process. There is still a possibility that a spike in the concentration of one of the interfering metals in solution will cause a change in the fluorescence intensity of FZ-1 which is not related to the concentration of zinc in solution.

3.7 Reference sensor development

It was observed that the pulsed excitation source suffered from shot-to-shot intensity fluctuations. This in turn will affect the sensor signals, causing a higher degree

of variance between data points. To correct for this, all of the work done to this point utilized a fast photodiode detector as a means of correcting for fluctuations in intensity. The method of correction is as follows. When an excitation pulse is generated by the laser, the fast photodiode records the intensity of the pulse and this data is collected by the oscilloscope. To reiterate, in the experimental design described in Chapter 2, the fast photo diode is located next to the pulsed laser and measures the intensity of reflected radiation as the pulse from the laser is coupled into the optical fiber. In an identical manner, the intensity of the fluorescence generated by FZ-1 is collected by a PMT. Both of these signals are transmitted to the oscilloscope. 200 of these individual signals, also referred to as traces, from both sources were averaged. As stated in Chapter 2, these averaged traces were then integrated. These integrated values describe the average energy of the pulses recorded by the respective detectors, PMT or fast photodiode. Because of this, the phrase "reference correction" indicates that there is a trace-to-trace correction process where the average of two hundred signal-pulse energies of the analyte-specific fluorophore is divided by the average energy of two hundred excitation traces, as recorded by the fast photodiode. While this was usually sufficient in laboratory settings, for remote monitoring an accurate reference close to the sensor site is required. An approach to resolve this issue involves developing a second crossed-fiber sensor connected in series with the zinc sensor. There are two characteristics required for the sensor materials of a reference. First, it must be rendered inert to all environmental or chemical influences. Second, the reference must also have spectral properties similar to the principal sensor with which it is paired (here FZ-1).

One method for preparing fluorophores resistant to environmental influences involves the use of polyacrylonitrile (PAN) as an encapsulating agent to fully protect the dye. This is accomplished by allowing the PAN to form an impermeable layer fully surrounding the dye, preventing species, such as dissolved oxygen, from changing the fluorescent emission properties of the dye. The reference material will then only undergo changes in fluorescence due to fluctuations with the intensity of the excitation pulse or potentially due to changes in temperature if in a non-controlled environment. Previously published work has developed a working procedure for dye encapsulation of the dye Rhodamine-110 (Rh-110).[21] Rhodamine-110 is a convenient choice as a reference sensor because the excitation and emission wavelengths of the zinc sensor will suffice for the reference sensor as well. The PAN-encapsulated Rh-110 was integrated into an optical fiber sensor in the same manner as the sensor containing FZ-1, with the polymer containing 10% of the Rh-110 suspension.

Upon integration of the reference sensor into the two-sensor array, the first step was to confirm that each sensor was recognized by the detector. Figure 3.20 shows a raw data output from the oscilloscope demonstrating that both sensors fluoresce at levels that are easily detectable. In Figure 3.20, the zero point on the x-axis is a relative measure, indicating the point when the laser fired. The fluorescence peaks shown on the x-axis are relative in time to the generation of the excitation pulse. The second step was to verify that utilizing a second sensor provided a reference that was either equal or better than the fast photodiode detector with regard to measuring pulse energy fluctuations. Over a five-day period, daily calibration curves were measured. Both methods utilized the same reference correction calculation as previously described. For the method utilizing Rh-

110, because both fluorescence signals were collected by the same PMT, 200 pulses were averaged. These averaged traces were analyzed individually using Origin 7.0, integrating only the areas of the traces where the peaks were detected, instead of the whole trace, as had been done previously. This change in procedure stemmed from the fact that the LabView program written for trace integration could not analyze independent regions of the same trace, only the trace as a whole. The data was plotted for comparison to see if either method proved to be more reliable over the long term. Using Rh-110 as a reference sensor provided a more reliable platform over a multi-day period as evidenced by Figures 3.21a and 3.21b, based on the fact that the linearity for each calibration curve was maintained. However, while the linearity for each calibration curve was maintained, the ratio of fluorescence intensities did vary from day to day. This is most likely due to the fact that both dyes (reference and analyte-specific) would undergo leaching from the PEG-DA polymer. However, they do not leach at the same rate and this explains why identical zinc concentrations for the calibration curves would have different values for different days.

Because the encapsulation process for Rh-110 was not always successful, a more reliable material was required. The commercially available material called Dragon Green was chosen as a replacement. Dragon Green does not refer to the dye used to generate the fluorescence. Rather it describes the entire system of both the fluorescent dye and the polymer used to encapsulate the dye. Neither of the individual components was provided by the company as these are considered proprietary technology. The dye is sold as resistant to interferences due to its proprietary manufacturing process.[22]

It should be noted that the fast photodiode detector, which was used initially to provide the pulse-energy reference, continued to be used in the experimental setup for providing the time at which the laser fired. That is the signal of the diode provided a time reference point for all measurements.

3.8 Sample analysis with independent verification

As the final step in the performance verification process of the zinc sensor, seven solutions containing unknown concentrations of zinc were created by Dr. Paul Henning, a research member of the Geissinger group. Each sample was divided into two portions. The first sample was analyzed using the sensor array while the second half of each sample was sent to SF Analytical, a laboratory certified by the Wisconsin Department of Natural Resources, which performed analysis using atomic absorption spectroscopy. The sensor array utilized the two-junction system with Dragon Green and FZ-1.

When the analysis by both methods was complete, a series of analyses were undertaken to prove the effectiveness of the two-sensor array. While performing the analysis using Dragon Green as the principal reference, the fast photodiode detector signals were also collected and utilized as a second, comparative reference. The ratio of the integrated signal from the sensor containing FZ-1 was referenced against both the integrated signal of the Dragon Green sensor and the integrated signal of the fast photodiode. Both values were compared against the expected value as provided by the preparer of the solutions. Figure 3.22 shows the precision and accuracy obtained when Dragon Green was used as the reference. As can be seen there is a significant

improvement versus results obtained using the fast photodiode, once again demonstrating why having a reference sensor is essential to the sensor platform.

The values of the solution concentration of zinc obtained using the FZ-1/Dragon Green sensor were compared to those obtained by atomic absorption. The data plotted in Figure 3.23 shows that the values were very similar. Statistical analysis using the student's t-test (α=0.05, N=4) determined that the zinc sensor gave statistically identical values for 5 out of the 8 samples when compared to the predicted values. Analysis also revealed that the zinc sensor gave statistically similar results for 5 out of 8 of the samples when compared to values obtained using atomic absorption by the outside laboratory. Table 3.2 summarizes all of these observations in tabular form. A final test, designed by Bland & Altman[23], was plotted to examine if persistent bias existed between the two methods. The test involves plotting the average value from the two different methods against the difference between the values from both methods. If bias is not present, the values will be evenly distributed around the zero error line. Once the data was plotted (Figure 3.24), it was determined that there was no significant bias between the two methods.

To summarize, an optical fiber-based sensor capable of monitoring zinc has been developed. This sensor, which is capable of rapidly and reversibly monitoring EPA relevant levels of zinc, when coupled with a reference sensor containing a chemically resistant compound, provides a new platform for the analysis of zinc in aqueous environments.
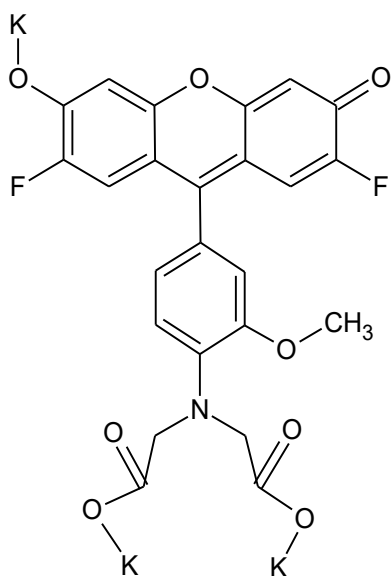
Figure 1a
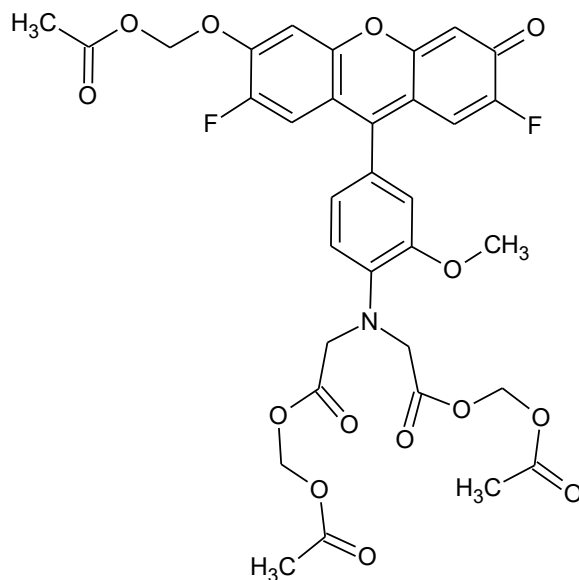
Figure 1b

Figure 3.1 Chemical structures for the tri-potassium (1a) and ester (1b) forms of FluoZin-1. The tri-potassium version is the water-soluble version and is the version of FZ-1 used for this study. By adding the ester groups, the dye becomes cell permeable. During introduction into the cell, cellular transport mechanisms will strip the ester groups, exposing the zinc recognitions units for analysis.
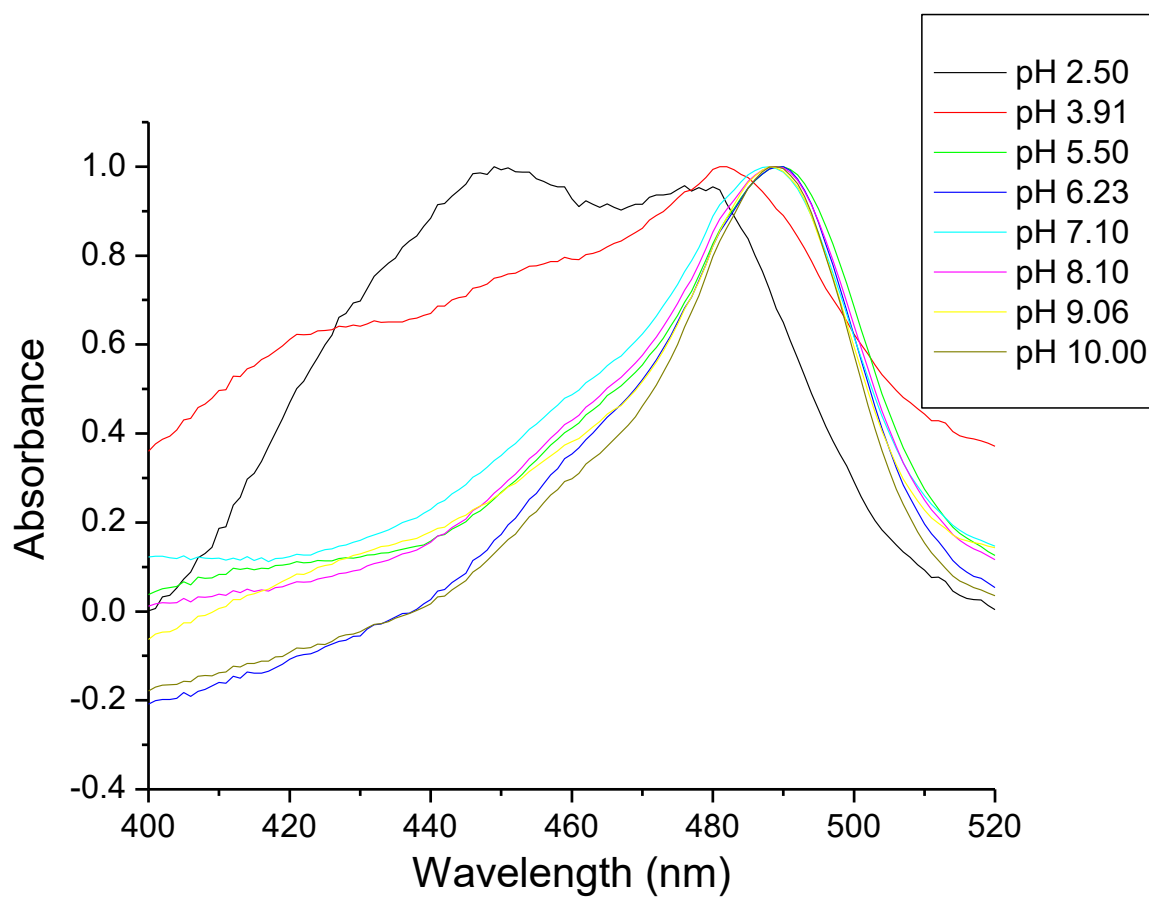
Figure 3.2 The normalized absorption profiles of FluoZin-1 shows the pH dependence of the absorption of the fluorophore. This change in absorbance is tied to the protonation or deprotonation of the hydroxyl group located on the xanthene ring of FZ-1 . Visually, solutions which were below pH 4.5 presented a light orange to clear color where solutions above pH 4.5 showed a strong orange coloration.
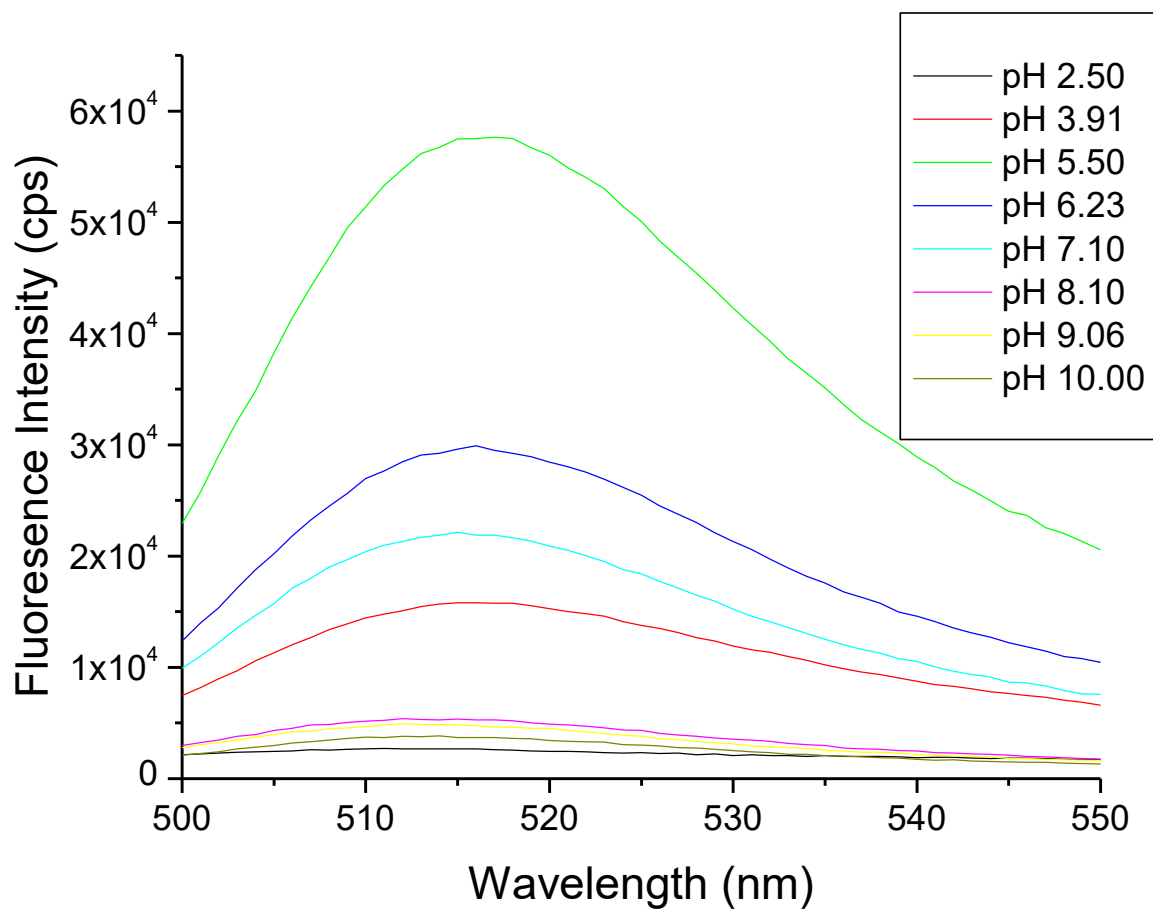
Figure 3.3 The fluorescence of FluoZin-1 is dependent on the pH of the solution. The maximum fluorescence intensity was obtained a pH of 5.5. Based on this observation, a pH 5.5 buffer consisting of 0.2 M sodium acetate and 0.2 M acetic acid was used for all subsequent measurements.
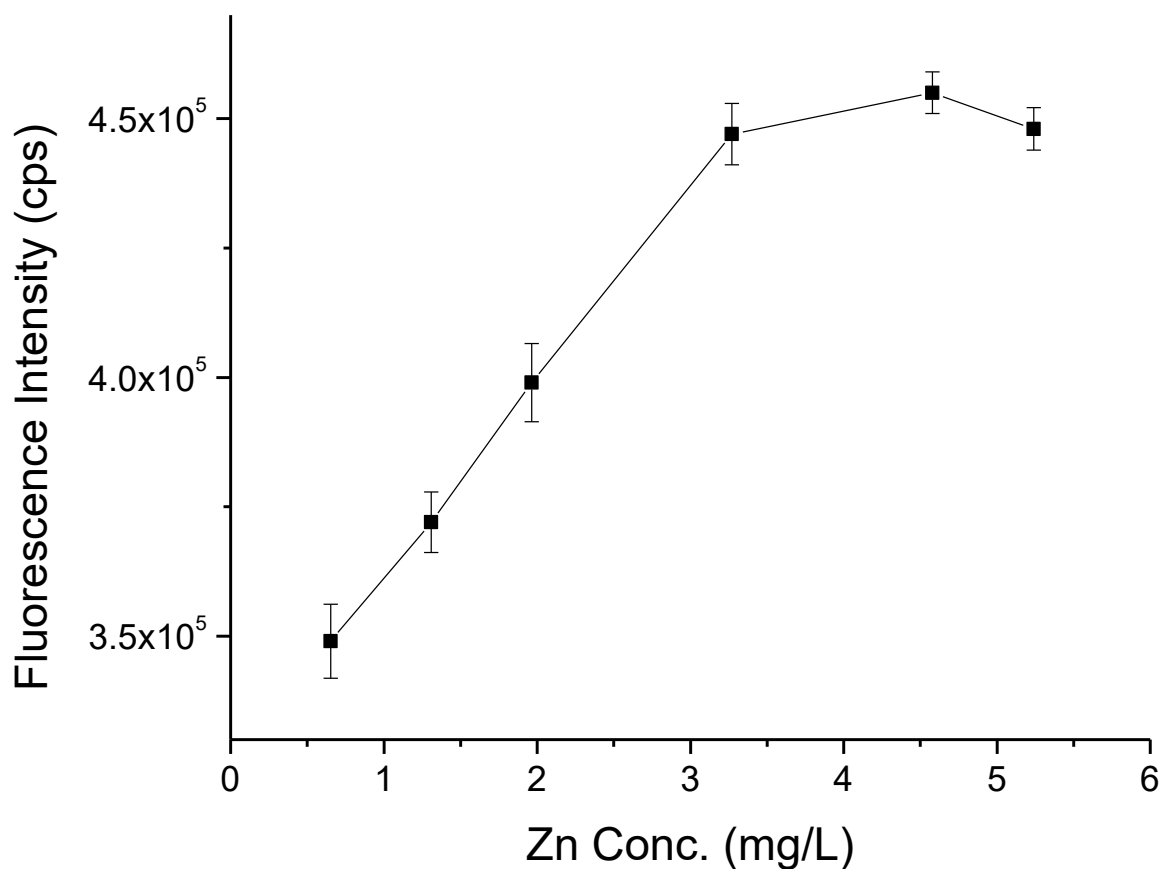
Figure 3.4 The linear dynamic range of FluoZin-1 in solution, confirming the range
  stated in manufacturer literature. The dye concentration in solution was
  held at 5.0×10^{-7} M in order to prevent dimerization of FZ-1. The
  manufacturer's literature had listed the range of measureable zinc
  concentrations in units of molarity. However, in keeping with EPA
  literature, all concentration units will be listed as mg/L or parts per million
  (ppm). For this and all future data plots, the abbreviation "cps" refers to
  counts   per   second,   a   measure   of   fluorescence   intensity.
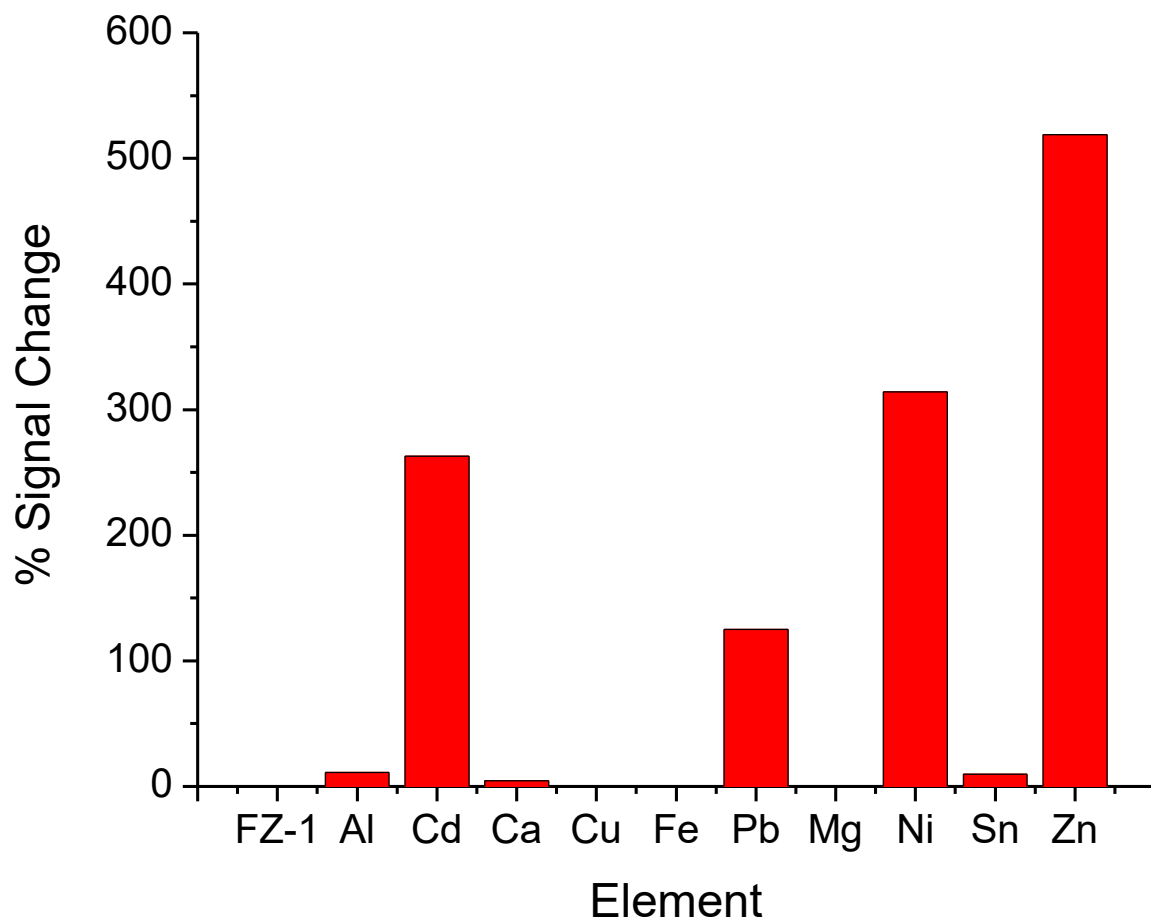
Figure 3.5 The percent change in fluorescent intensity of FluoZin-1 when exposed to individual elements in solution. Each element had a concentration of 5 mg/L in solution. The % signal change refers to the change in fluorescence intensity between a 5.0×10^{-7} M solution of FZ-1 in a clean (non-metal containing) solution and a solution containing the metal species listed.

Figure 3.6 Multiple calibration curves of zinc in the presence of increasing amounts of cadmium. Each data point shown is the integrated area of a fluorescence scan which was determined by averaging five individual fluorescence scans. The scans were averaged internally by the software provided with the fluorimeter and displayed as one scan. Error analysis was not provided by the software which performed the averaging operation. While each calibration curve was shifted upwards as the interfering species concentration was increased, the linearity of each calibration curve was maintained. Preserving the linear relationship of each curve allows for periodic calibration correct for the shift in intensity due to the presence of interfering species.
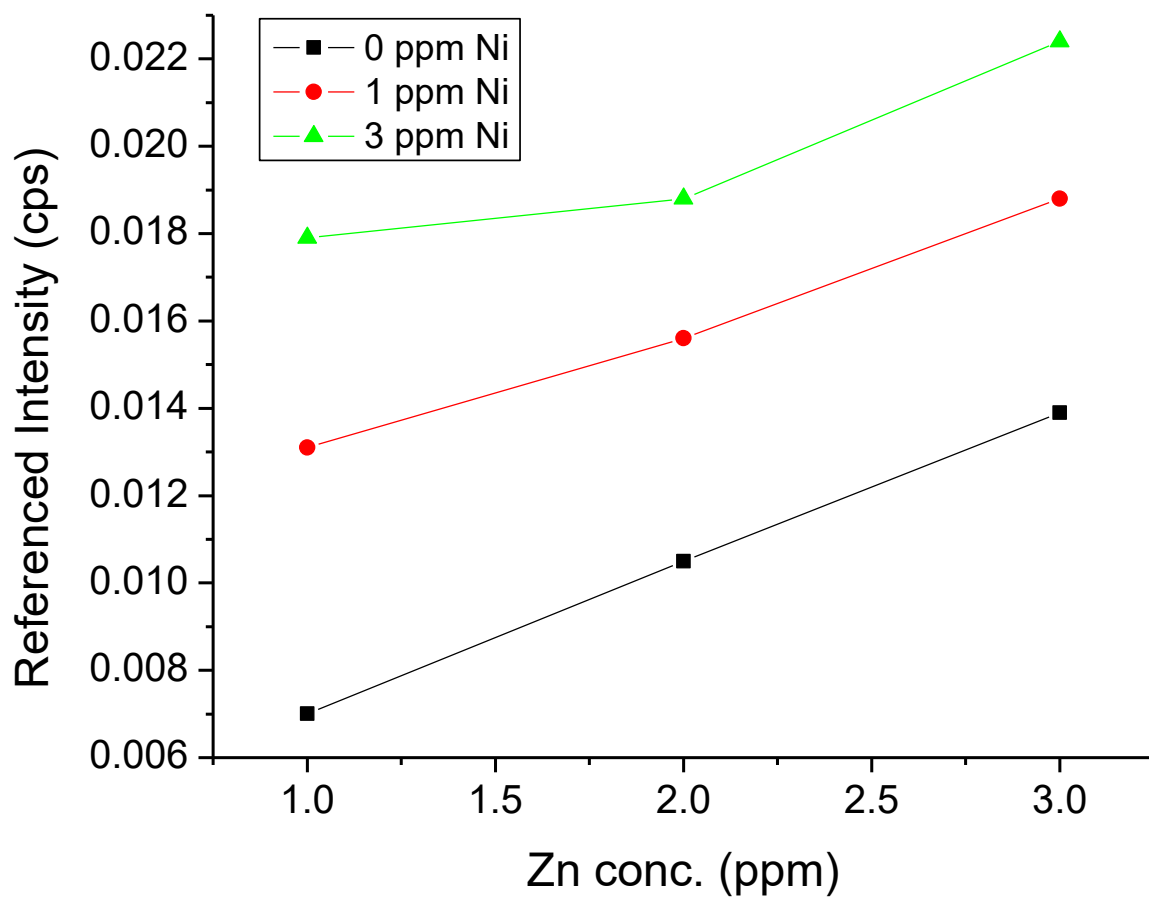
Figure 3.7 Multiple calibration curves of zinc in the presence of increasing amounts of nickel. Each data point shown is the integrated area of a fluorescence scan which was determined by averaging five individual fluorescence scans. The scans were averaged internally by the fluorimeter and displayed as one final scan. Error analysis was not provided by the software which performed the averaging operation.

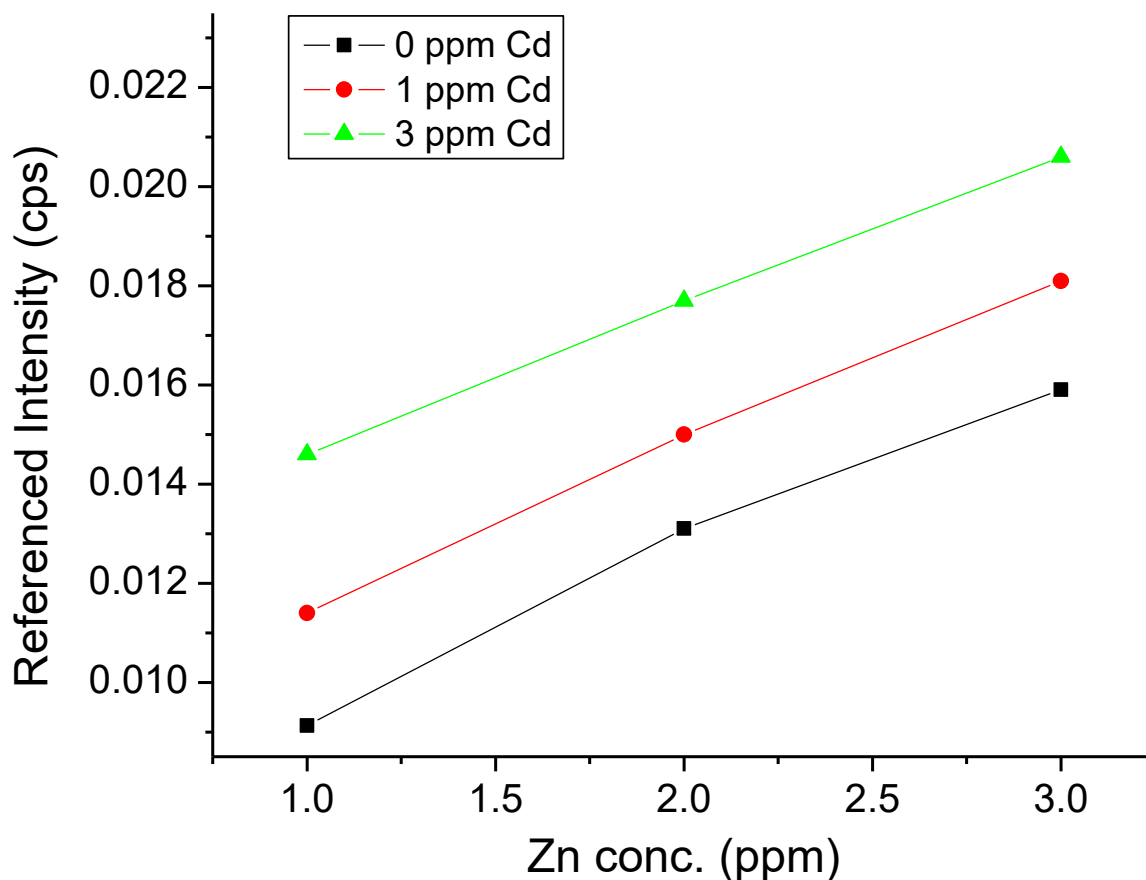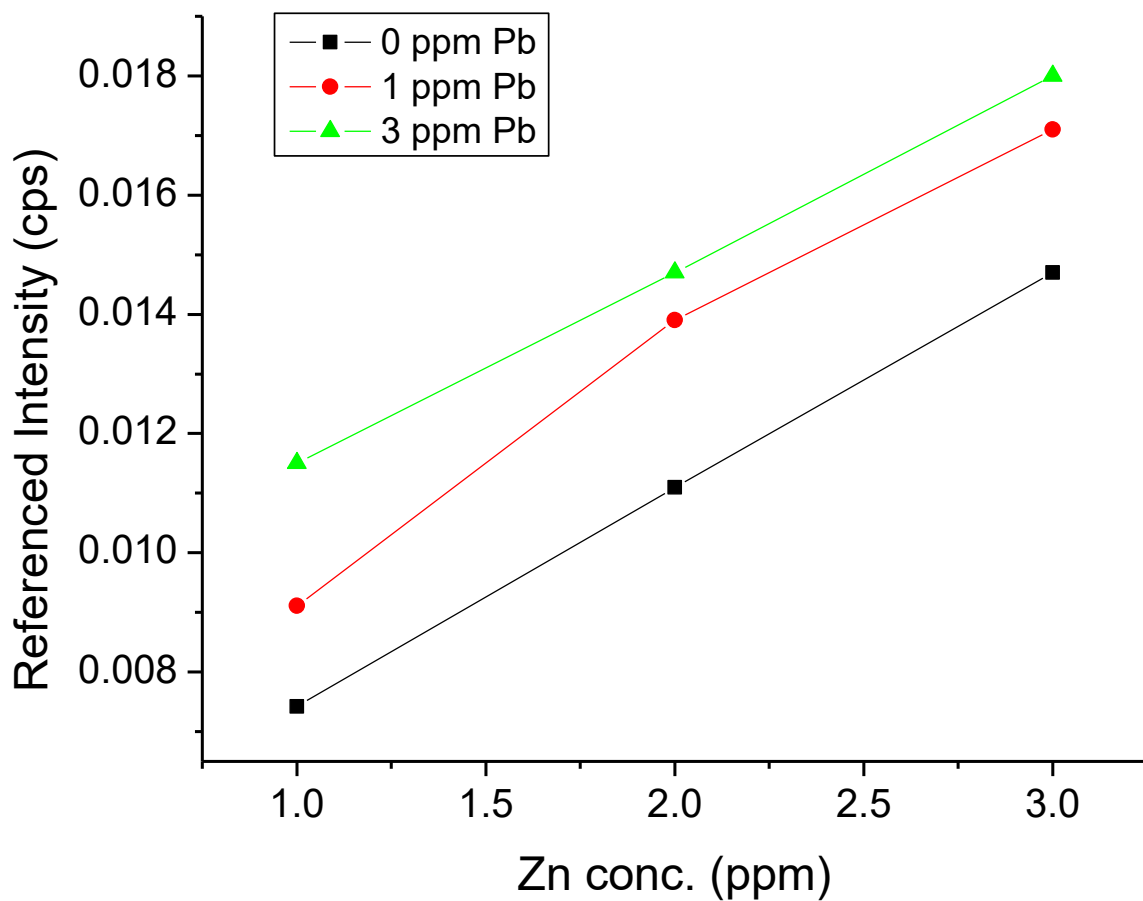**Figure 3.8** Multiple calibration curves of zinc in the presence of increasing amounts of lead. Each data point shown is the integrated area of a fluorescence scan which was determined by averaging five individual fluorescence scans. The scans were averaged internally by the fluorimeter and displayed as one final scan. Error analysis was not provided by the software which performed the averaging operation
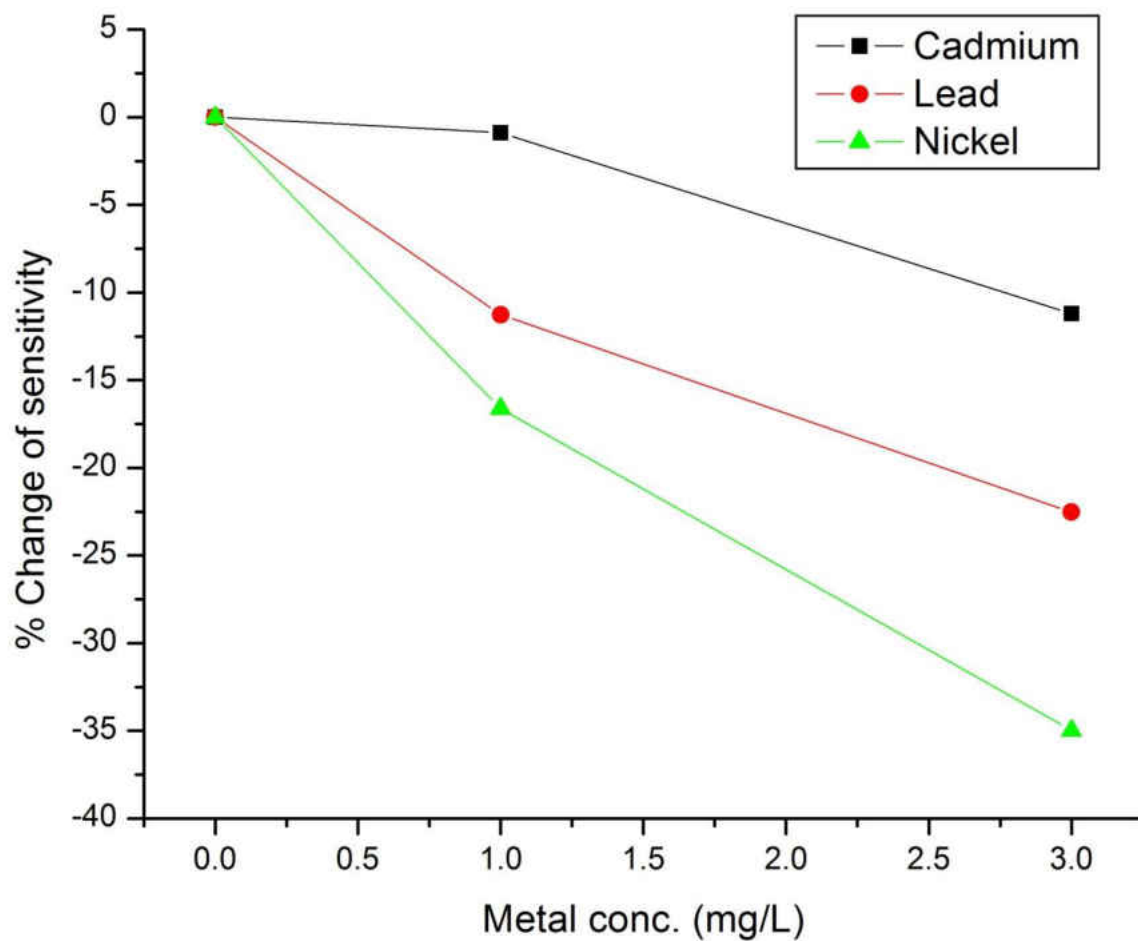
Figure 3.9 The % change in the sensitivity (i.e. the slope of a calibration curve) as the concentration of a competing metal species is increased. The % change is calculated by using the slope determined for a calibration curve where zinc is alone in solution as the baseline values. The slopes of the other calibration curves with competing metals present were compared against these baseline values to obtain the % change of sensitivity. A separate baseline value was obtained for each metal species tested as samples were analyzed on different days
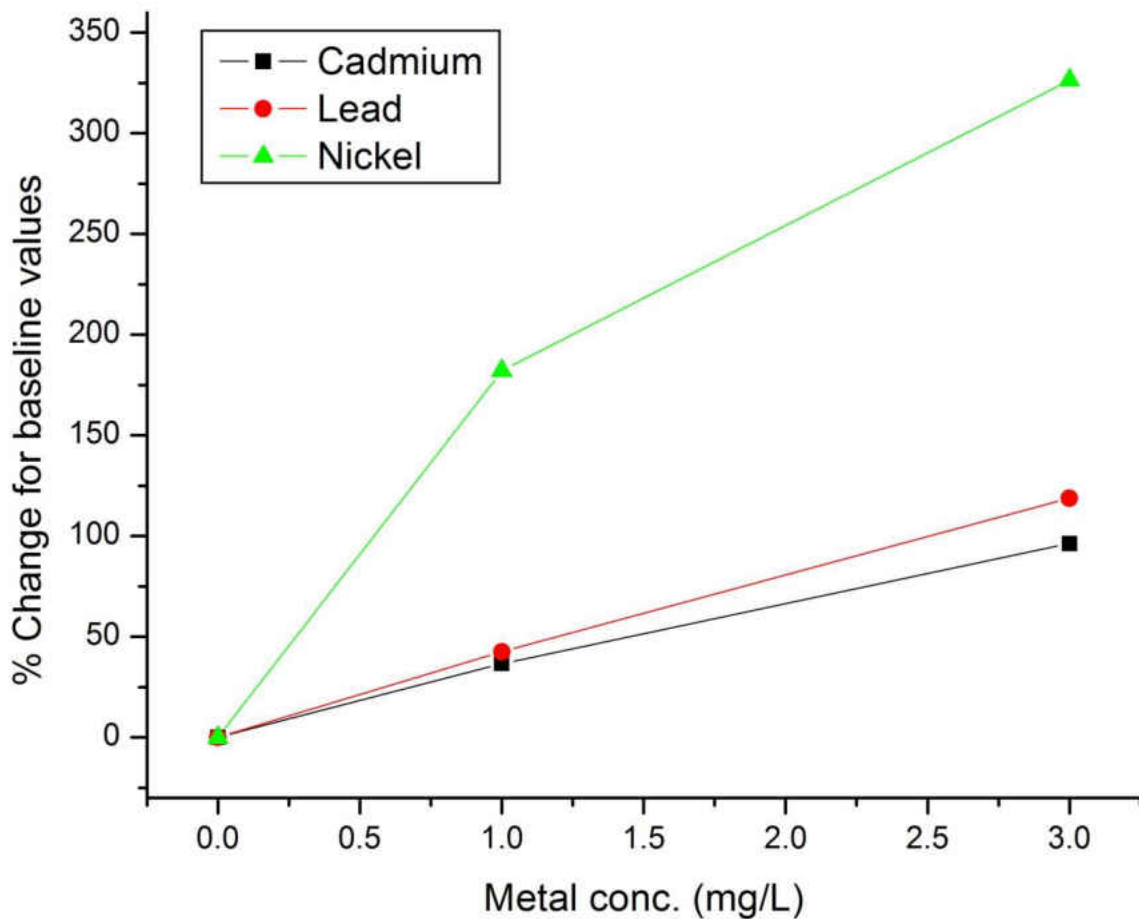
Figure 3.10 The percent change of the fluorescence for FluoZin-1 solutions as the concentrations of competing species are increased. The y-axis in this case refers to the fluorescence intensity noted for a solution of FZ-1 when no zinc is present as the concentration of the other metals species are increased. The percent change indicates the amount of change in fluorescence intensity between a solution containing only FZ-1 and a solution containing FZ-1 and one interfering metals species.
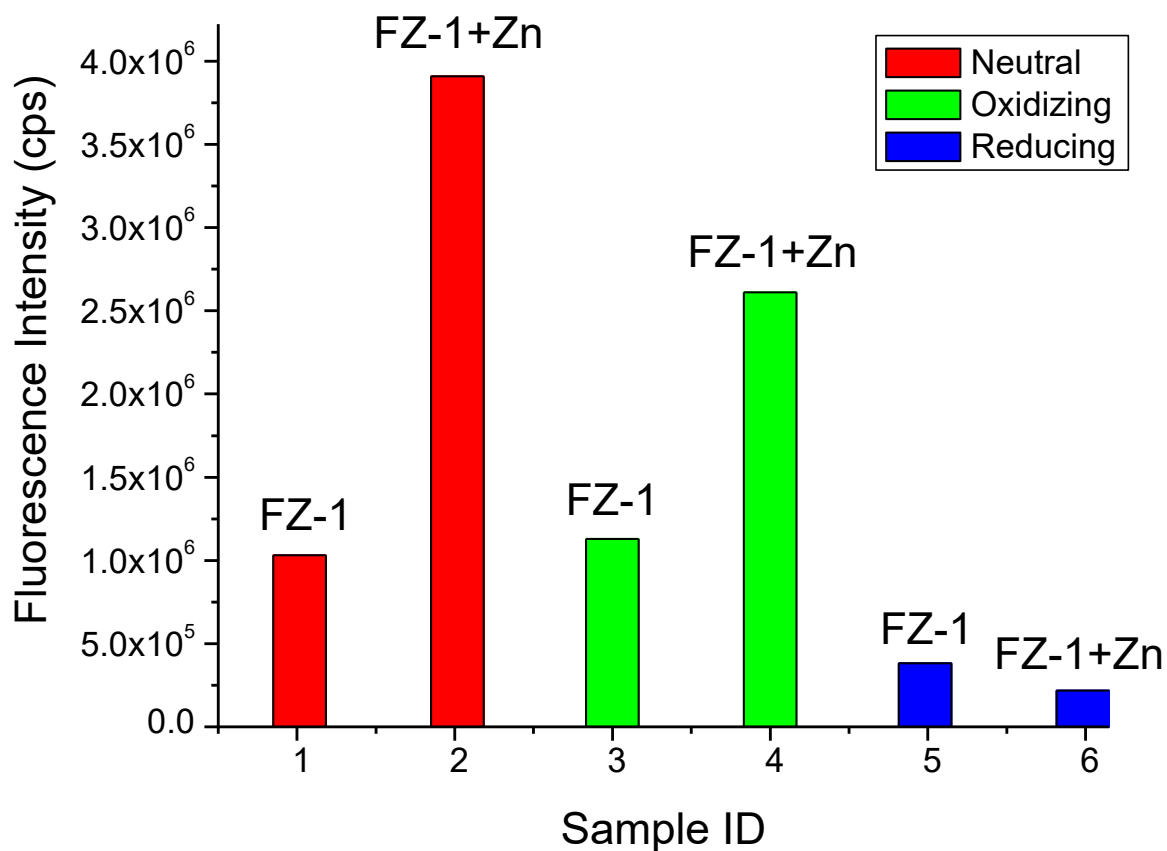
Figure 3.11 The effect of oxidizing and reducing environment upon FluoZin-1 with and without zinc present. See text for a further discussion of these results. The odd-numbered samples refer to the fluorescence response of FZ-1 alone in solution when exposed to the different solution environments while the even-numbered samples have introduced 1 mg/L of zinc into the solutions.
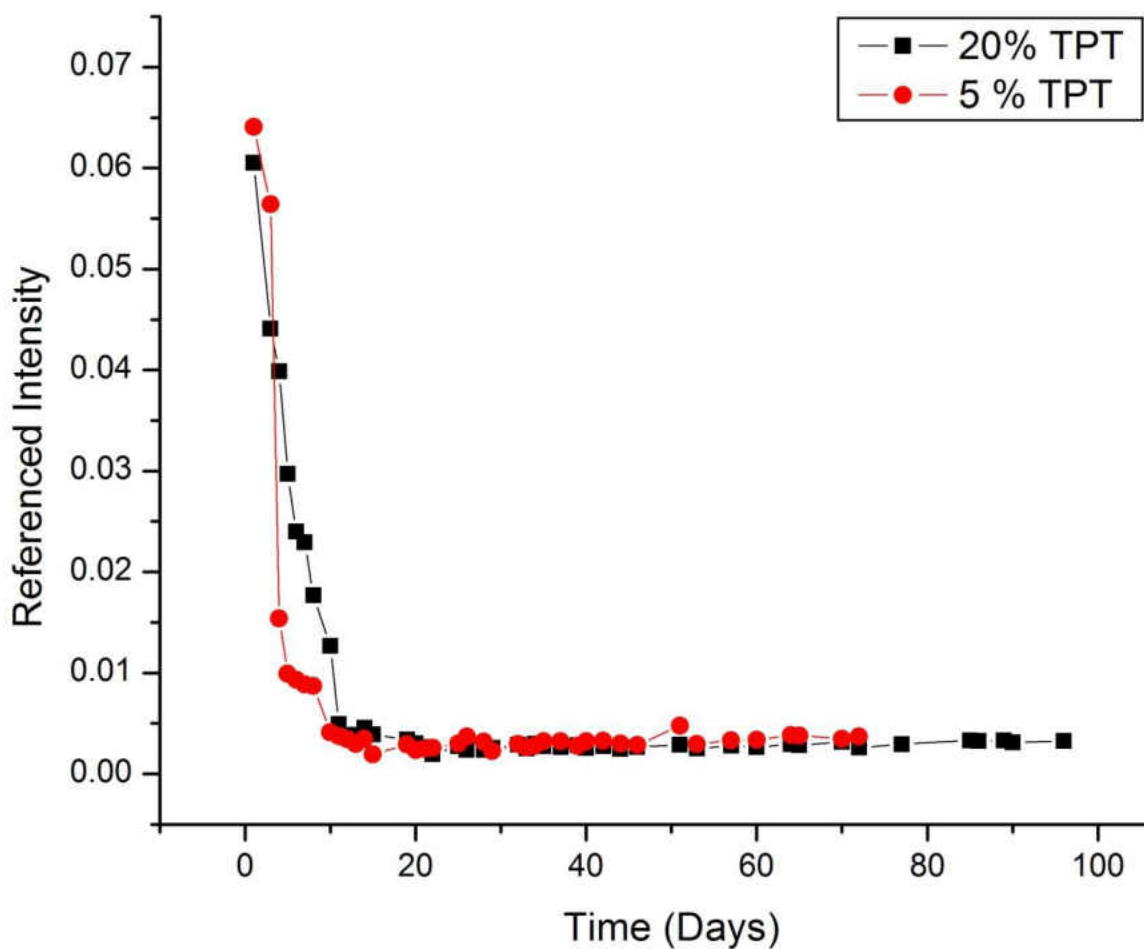
Figure 3.12 A comparison between polymer solutions containing 5% and 20% TPT to determine the rate of dye leaching and lifetime of the polymer films. Displayed is an average value obtained by four films for each polymer type.
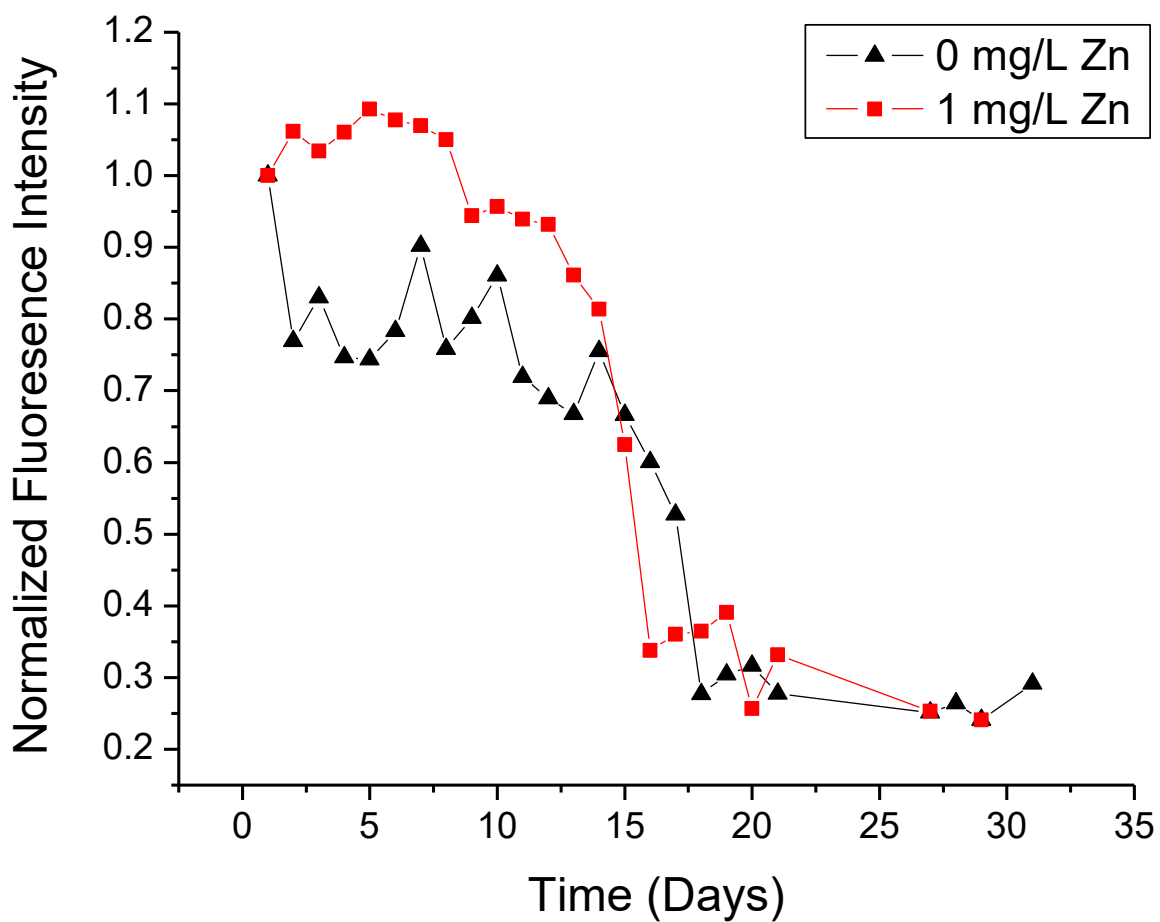
Figure 3.13 A comparison of polymers containing 25% TPT. One set of films was exposed to a 0 mg/L zinc environment, while the other set of films were immersed in 1 mg/L Zn solutions. Displayed are traces depicting the average trend of three films.
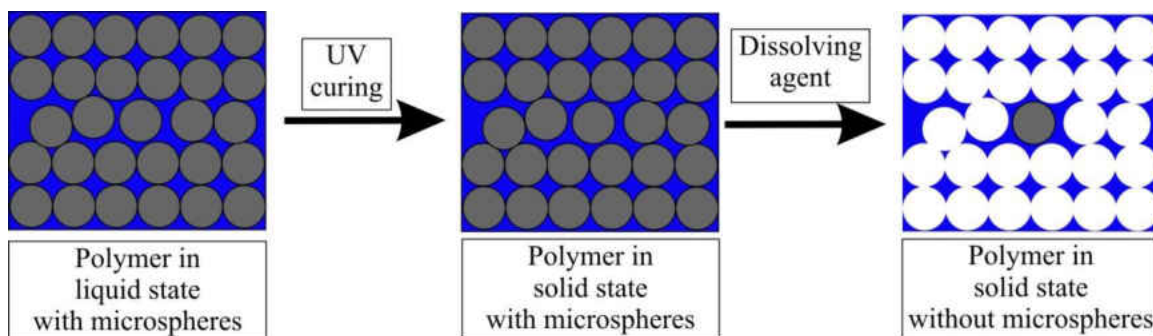
Figure 3.14 A schematic describing the process of micro-templating. By having a high concentration of microspheres, channels are created which allow for rapid passage through the polymer. Note that the one microsphere located in the center of the polymer after application of the dissolving agent was not in contact with any other microsphere due to an insufficient number of microspheres in that region. This prevented the dissolving agent from penetrating the polymer to dissolve it.
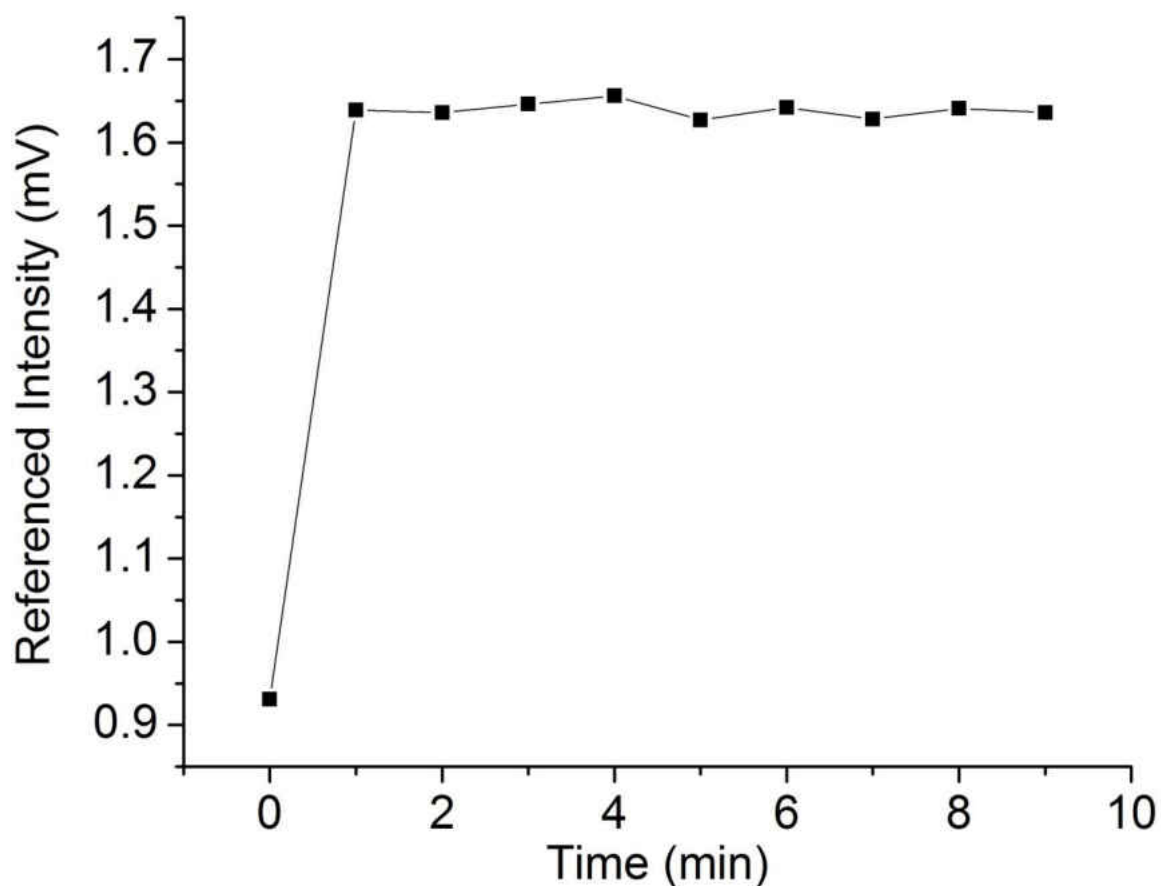
Figure 3.15 The amount of time required for a zinc sensor with a micro-templated polymer to reach signal equilibrium after the introduction of a 0.66 mg/L zinc solution. The y-axis refers to the pulse-to-pulse intensity correction process described in the text. Figures 3.15 through 3.19 were collected using a single sensor region with a fast photodiode detector located next to the laser providing the intensity correction factor.
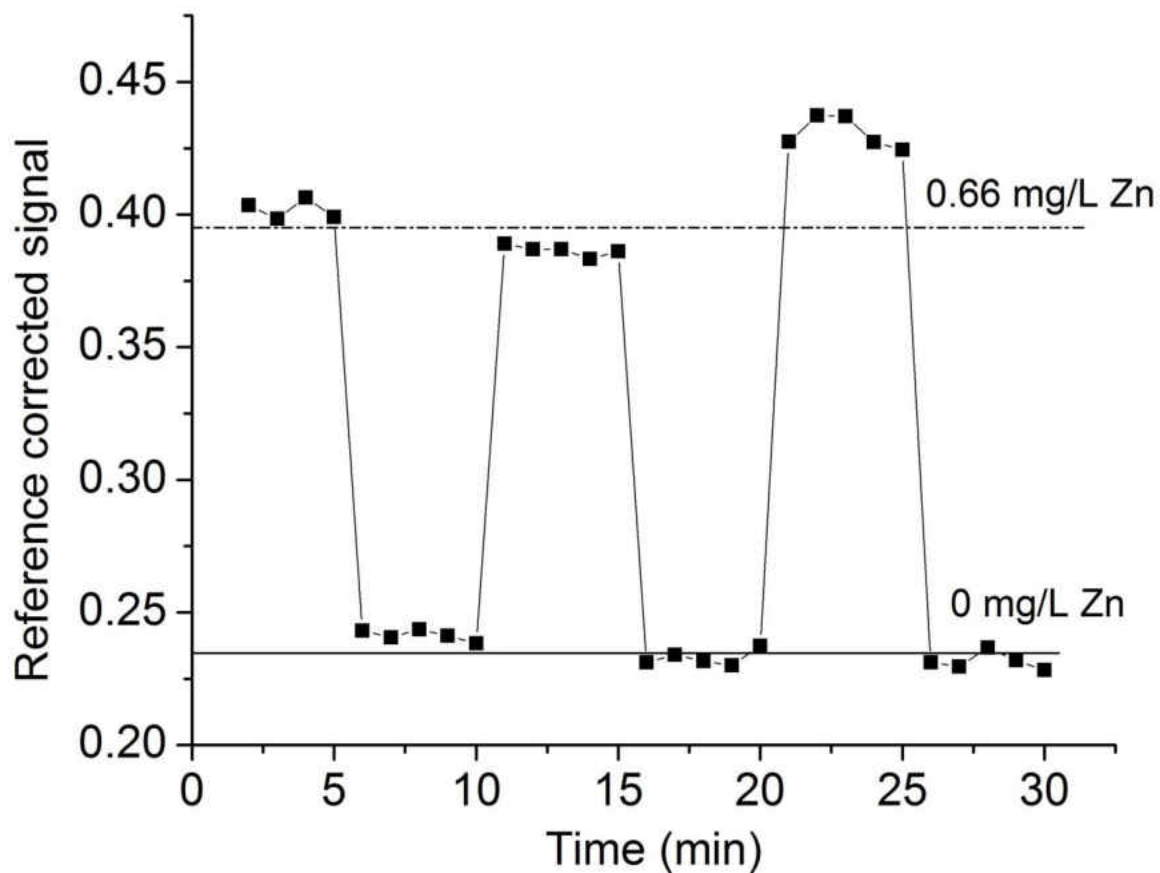
Figure 3.16 Depiction of the response time and reversibility for FluoZin-1 within a micro templated polymer on a crossed fiber sensor. The reversibility of the sensor was generated by immersing the sensor within ultrapure water. The concentration difference between the ultrapure water and the sensor causes zinc to detach from FZ-1 and move into solution, regenerating the sensor for subsequent analysis.

Trial number	Limit of Detection (in mg/L of Zn)	Limit of Quantitation (in mg/L of Zn)
1	0.004	0.042
2	0.010	0.036
3	0.009	0.035
4	0.016	0.047
Average value	0.010 (±0.006)	0.040 (±0.008)

Table 3.1 Individual values used to determine the limit of detection and limit of quantitation.
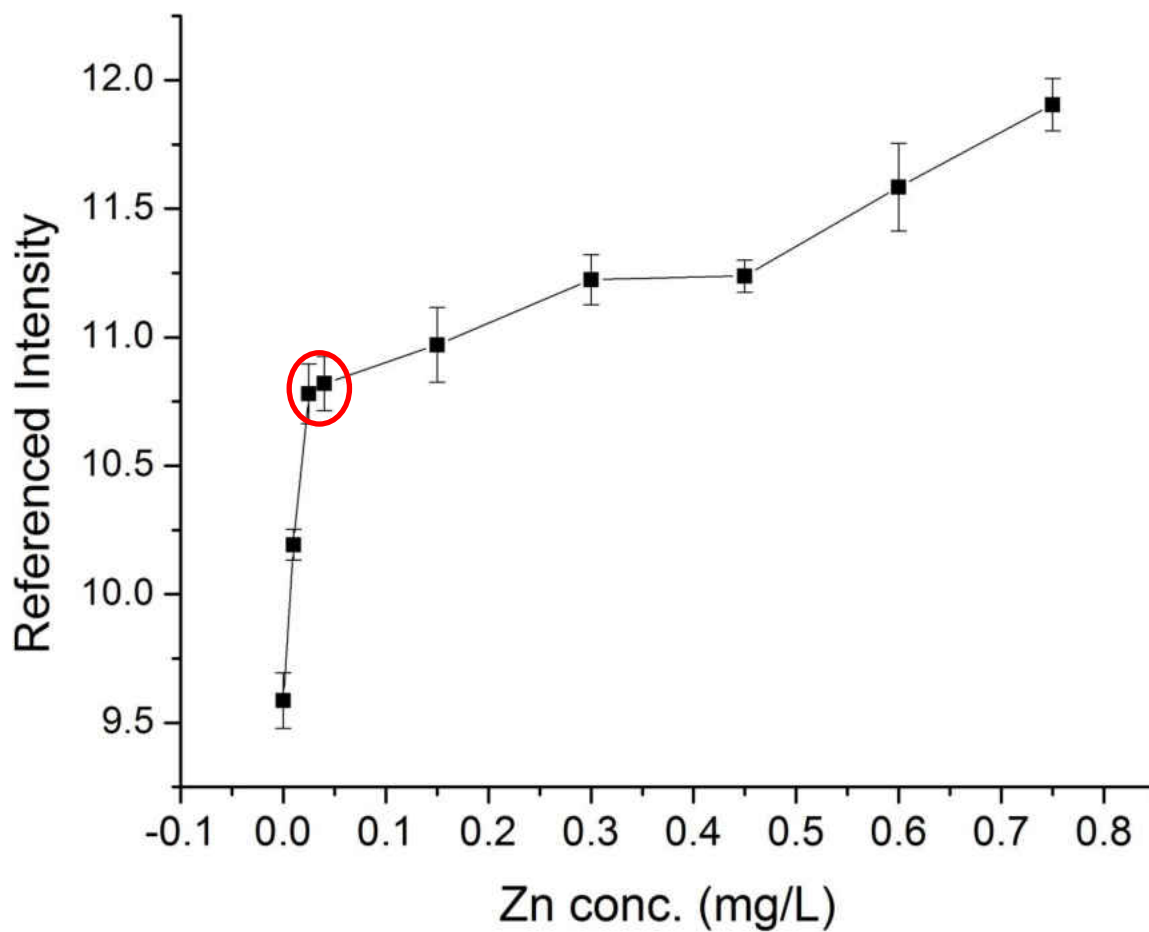
Figure 3.17 The non-linear trend exhibited by the zinc sensor at low zinc concentration. The point at which the slope of the line changes, denoted by the red circle, is the same zinc concentration as the previously measured limit of quantitation.
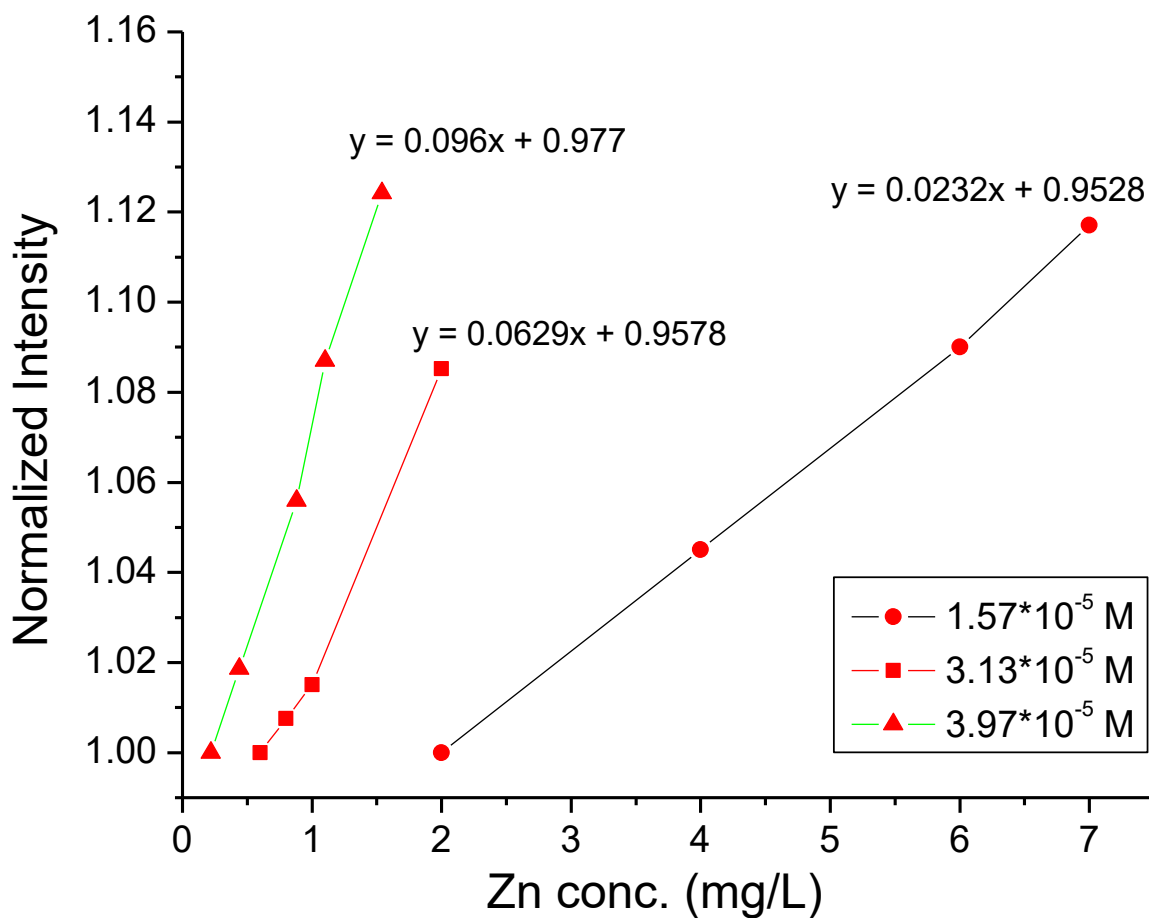
Figure 3.18 The relationship between the concentration of FluoZin-1 and the linear dynamic range of the sensor. As the concentration of the fluorophore within the polymer decreases, there are less available binding sites. This decreases the probability of a zinc/fluorophore interaction within the polymer so even when zinc is present at equal concentrations, the change in the probability of a zinc/fluorophore interaction will change the applicable linear dynamic range.
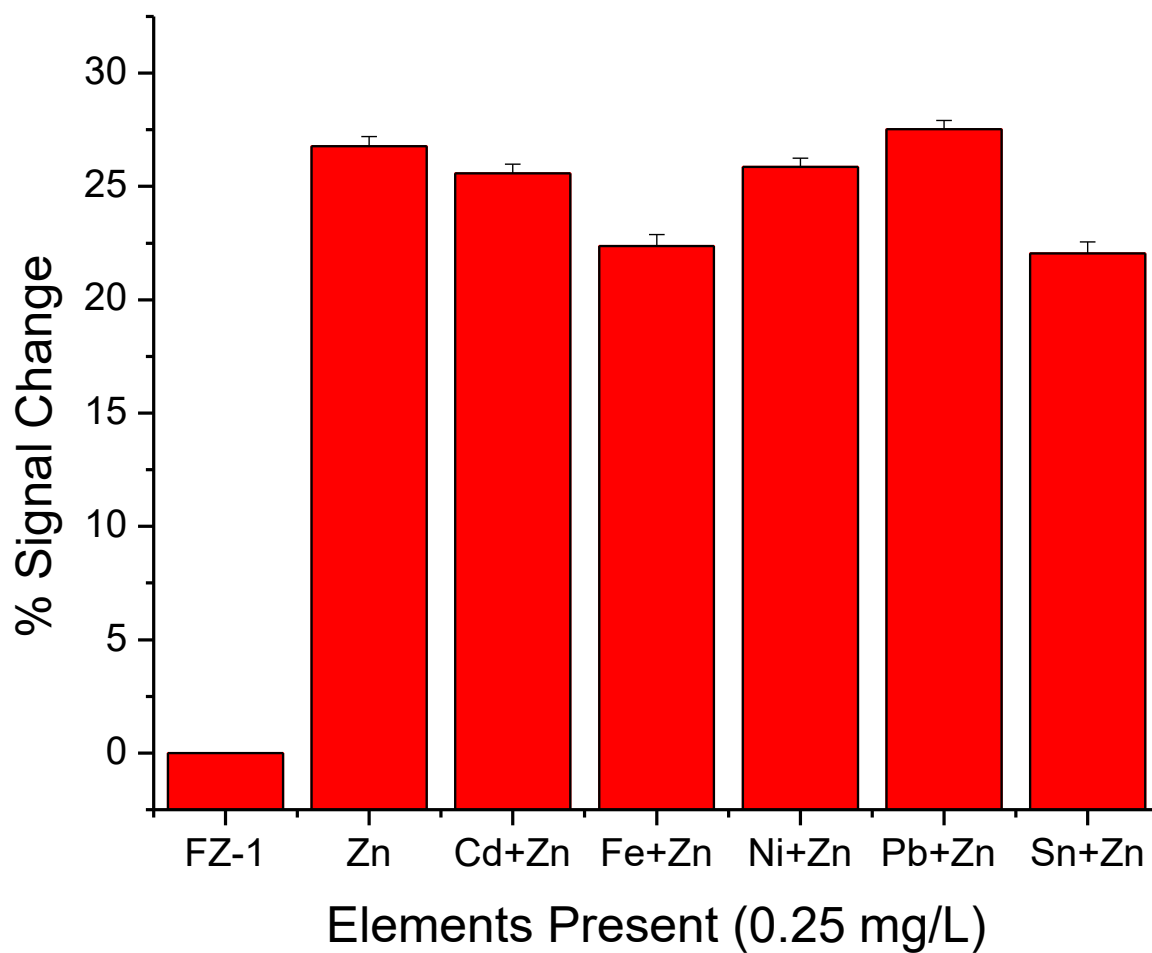
Figure 3.19 A study investigating the behavior of FlouZin-1 in the presence of zinc and an interfering species while integrated within the crossed-fiber sensor platform.
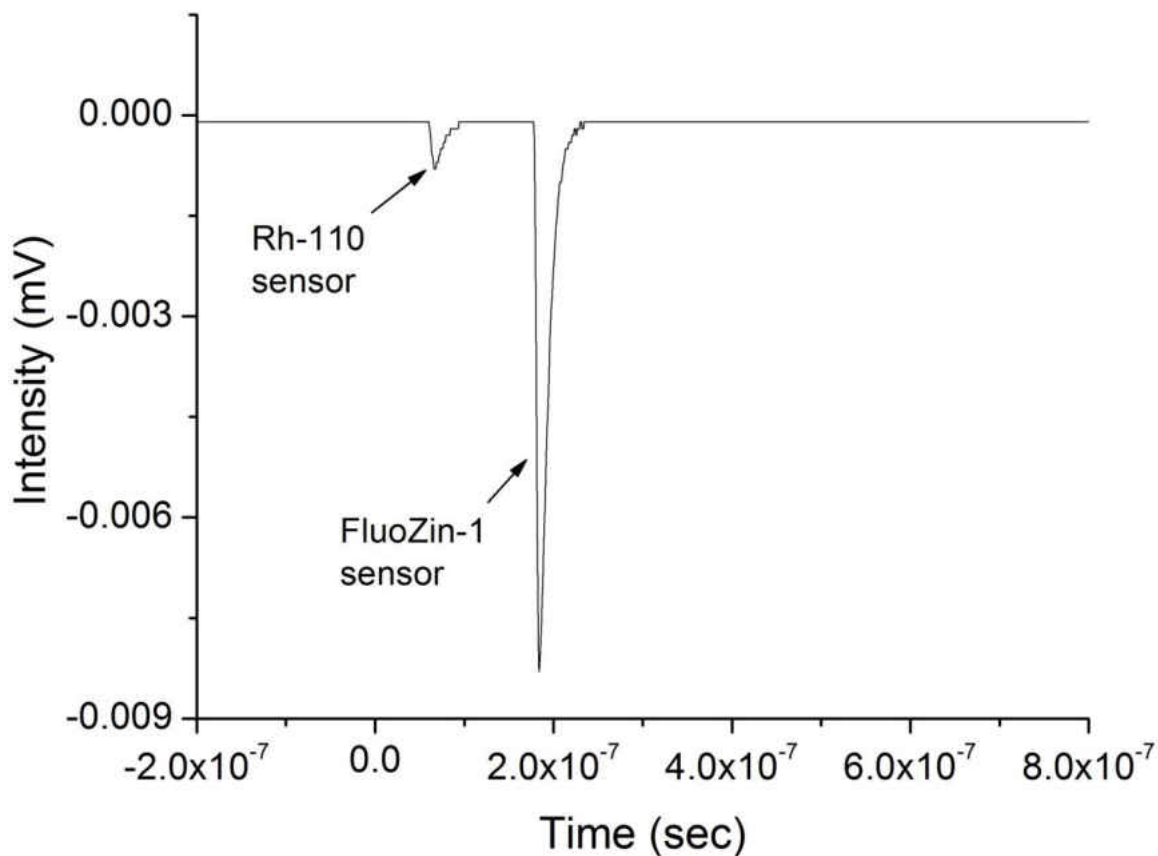
Figure 3.20 Raw data collected from the oscilloscope demonstrating that both sensor regions in a dual sensor array exhibit detectable fluorescence simultaneously. The spacing on the emission fiber between the two regions was approximately 15 meters and 200 individual oscilloscope traces were averaged to produce this figure. To re-iterate, the time listed on the x-axis is relative, with t_0 being when the laser fired.
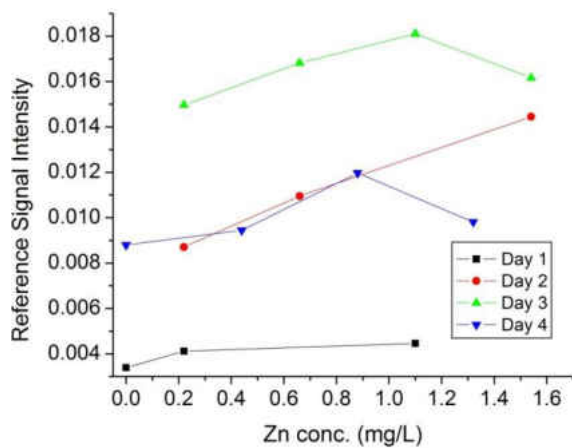
Figure 3.21a Daily calibration using FZ-1 to analyze zinc solutions with a fast photodiode located at the excitation source acting as the pulse energy reference.
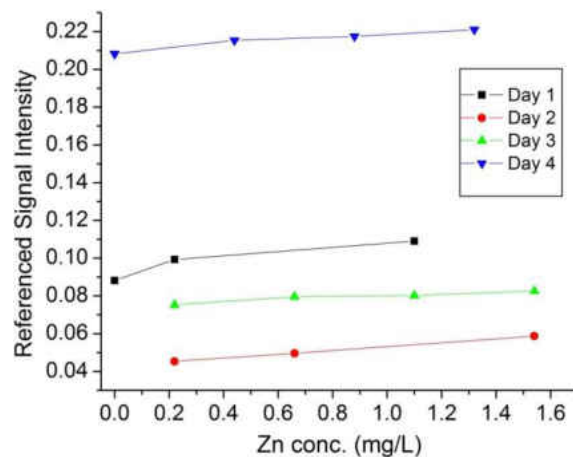
Figure 3.21b Daily calibration using FZ-1 to analyze zinc-containing solutions with an optical fiber sensor containing Rh-110 located in proximity to the sensor containing FZ-1. The Rh-110 sensor acted as the reference for excitation pulse energy.
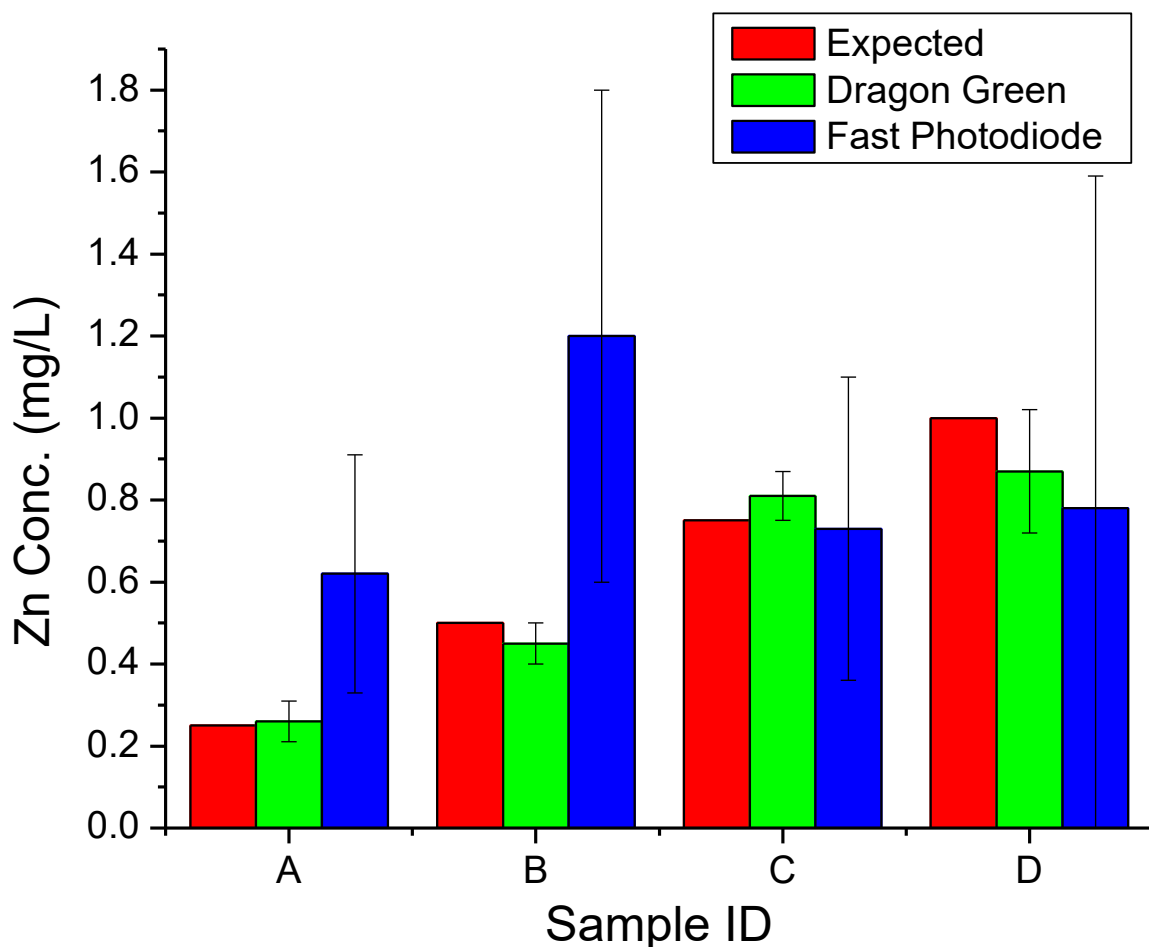
Figure 3.22 A comparison between using a sensor region containing Dragon Green versus using the fast photodiode as an intensity reference for the zinc sensor while performing sample analysis. The expected values are the values supplied by Dr. Henning, the preparer of the samples. The accuracy of the sensor array using Dragon Green is improved and the variability between measurements is decreased when compared against the values obtained by using the fast photodiode. Both of these characteristics support the need for having a second optical fiber-based sensor to provide a means of analyzing the fluctuations in excitation pulse intensity.
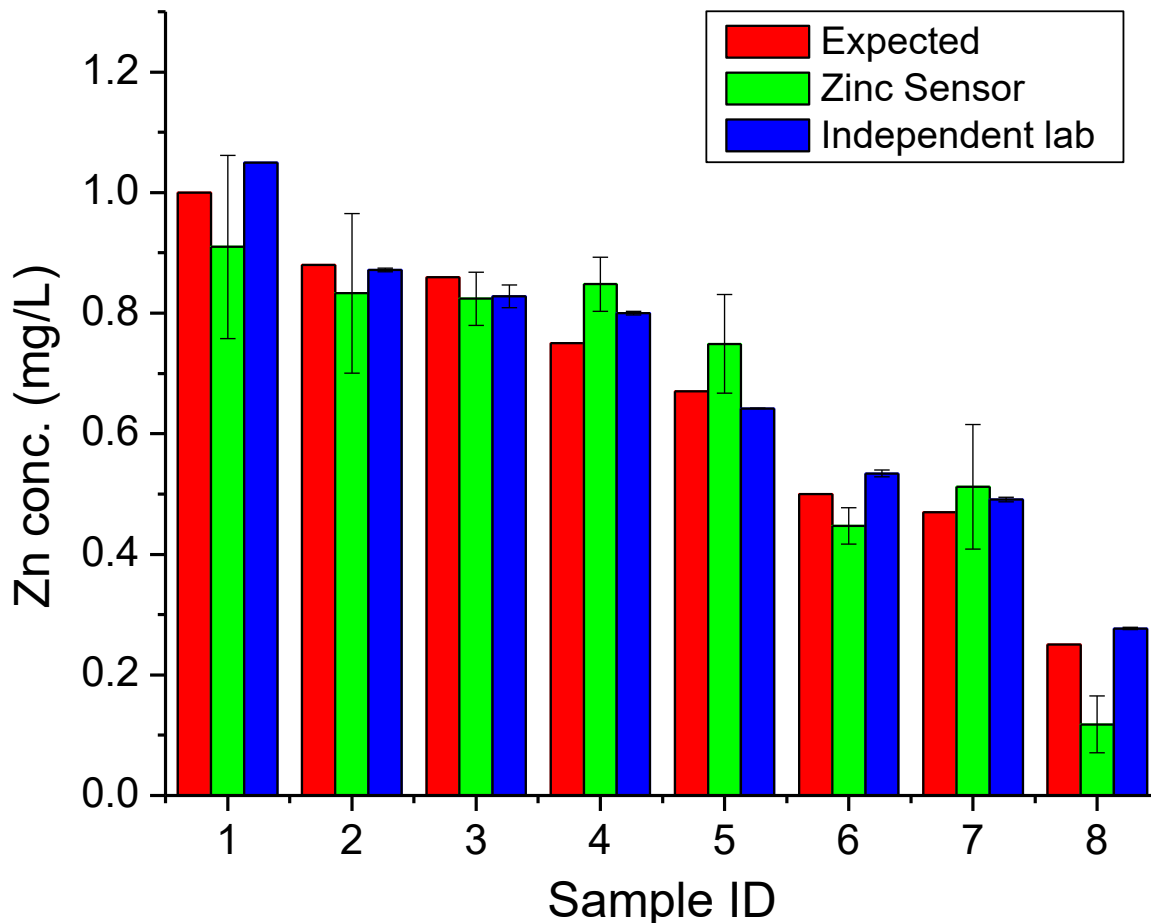
Figure 3.23 A comparison of methods for the analysis of zinc in aqueous environments. Each set of three bars represents the concentration of zinc determined or predicted for a particular sample. The expected values were the concentrations of the solutions based on sample preparation. The red bars are provided to show how well both methods performed against the expected value, but the more important relationship involves the comparison between the values obtained for the optical fiber-based sensor (green) and atomic absorption spectroscopy (AAS) in blue. For most environmental samples, a theoretical true value is not known so the optical fiber-based sensor must perform as well as the currently accepted technology, in this case AAS.

Expected values (mg/L)	Optical fiber sensor (mg/L)	Independent lab (mg/L)	T-test$_{theoretical}$	T-test$_{outside\ lab}$
1	0.910 (±0.152)	1.050 (±0.000)	Pass	Pass
0.88	0.833 (±0.055)	0.872 (±0.003)	Pass	Pass
0.86	0.824 (±0.044)	0.828 (±0.019)	Pass	Pass
0.75	0.848 (±0.045)	0.800 (±0.003)	Fail	Pass
0.67	0.749 (±0.082)	0.642 (±0.000)	Pass	Fail
0.5	0.447 (±0.030)	0.534 (±0.006)	Fail	Fail
0.47	0.512 (±0.104)	0.491 (±0.004)	Pass	Pass
0.25	0.118 (±0.047)	0.277 (±0.002)	Fail	Fail

Table 3.2 A tabular listing of the concentrations of zinc as determined by the optical fiber and the independent lab using atomic absorption spectroscopy. Also listed are the results of the student's t-test. Values where $t_{crit} > t_{calc}$ are listed as "pass" indicate no statistical difference existed between the two examined methods.
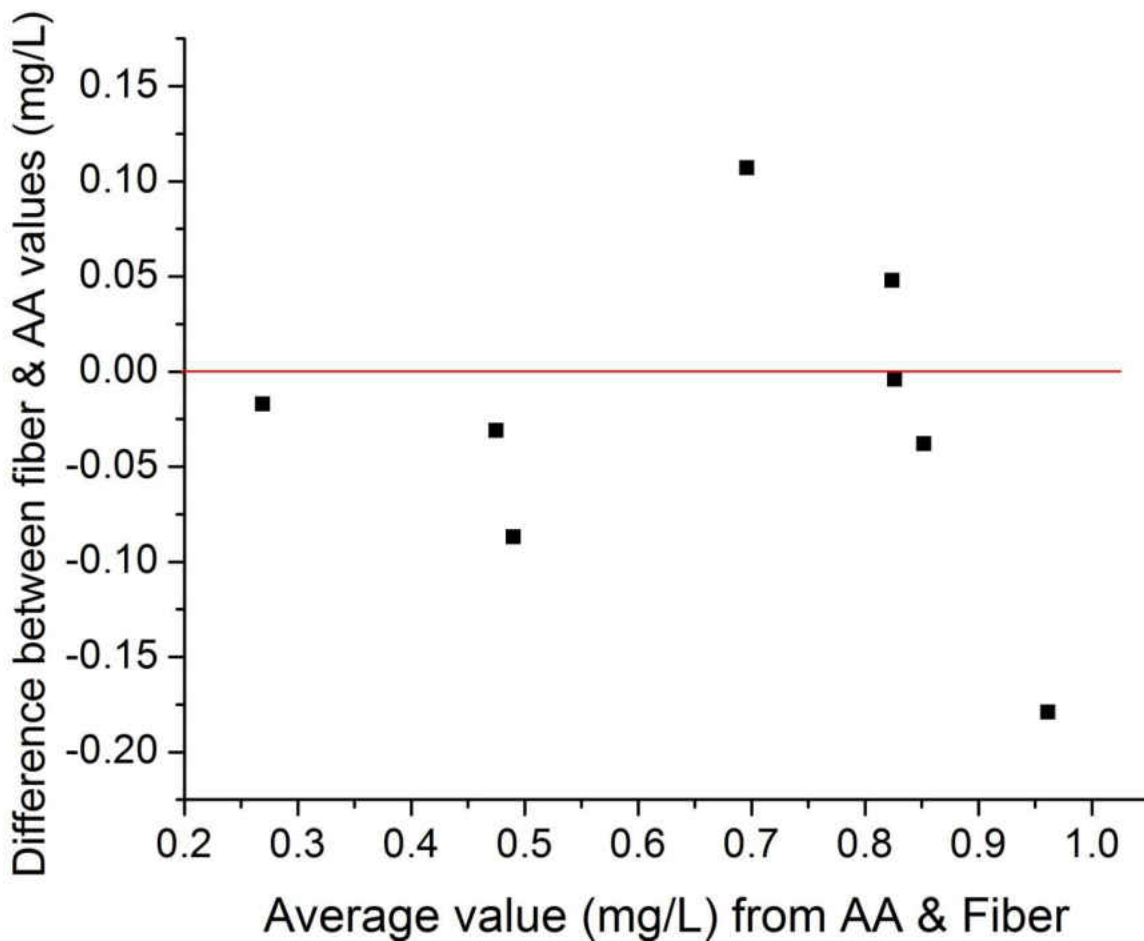
Figure 3.24 Results of the Bland-Altman test demonstrated that there was no significant bias between the two methods (optical fiber-based and AA) for zinc analysis. If the methods of analysis provided identical results, all the point would fall on the red line. This test does not definitively rule out bias, but it provides an indication that if bias is present, it is not at a significant level.

References

1. Invitrogen. Fluorescent Indicators for Zinc.
    http://tools.invitrogen.com/content/sfs/manuals/mp07990.pdf (March 2009)

2. Wei. Y.; Dax, F. Selective Metal Binding to a Membrane-embedded Aspartate in
    the Escherichia coli Metal Transporter YiiP (FieF). *J. Biol. Chem.* **2005**, *208,*
    33716-33724

3. Lee. B.; Chu, T.; Dill, K.; Zuckerman, R. Biomimetic Nanostructures: Creating a
    High-Affinity Zinc-Binding Site in a Folded Nonbiological Polymer. *J. Am.
    Chem. Soc.* **2008**, *130*(27)*,* 8847-8855

4. Royzen, M.; Dai, Z.; Canary, J. Ratiometric Displacement Approach to Cu(II)
    Sensing by Fluorescence. *J. Am. Chem. Soc.* **2005**, *127*(6), 1612-1613

5. de Silva, A.; Gunaratne, H.; Gunnlaugsson, T.; Huxley, A.; McCoy, C.;
    Rademacher, J.; Rice, T. Signaling Recognition Events with Fluorescent Sensors
    and Switches. *Chem. Rev.* **1997**, *97*(5), 1515-1566

6. Life Technologies. FluoZin-1 Tripotassium Salt cell impermeant.
    https://products.invitrogen.com/ivgn/product/F24180?ICID=search-product
    (October 2009)

7. Orte, A.; Crovetto, L.; Talavera, E.; Boens, N.; Alvarez-Pez, J. Absorption and
    Emission Study of 2',7'-Difluorofluorescein and Its Excited-State Buffer-
    Mediated Proton Exchange Reactions. *J. Phys. Chem. A.* **2005**, *109,* 734-747

8. Lide, D., Ed. *Handbook of Chemistry and Physics,86*[th] *ed.;* CRC Press: New
    York, 2006

9. U.S. Environmental Protection Agency. Electroplating and Metal Finishing Point
    Source Categories; Effluent Limitation Guidelines, Pretreatment Standard and
    New Source Performance Standards. *Federal Register*. **1983**. *48*(137), 32462-
    32488

10. Ogawa, S.; Yoshimura, E. Determination of thermodynamic parameters of
    cadmium(II) association to glutathione using the fluorescent reagent FluoZin-1.
    *Anal. Biochem.***2010**, *402(2):* 200-202.

11. Henning, P. E.; Geissinger, P. Application of time-correlated single photon
    counting and stroboscopic detection methods with an evanescent-wave fibre-optic
    sensor for fluorescence-lifetime-based pH measurements. *Meas. Sci. Technol*.
    2012, *23*, 045104

12. Rigo, M.V., Plasmonic Optical Fiber Sensor for Oxygen Measurement. Ph.D.
    Thesis, University of Wisconsin-Milwaukee, Milwaukee, WI, May 2009

13. International Union of Pure and Applied Chemistry. IUPAC Gold Book. http://goldbook.iupac.org/L03540.html (January 2013)

14. Volker, T.; Schatzlein, D.; Mercuro, D. Limits of Detection in Spectroscopy. *Spectroscopy* **2003**, *18*, 112-114.

15. Skoog, D., West, D., Holler, F., Crouch, S. *Fundamentals of Analytical Chemistry*, 8th Ed; Thomson Brooks/Cole, Belmot, CA; 2004

16. Nakashima, T.; Yamada, Y.; Yoshizawa, H., Synthesis of Monodisperse Polystyrene Microspheres by Dispersion Polymerization Using Sodium Polyaspartate. *Colloid & Polymer Science* **2007,** *285*, (13), 1487-1493.

17. Hong, J.; Hong, C. K.; Shim, S. E., Synthesis of Polystyrene Microspheres by Dispersion Polymerization Using Poly(vinyl alcohol) as a Steric Stabilizer in Aqueous Alcohol Media. *Colloids and Surfaces A: Physicochemical and Engineering Aspects* **2007,** *302*, (1-3), 225-233.

18. Cepak, V., Hulteen, J., Che, G., Jirage, K., Lakshmi, B., Fisher, E., Martin, C., Yoneyama, H. Chemical Structures for Template Syntheses of Composite Micro- and Nanostructures. *Chemisty of Materials* **1997**, *9(5)*, 1065-1067

19. Henning, P. E.; Application of Advanced Time-Resolved Fluorescence Detection Techniques for Remote pH Sensing with Optical Fibers. Ph.D. Thesis, University of Wisconsin-Milwaukee, Milwaukee, WI, May 2009

20. Ogawa, S., Yoshimura, E. Determination of thermondynamic parameters of cadmium (II) association to glutathione using fluorescent reagent FluoZin-1. *Analytical Biochemistry* **2010**, *402*, 200-202

21. Kürner, J., Klimant, I., Krause, C., Preu, H., Kunz, W., Wolfbeis, O. Inert Phosphorescent Nanospheres as Markers for Optical Assays. *Bioconjugate Chemistry*, **2001**, *12*, 883-889

22. Bangs Laboratory, Inc. Dragon Green Intensity Standard. http://www.bangslabs.com/sites/default/files/bangs/docs/pdf/PDS%20704.pdf (February 2013)

23. Altman, D., Bland, J. Measurement in Medicine: the Analysis of Method Comparison Studies. *The Statistician*, **1983**, *32*, 307-31

Chapter 4

Copper Sensor Development and Characterization

4.1 Fluorescent sensor introduction

In this study a fluorophore capable of monitoring copper in solution was examined. The fluorescent sensor, hereafter referred to as DDETA, was prepared using the method published by Li et.al.[1] This scheme allows for the covalent attachment of the fluorophore directly to the optical fiber. This change in the way in which the fluorophore is integrated into the optical sensor has both negative and positive impacts on the crossed-fiber design. Covalent attachment of the fluorophore to the optical-fiber core will minimize or eliminate the risk of dye leaching. Furthermore, the molecule is held in very close proximity to the optical-fiber core, maximizing the strength of the interaction of the evanescent wave with the fluorophore. On the other hand, the bulky dansyl group, which gives rise to the fluorescence of the compound, limits – because of steric hindrances – the number of fluorophores that can be attached to the optical fiber. Also, the overall surface area of the optical fibers in a sensor junction is small. These two conditions cause the calibration range of the sensor to have a fixed value, in contrast to the zinc sensor. The third potential problem is that the maximum excitation wavelength is at 365 nm. While this is of no concern for measurements in a fluorimeter, for remote sensing with optical fibers over long distances, this wavelength will suffer from absorption losses in the fiber core. However, the optical fibers used in the crossed-fiber array have high-OH content, which improves the transmission properties in the near UV.[2] This issue will be addressed in a later section.

Sensor recognition requires that copper exist as a +2 ion and will induce fluorescence quenching because the paramagnetic nature of copper allows for the excited state of the fluorophore to undergo a singlet to triplet state conversion.[3] This in turn

reduces the fluorescence generated by the fluorophore, as only relaxation of the singlet state can generate fluorescence. The binding of copper occurs at the dimethylamino group located at the end of the molecular chain, which is attached to the naphthalene group. However, the overall sensitivity of the molecule is enhanced by the amino groups located within the molecular chain connecting the copper recognition unit to the optical-fiber-core surface. Other copper-specific fluorophores have been created using amino groups as a means of selectively binding with copper.[4] So although copper binds at the dimethylamino site, other amino groups located within the chain help to stabilize the binding.

Dansyl chloride, by itself, is not a fluorescent compound.[5] This lack of fluorescence is due to the presence of a large electron withdrawing group, sulfonyl chloride.[6] This allows intersystem crossing to occur, creating a non-radiative route of relaxation for the molecule. This crossing into the triplet state may result in the generation of phosphorescence, a type of emission that is weaker in intensity and has longer luminescent lifetimes when compared to fluorescence. This type of radiative decay is usually not observed when the fluorophore is in solution at room temperature. Instead, non-radiative relaxation from the triplet state back to the ground state will be the primary means of relaxation in solution. However, after reacting with an amine-containing compound at the sulfonyl site, the overall molecule will become fluorescent. This has made dansyl chloride an ideal tag for numerous studies, including proteins and illegal narcotics.[7, 8] For the mentioned studies, the dansyl chloride does not serve as a sensor, providing specific recognition of various analytes. Rather, due to the propensity of dansyl chloride to react quickly with primary, secondary or tertiary amines, various

substances can be tagged with dansyl chloride, modifying the compounds of interest so that the compounds fluoresce. In the study involving illegal narcotics, each compound of interest, usually the active ingredient of the narcotic, was tagged with dansyl chloride. The samples were then introduced onto a thin-layer chromatography plate. After the separation process was completed, the plate was exposed to UV radiation and the fluorescence of the now-tagged compounds would allow for identification of the compound based on the retention behavior on the chromatography plate.

A benefit of using dansyl-chloride functionalized compounds is the fact that the fluorophore exhibits a large Stokes shift of 130 nm. This is due to a change in the planarity of the dimethylamino group in polar environments. Upon excitation of the copper fluorophore, the dimethylamino group, located at the end of the molecular chain, attached to the naphthalene ring, rotates so that it is out of the plane with relation to the naphthalene ring of the dansyl group.[9] The twisting during excitation is referred to as the Twisted Internal Charge Transfer (TICT) process, which decreases the energy gap between the excited state and ground state, causing fluorescence to occur at a longer wavelength. This process is illustrated in Figure 4.1.

4.2 Fluorescence quenching classification

There are two ways in which an analyte may interact and induce fluorescence quenching of the fluorophore in solution. The first involves a purely collisional process between the quenching species (Q) and the fluorophore (F) and is referred to as collisional quenching. After the collision, the quenching species will immediately separate from the fluorophore. The second type of fluorescence quenching involves a

direct coupling between the fluorophore and quenching species via some type of binding or electrostatic coupling. These interactions refer to a coupling which occurs for a length of time longer than the excitation and emission cycle. Due to the semi-permanency of the binding, this is referred to as static quenching.

Collisional quenching, or dynamic quenching, is defined as the when the quenching species interacts with the fluorophore after the fluorophore has reached an excited state.[10] The mechanism for excitation and subsequent fluorescence in the presence of a collisional quenching species is illustrated in Figure 4.2. These collisions are often rate limited due to the diffusion of the quenching species in solution. For the sensor investigated here, the fluorophore will remain fixed in place, so the only diffusion occurring will consist of the quenching species migrating in solution. The relationship between the concentration of the quenching species, [Q], is inversely proportional to the change in fluorescence intensity observed between when the quenching species is present and when it is not.[11] This inverse relationship allows for the development of the Stern-Volmer equation which describes the correlation between [Q] and the ratio of fluorescence quenching. The equation is shown below, where k_q depicts the radiative decay rate in the presence of the quenching species, τ_0 is the lifetime of the fluorophore in the absence of the quenching species and I_0 and I are the fluorescence intensities in the absence and presence of the quenching species, respectively.

$$\frac{I_0}{I} = 1 + k_q \tau_0 [Q] \qquad \qquad \text{(Eqn 4.1)}$$

The lifetime component of this equation brings to light a key point which distinguishes dynamic quenching. Because dynamic quenching occurs after the

fluorophore undergoes excitation, the subsequent energy transfer will have the effect of shortening the excited state lifetime of each affected molecule. As such, the relationship between the change in lifetime of the fluorophore and [Q] will be inversely linear. This linear relationship once again yields a second Stern-Volmer equation describing the change in lifetime and [Q].

$$\frac{\tau_0}{\tau} = 1 + k_q \tau_0 [Q] \qquad\qquad\qquad \text{(Eqn.4.2)}$$

For both equations, the variables k_q and τ_0 are often combined to form K_{sv}, referred to as the Stern-Volmer constant.[6] Using either the intensity ratio or the lifetime ratio will provide the user with the Stern-Volmer coefficient. Fluorescence intensity is often measured as steady-state fluorescence where no fluorescence lifetime data is obtainable. However, the fluorescence lifetime inherently dictates how intense fluorescence will be. If an excited state lifetime is cut in half by dynamic quenching, this means that only half of the possible fluorescence is generated, which will reduce the measured fluorescence intensity. It should also be noted that it is not uncommon for fluorophores to deviate from the inversely linear relationship predicted by the Stern-Volmer relationship. There are many reasons for this, including the formation of non-fluorescent complexes, or competitive interactions between different fluorophores for the same quenching species.

Static quenching occurs when the quencher and the fluorophore are bound together. This binding prevents the fluorophore-quencher complex from undergoing excitation with subsequent fluorescence at the excitation and emission wavelengths of the fluorophore. However, fluorophores to which no quencher is bound will maintain their excitation and emission properties. The relationship generated between [Q] and the

change in fluorescence intensity (I) is inversely linear, just as for dynamic quenching and yields the following equation:

$$\frac{I_0}{I} = 1 + K_s[Q] \qquad \text{(Eqn 4.3)}$$

Note that the Stern-Volmer coefficient K_{sv} has been replaced with K_s. Because the fluorophore does not undergo an excitation/emission cycle when bound to the quenching species, the lifetime of the excited state will not change. The amount of fluorescence quenching is now tied to the rate of formation for the chemical reaction, F+Q→FQ, and as such K_s then represents the rate of formation for the final, non-fluorescent product.

$$K_s = \frac{[FQ]}{[F][Q]} \qquad \text{(Eqn. 4.4)}$$

This change allows for the relationship between the fluorescence intensity and Q to be quantified.

There may be times where the exact nature of the fluorescence quenching is unknown. Several comparisons can be made in order to determine which type of fluorescence quenching is occurring. While both dynamic and static processes lead to quenching of the fluorescence intensity, only dynamic quenching causes a simultaneous change in the fluorescence lifetime. Lifetime studies would reveal this change, or lack thereof, and allow for tentative identification. For static quenching, because the binding between Q and F have reached equilibrium before excitation occurs, a change in the absorption profile would be observed due to the change in the spectral features of the new complex when compared to the original fluorophore. Lastly, changes in temperature may

provide an insight as to the type of quenching occurring. For static quenching, higher temperatures will result in lower amounts of quenching due to the increase in instability within the FQ complex, thus decreasing the slope of the Stern-Volmer linear relationship. However, an increase in temperature for a dynamic quenching system will result in an increase in the amount of fluorescence quenching. At higher temperatures, more energy will be supplied to the quenching species, allowing it to move more freely in solution and increase the probability of colliding with the fluorophore. The Stern-Volmer plot in this case will exhibit an increase in the slope of the line.

Lastly, there is the possibility that both mechanisms occur simultaneously. If this is the case, the linear relationship obtained for either system will no longer be maintained. For dynamic systems, this may be due to the fact that [Q] is so high that a quenching molecule will always interact with the fluorophore. Static quenching systems may undergo collisional quenching from unbound Q in solution colliding, but not binding, to fluorophores. In order to account for the mixing of the two mechanisms a new relationship is created where the effect of both systems are accounted for and combined to yield a final equation of

$$\frac{I_0}{I} = (1 + K_{sv}[Q])(1 + K_s[Q]) \qquad \text{(Eqn. 4.5)}$$

4.3 Fluorescent compound attachment confirmation

To confirm successful synthesis of the copper-sensitive fluorophore, a quartz absorption cuvette underwent the synthesis process to create the copper-specific sensor. Upon completion of the synthesis process, UV-Vis and front-face fluorescence

spectroscopy were employed to confirm the covalent attachment of the fluorescent molecule to the glass surface by comparing the absorption and fluorescence spectral profiles provided in the literature against the spectra obtained experimentally. It was cited in the literature that λ_{ex} = 330 nm while λ_{em}=500 nm.[1] The UV-Vis absorption profile confirms that the absorption maximum occurs at approximately 330 nm. (Figure 4.3) However, the original work and research performed here both corroborate that the absorption of glass at this wavelength will be significant, so a longer excitation wavelength (365 nm) was chosen for analysis. Examination by front face fluorescence confirmed an emission wavelength of 495 nm. (Figure 4.4) These spectral features verified that the successful creation and attachment of the fluorophore to a glass surface was achieved.

4.4 Mechanism of fluorescence

It is strongly suspected that the copper fluorophore, DDETA, principally undergoes static quenching. The literature has stated that the copper binds to DDETA, due to the affinity of transition metals for the amino groups located within the sensor.[1,4] Additionally, a strong ionic interaction can be suspected as the literature states the need of a chelating agent to regenerate the fluorophore and remove bound copper ions. If collisional quenching was the sole mechanism, simply introducing a solution free of copper would restore the fluorescence back to the original intensity.

To determine what type of quenching mechanism existed, a quartz cuvette was exposed to the copper-specific sensor synthesis process. After the synthesis was completed, the cuvette was analyzed using both UV-Vis and fluorescence spectroscopy.

Analyzing the UV-Vis absorption profile in the presence of increasing copper concentrations yielded a significant change of the absorption profile (Figure 4.5) indicating that there was binding between the copper and the fluorescent molecule. All of the solutions analyzed by the UV-Vis method were also analyzed by front-face fluorimetry. A calibration curve showed a linear relationship between the fluorescence-intensity quenching and copper concentration (Figure 4.6) but after applying the Stern-Volmer relationship (Eqn 4.3) a non-linear relationship was obtained. (Figure 4.7) This non-linear relationship does not conclusively prove what type, or types, of fluorescence quenching is occurring so more study is required in order to determine the exact quenching mechanism or combination of mechanisms. In the future, a study of DDETA's fluorescence lifetime and the change, or lack thereof, of the fluorescence lifetime of DDETA in the presence of copper will provide a more definitive answer towards what type of quenching mechanism is occurring.

4.5 Optical fiber and fluorophore integration

After confirming that the fluorophore was successfully synthesized and attached to a glass surface, integration within the optical-fiber-sensor platform was undertaken. The process for preparing the fibers started in an identical fashion as for all other sensors. Outer cladding and buffer materials were removed using a Bunsen burner with subsequent acetone washing and nitric-acid immersion for two hours. To perform the synthesis, the optical fibers had to be bent in order to fit within the reaction glassware, one being an Erlenmeyer flask. The exposed cores, if not overheated, could withstand the strain of mild bending. This was required to perform both synthesis steps. After the synthesis was completed, the fibers were placed within the polypropylene blocks

designed for single crossed-fiber sensors. The sensor was placed into the sample analysis chamber, and excited with laser pulses generated at 365 nm. Confirmation of a successful synthesis was indicated by the observation of fluorescence, as recorded by the PMT after passing through an optical filter to remove any scattered excitation light. A three point calibration curve with copper was collected as a second level of confirmation.

During the course of the research two different sensor versions were investigated. Because DDETA is directly attached to the optical fiber, there is no need for the PEG-DA polymer to serve as a dye-encapsulating agent. However, the polymer has another function, namely as a means of keeping the fibers at a fixed distance from each other. Because evanescent waves are exponentially decaying[12], small changes in fiber position will potentially lead to large changes in fluorescence intensity, even without change in the analyte concentration. Therefore, locking the fibers to each other should reduce the overall variability of the sensor.

However, an argument can also be made for the removal of the polymer from the optical-fiber sensor. Addition of the polymer will cause two negative effects. The first is that the polymer may potentially block copper-sensor molecules. While this is also the case for the zinc sensor, more zinc-specific dye could be added to compensate for this. The size of the copper molecule and the length of the exposed fiber limits the number of fluorophores which can be placed on the optical fiber, so blocking of potential fluorophores might have serious implications on the copper sensor. These potential negative effects could involve the reduction of the linear dynamic range, a decrease in the sensitivity of the sensor or an increase in the response time. The decrease in sensitivity and the linear dynamic range stem from the fact that having the polymer obscure binding

sites will limit the total number of possible fluorophore-metal interactions. This will lead to a more rapid saturation of the fluorophores, truncating the linear dynamic range. Also, when fluorophore-metal interactions do occur, the change in fluorescence will be less, as some of the fluorophores are covered by the polymer and remain unperturbed by the changes in copper concentration. This reduction will result in a less-sensitive sensor. The response times may suffer as a result of the time required for the metal species to permeate the polymer to reach the fluorescent sensors. To minimize these effects and still retain the structural stability afforded by the polymer, the polymer will undergo micro-templating in the same manner as for the zinc sensor. This will also minimize the sensor-response time. The polymer consists of 60% (v/v) PEG-DA, 1% (w/v) DMPA, 5% (v/v) TPT and 35% (v/v) ultrapure H_2O.

As stated in previous chapters, the nitrogen pumped-dye laser suffers from shot to shot energy fluctuations. Coupled with the fact that the transmission capability of the optical fiber at 365 nm is reduced, this can lead to significant levels of variability when analyzing samples using the copper sensor. As a way to compensate for these combined fluctuations, 20-1000 individual data sets were internally averaged by the oscilloscope to give the compiled data point which would be used in the calculations. Four or five of these compiled data points are then averaged together per sample analyzed for all analyses of copper solutions. With a laser-pulse-repetition rate of approximately 3 - 4 Hz, 1000 data sets could require up to 5-7 minutes of collection time. Lastly, the inclusion or exclusion of the PEG-DA polymer with the crossed-fiber setup may affect the number of pulses required to obtain a stable signal. A plot of the number of pulses versus the percent relative standard deviation obtained for each pulse count was created,

for sensor junction with and without PEG-DA to determine if the use of PEG-DA would affect the number of pulses required. Figure 4.8 demonstrates that averaging 200 data point would be sufficient for data collection purposes and that the PEG-DA had no significant effect on the variability of the data sets.

After confirming successful creation of the sensor by performing a three point calibration curve with copper, the investigation transitioned to examining several key properties regarding performance characteristics of the copper sensor. The susceptibility of the fluorophore to changes in pH and temperature was investigated initially. Based on the chemical structure of the fluorophore, it was expected that the fluorophore would not undergo any change in fluorescence due to changes in pH. This is due to the lack of pH dependent sites on the molecule that are subject to protonation or deprotonation. Initially the compound appeared to suffer from a pH dependence, showing a decrease in fluorescence intensity as the pH increased.(Figure 4.9) However, work done in parallel within the Geissinger group had discovered that the PEG-DA polymer affected the fluorescence of dyes encapsulated within as the pH was changed.[12](Figure 4.10) The comparison of the trends noticed in the data led to the conclusion that the pH dependence of the copper sensor was dictated by the susceptibility of the polymer to pH fluctuations. As a result of this study, un-buffered 18 MΩ*cm water was used for all future experimentation. It was also determined that the fluorescence intensity was not significantly dependent on temperature over a range of 0 °C - 40 °C. (Figure 4.11) During the temperature-dependence measurements, the polymer was not employed on the optical fiber. Research has shown (Figure 4.12) that the polymer can affect fluorescence emissions generated from within the polymer as the temperature changes.[12] These

observations have demonstrated that the polymer will scatter less light as the temperature increases until a temperature of about 60° C is reached. After this point, the polymer begins to soften, increasing the amount of scattered light within the polymer. As such, the polymer was not included in order to determine the relationship between DDETA and temperature. It should be noted that while the data to this point suggests that the use of the PEG-DA polymer will be detrimental to the sensor performance; further examination will demonstrate the benefits of using the PEG-DA polymer.

The response time and reversibility of the sensor were investigated next. Because copper binds to the fluorophore, a means of copper removal was required in order to regenerate the sensor molecule. It was noted in the original paper that EDTA was required to remove the copper from the binding site.[1] A mild (0.05 M) solution of EDTA, adjusted to pH 9 using six NaOH pellets in order to maximize chelating potential, was used to facilitate this removal. The pH adjustment was required in order to maximize the removal efficiency by deprotonating the EDTA binding sites. As seen in Figure 4.13 the response time of a sensor without PEG-DA was less than 1 minute and the sensor exhibited the capability to be regenerated. Using a sensor encapsulated with PEG-DA caused longer response times of 3 minutes, but the sensor could still be regenerated with EDTA.

As mentioned earlier, one concern raised during the development of the copper sensor was that excitation pulses emitted at 365 nm would suffer significant intensity losses while traveling through the optical fiber. A means of correcting for this feature would be to red-shift the excitation wavelength, providing for better transmission capabilities over distances. With this in mind, four calibration curves were obtained for

four different excitation wavelengths. The same solution was used for each wavelength for each concentration of copper and the wavelengths were cycled from shortest to longest each time. Figure 4.14 demonstrates that there is a relationship between the excitation wavelength and the ability to obtain linear calibration curves. This data indicated that the excitation wavelength remains at 365 nm. The error associated with these measurements is significant. This is because initial research with the copper sensor attempted to use the same optical filter, a 515 narrow bandpass filter, that had been used for detecting the zinc sensor signal to reduce the complexity of multi-analyte analysis. However, a switch to a 500 nm long pass filter was eventually decided upon as this improved the precision during data collection.

The comparison between using a sensor encapsulated with the PEG-DA polymer against a sensor without the polymer continued by focusing on the figures of merit, including the limit of detection, limit of quantitation, and linear dynamic range. As predicted, when comparing the linear dynamic range for each sensor, the sensor which did not utilize the polymer had a linear dynamic range of 0 – 6 mg/L (Figure 4.15) with a LOD of 1.50 mg/L and a LOQ of 3.30 mg/L. Using the sensor that contained the polymer yielded a smaller range of 0-2 mg/L (Figure 4.16) but also had a LOD of 0.18 mg/L and a LOQ of 0.68 mg/L. It should be noted that EPA regulations dictate that an average of 2.07 mg/L of copper may be discharged over a 30 day period.[13]

After determining the figures of merit, characterization of the sensor's response to other divalent cations was investigated. The sensor was exposed to equal concentrations (1 mg/L) for each individual metal and the percent change in fluorescence intensity when compared to a clean solution was determined. Two effects are evident from the results

shown in Figure 4.17. The first is that the fluorophore only shows significant fluorescence quenching in the presence of copper. Secondly, the cation which causes the next largest change in signal is zinc, exhibiting fluorescence enhancement. In the original paper, DDETA showed a low affinity for zinc, demonstrating a slight change in the fluorescence intensity.[1] The literature does not provide the percent signal change observed for zinc but examination of the graphical data provided estimates that the amount of signal change is approximately equal to the values obtained here. The ability to successfully measure copper in the presence of zinc will be discussed in a later chapter.

4.6 Reference Sensor Development

As for the zinc sensor, a reference sensor was also required for the copper sensor. Quinine sulfate is often used as a fluorescence reference standard when examining other compounds undergoing excitation at 365 nm.[14] Initial investigation of quinine sulfate revealed that the fluorophore suffered from a significant change in fluorescence when exposed to divalent cations in solution. (Fig. 4.18) Because of this, the PAN encapsulation method described in Chapter 3 was employed as a means of protecting the dye from interferences. Because the amount of quinine required for a fluorescence signal strength comparable to that of DDETA had to be determined, the encapsulation process was performed three times. During each of the procedures, the amount of the fluorophore was varied. It was expected that a balance could be struck between the encapsulating ability of PAN and the fluorescence signal strength. Having a high amount of the fluorophore within the PAN would increase the overall fluorescence signal. However, having too much quinine sulfate in solution would result in the available PAN being consumed before total encapsulation of most molecules could be induced. This would

leave the dye vulnerable to exposure by any interferent when immersed in solutions of interest. Quinine sulfate masses of 5, 15 and 25 mg were used during the encapsulation process. Once the procedure was completed, fluorescence spectra of each of the encapsulated materials, as well as quinine sulfate in free solution, were collected. Each solution was then spiked with 1 mg/L Cu and the change in fluorescence recorded. It was noted that the smallest change in signal was noted for the PAN procedure which used 15 mg of quinine sulfate. (Figure 4.19) It should be noted that there was still some change in signal produced from the 15 mg sample but this is attributed to the difficulty in adding identical concentrations of PAN encapsulated material placed in the cuvette. While the PAN material was thoroughly mixed before addition, the ability to pipette identical amount into a cuvette for measurement purposes was difficult due to some of the PAN was still aggregating in solution. Also the PAN, while in solution, would begin to settle to the bottom of the cuvette. The inconsistency of this process will also influence the fluorescence signal for the PAN solution.

4.7 Sample Analysis

The final step of the copper sensor validation involved the analysis of several unknown samples. A long-term goal for the sensor described here would be to remotely deploy the sensor in environments that would make daily calibration difficult. As such, other methods of sample analysis are required. Because the fluorophore undergoes fluorescence quenching and a 1:1 complex between copper and DDETA forms, a predictive equation analogous to the Stern-Volmer relationship was sought. The equation would be modeled after equation 4.3, but K_s would be replaced by K' yielding the equation:

$$\frac{I_0}{I} = 1 + K'[Q] \qquad \text{(Eqn 4.6)}$$

To determine K′, three calibration curves were obtained for the same copper sensor array. For each of these calibration curves, the concentration of copper was plotted against the ratio of fluorescence from a clean solution (i.e. copper-free) and to that of the same solution after the addition of copper. The slope of the line provided a K′ for each day. These three values were then averaged to provide the K′ used during sample analysis.

Seven copper-containing samples were prepared by Dr. Paul Henning and the concentrations were unknown at the time of analysis. These samples were analyzed five days after the final calibration used for determining K′. No calibration of any kind was performed the day that sample analysis was undertaken. After analyzing all of the samples, the collected data was inserted into Equation 4.6 and plotted in Figure 4.20 in comparison against the expected values. Table 4.1 compares the expected of the copper concentration as supplied by Dr. Henning and the values obtained using Equation 4.6. As shown, the values obtained by the copper sensor agree well with the expected values supplied by the third party. The student's t-test demonstrated that five out of the seven calculated values were statistically indistinguishable from the prepared values. Application of the Bland-Altman test (Figure 4.21) revealed the possibility of bias due to the number of reported values lower that the expected concentrations of copper, but this error was small when compared to the actual values obtained.

In conclusion, a successful copper sensor has been created capable of monitoring environmentally relevant levels of copper. The sensor is resistant to most divalent cations and to changes in pH and temperature while offering the potential for a sensor that allows for a reduction in the need of daily calibration. Further development has afforded a reference sensor, comprising of PAN- encapsulated quinine sulfate, to provide for more reliable measurements over long distances.
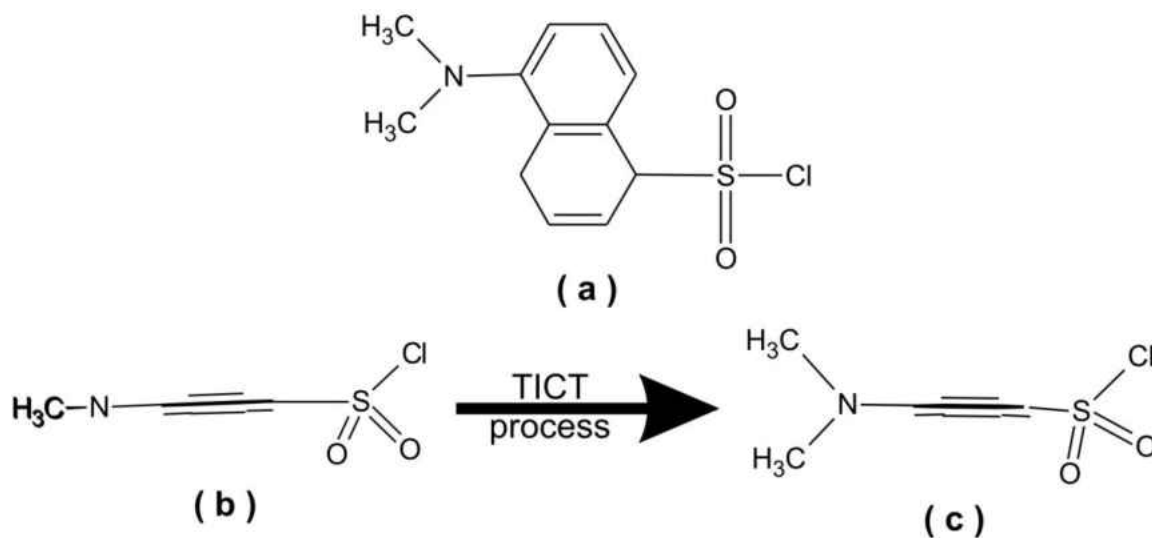
Figure 4.1 Illustration of the twisted internal charge transfer (TICT) process undertaken by dansyl chloride. Dansyl chloride (**a**) is rotated 90° around the naphthalene ring yielding a planar molecule (**b**). The TICT process yields the final spatial orientation of the amino group where the methyl groups rotate out of the plane of the ring (**c**).
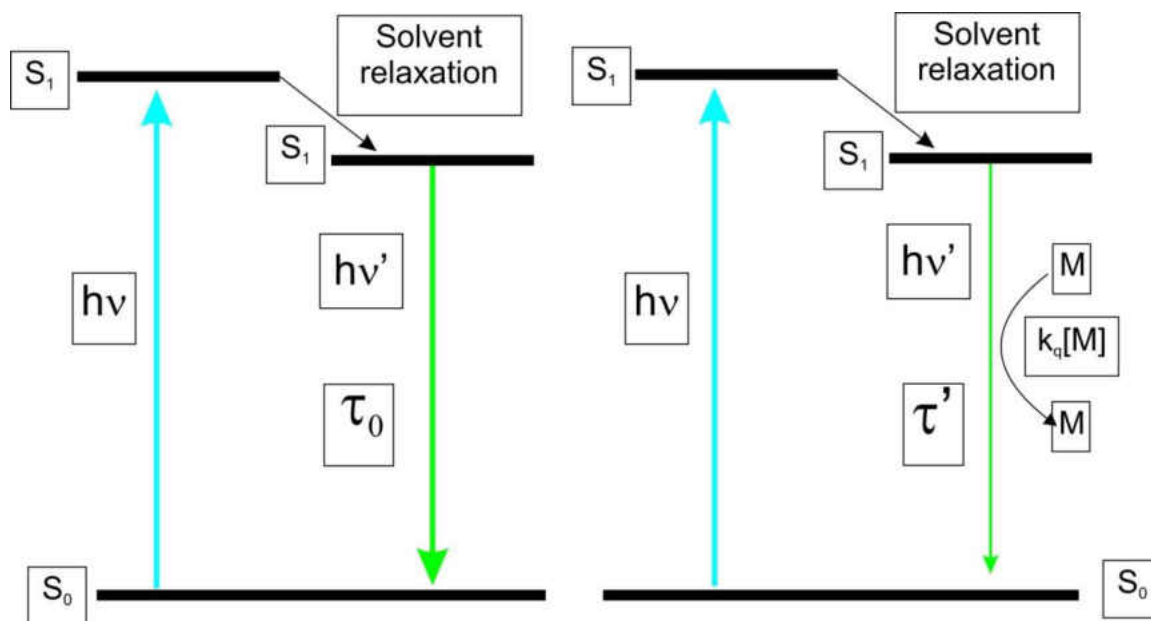
Figure 4.2 Two simplified Jablonski diagrams, where the one on the left denotes the fluorescence of a molecule in the absence of a metal species (M) acting as a fluorescence quencher. The second diagram, on the right, illustrates the process that occurs during dynamic quenching when a metal species collides with the fluorophore, partially quenching the fluorescence signal. Both examples are excited at the same wavelength (hν) and both examples fluoresce at the same wavelength (hν'). In the case of the quenched species however, the excited state lifetime of the molecule decreases ($\tau_0 \rightarrow \tau'$) which in turn causes the decrease in fluorescence intensity. The quenching is due to the metal in solution colliding with the fluorophore while in an excited state. The collision transfers some of the energy to the metal species, which is dispersed via non-radiative pathways. The rate of this transfer is described by k_q, the bimolecular quenching constant, and is dependent on the concentration of the metal quenching species [M] in solution. Figure adapted from Ref. 11
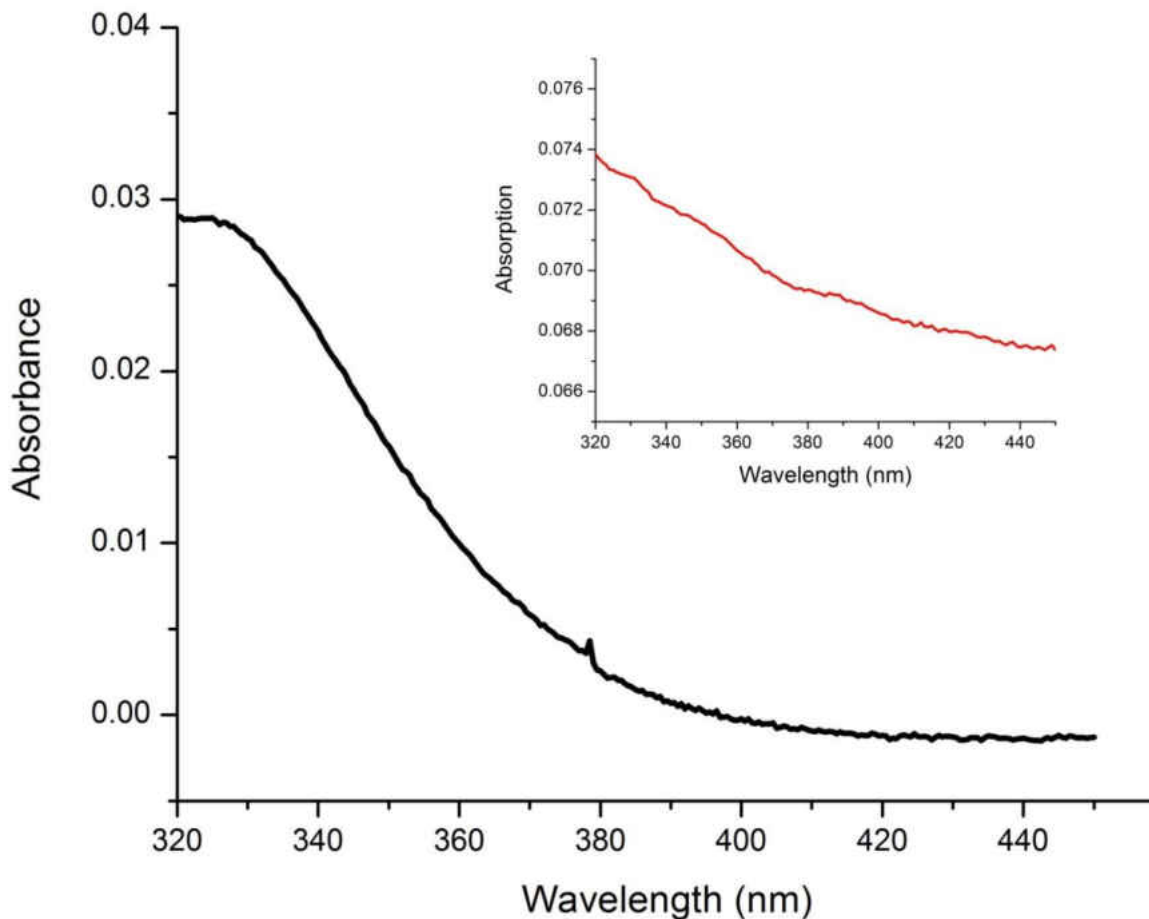
Figure 4.3 The reference-corrected absorption spectrum for a cuvette coated with the copper-specific sensor, DDETA. The peak occurring at 380 nm was attributed to a small section of the functionalized cuvette which had a slight discoloration, most likely due to contaminants on the cuvette before the synthesis of the copper sensor which could not be removed during the pre-synthesis cleaning. While the maximum absorption is observed at 330 nm, longer wavelengths will be required for analysis due to the co-absorption by silica at 330 nm. The insert above is the absorption profile of a silica cuvette, the same material as the optical fiber. The higher absorption losses observed at 330 nm support the rationale for changing the excitation wavelength. While the absorption differences were not large between 330 and 365 nm, the width of the glass used for this spectra was only 2.5 mm thick. As such, the difference in absorbance will be magnified as the lengths of fiber are increased.
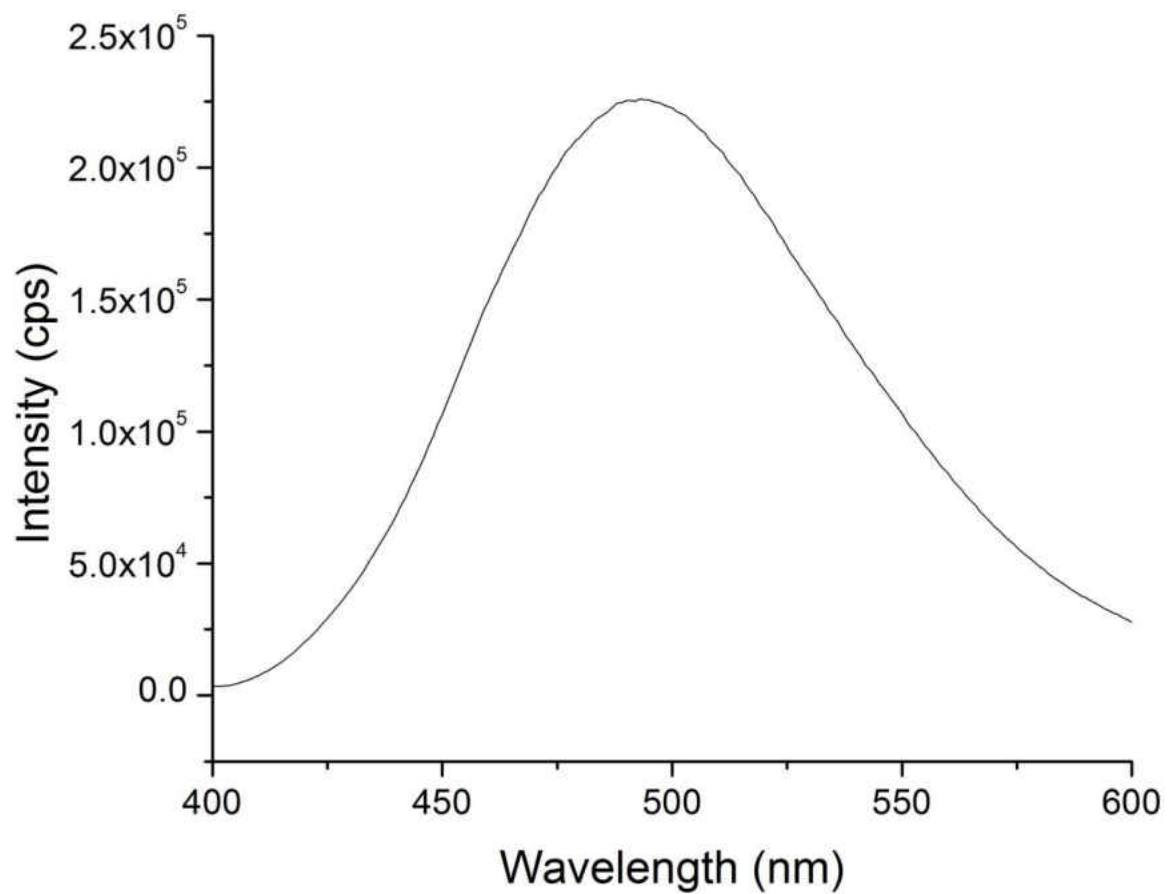
Figure 4.4 The fluorescence spectrum of a cuvette coated with the copper sensor, DDETA, where $\lambda_{ex} = 365$ nm.
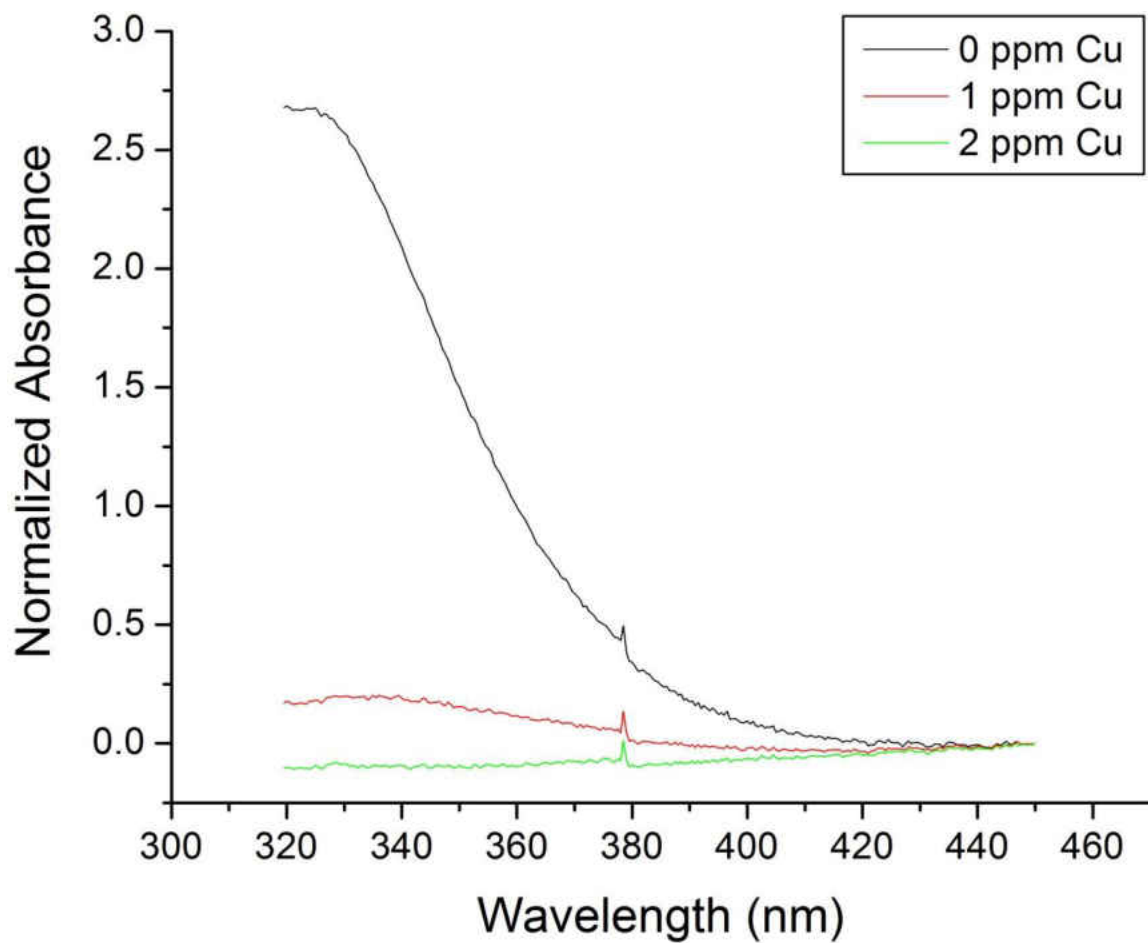
Figure 4.5 The UV-Vis absorption profile for DDETA as a function of copper concentration. The strong influence that copper exerts on the absorption profile confirms the statement that copper binds to DDETA.
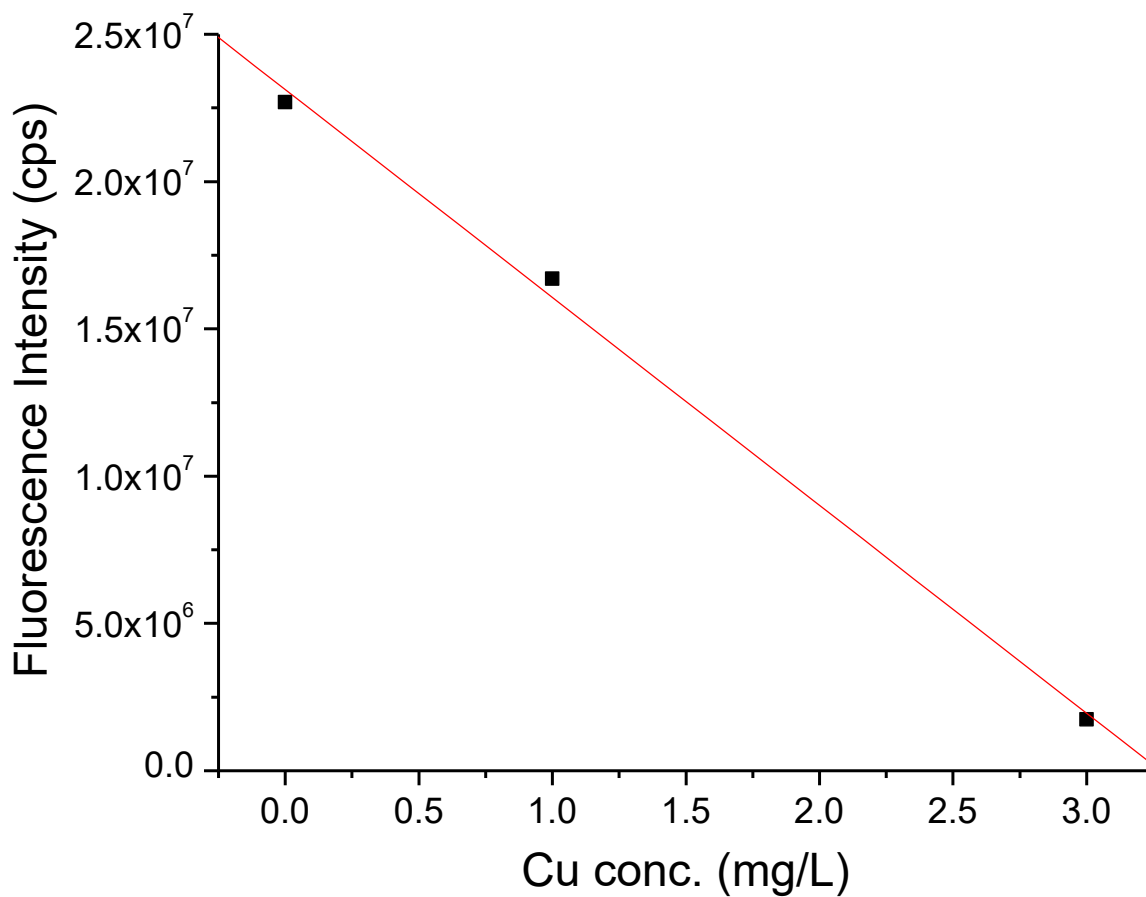
Figure 4.6 A front-face fluorescence calibration curve for copper using DDETA attached to a quartz cuvette where λ_{ex} = 365 nm. Five individual fluorescence scans were averaged internally using the software provided with the fluorimeter to yield each data point shown here. However, statistics on the replicate measurements are not provided by the software after the analysis.
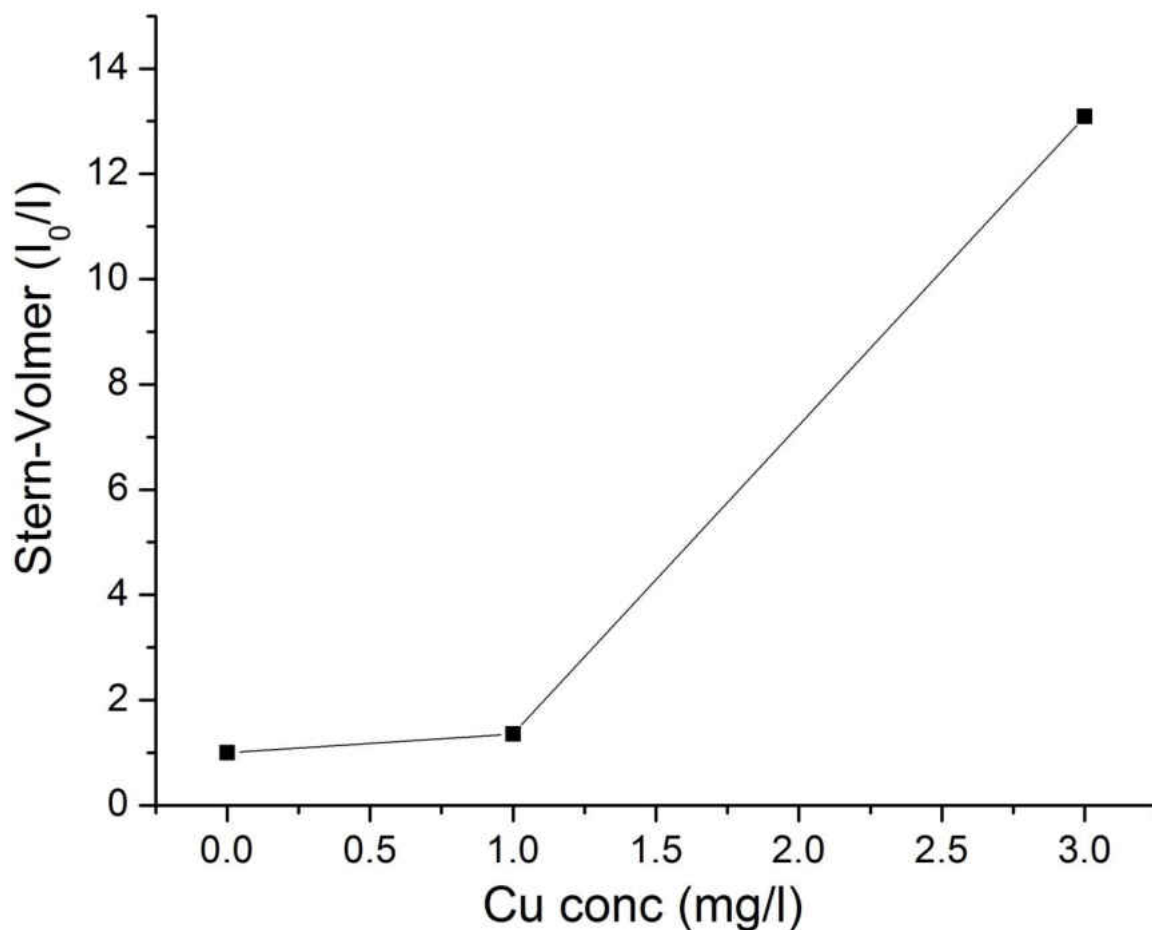
Figure 4.7 Applying the Stern-Volmer relationship to the data from **Figure 4.6** provided inconclusive results when attempting to examine the mechanism of fluorescence quenching. It is stated in literature that the binding of copper to DDETA will cause static quenching to occur.[1] However, it is still possible for collisional quenching to affect the fluorescence of DDETA. These collisions could result from unbound copper in solution colliding with, but not binding to, DDETA. Other species, such as dissolved O_2, may also cause collisional quenching.
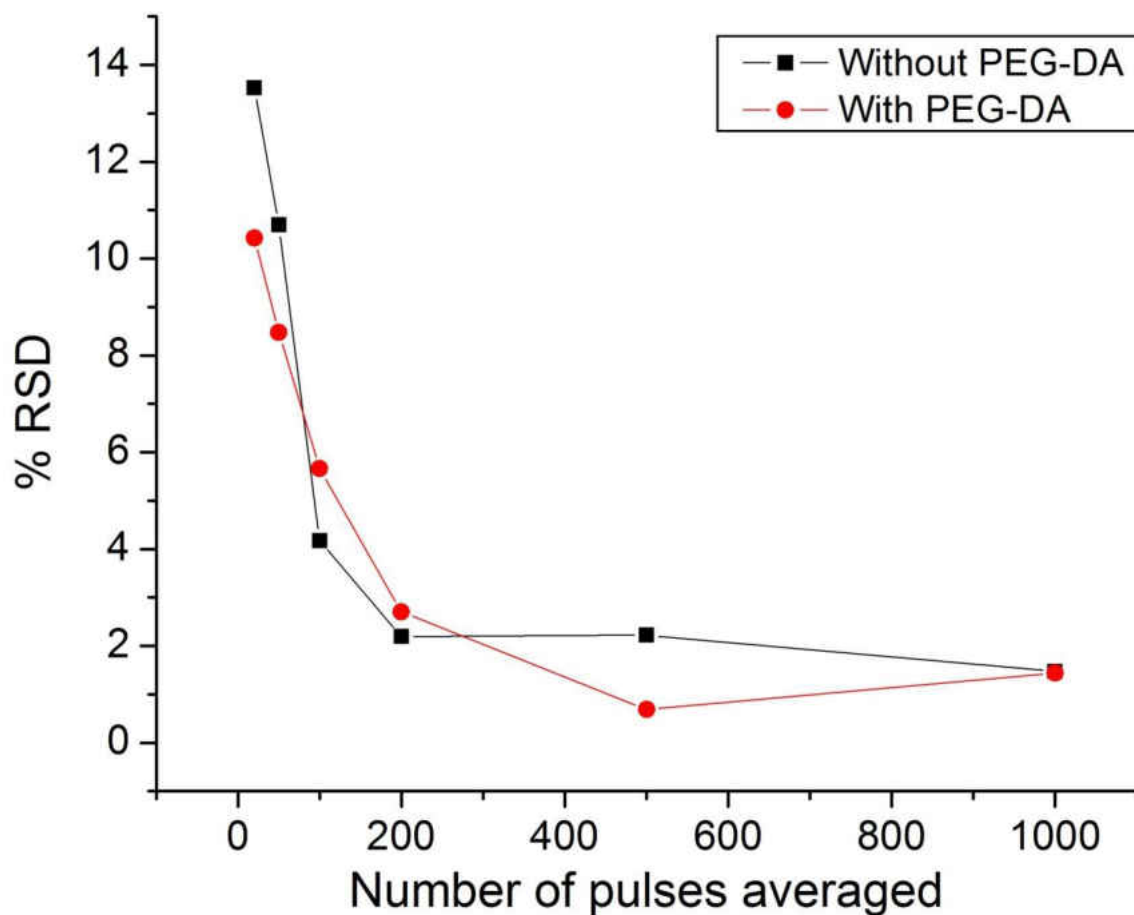
Figure 4.8 Determination of the lowest number of laser pulses required to minimize the variation occurring during data analysis. Each point plotted consists of four separate data points, where an individual point averaged the number of pulse listed on the x-axis. Any gain in precision obtained for the number of pulses internally averaged being greater than 200 are offset by the amount of time required for data collection. Therefore, the most efficient number of pulses to be averaged together will remain at 200.
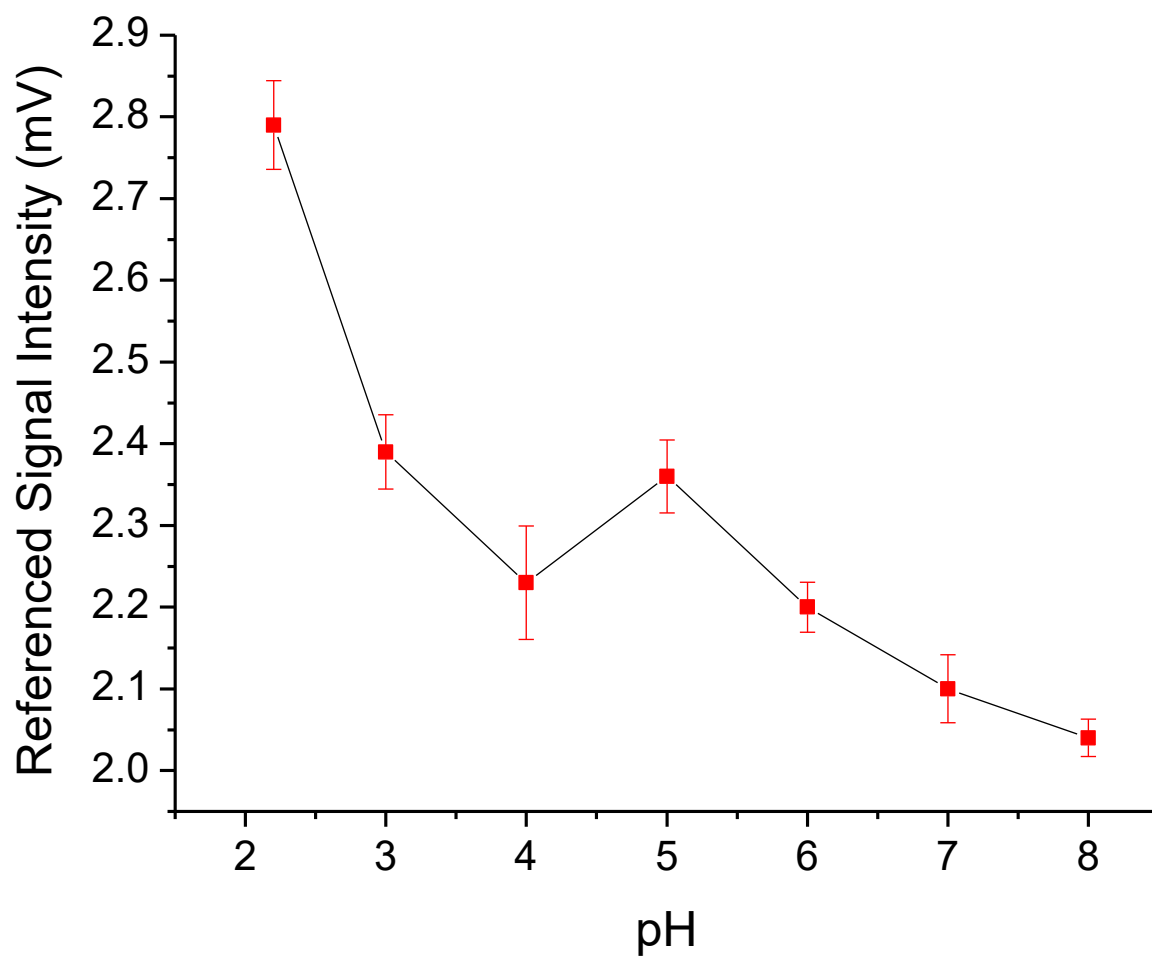
Figure 4.9 Changing the pH of a copper sensor containing the PEG-DA polymer causes a decrease in fluorescence intensity as the pH is increased.
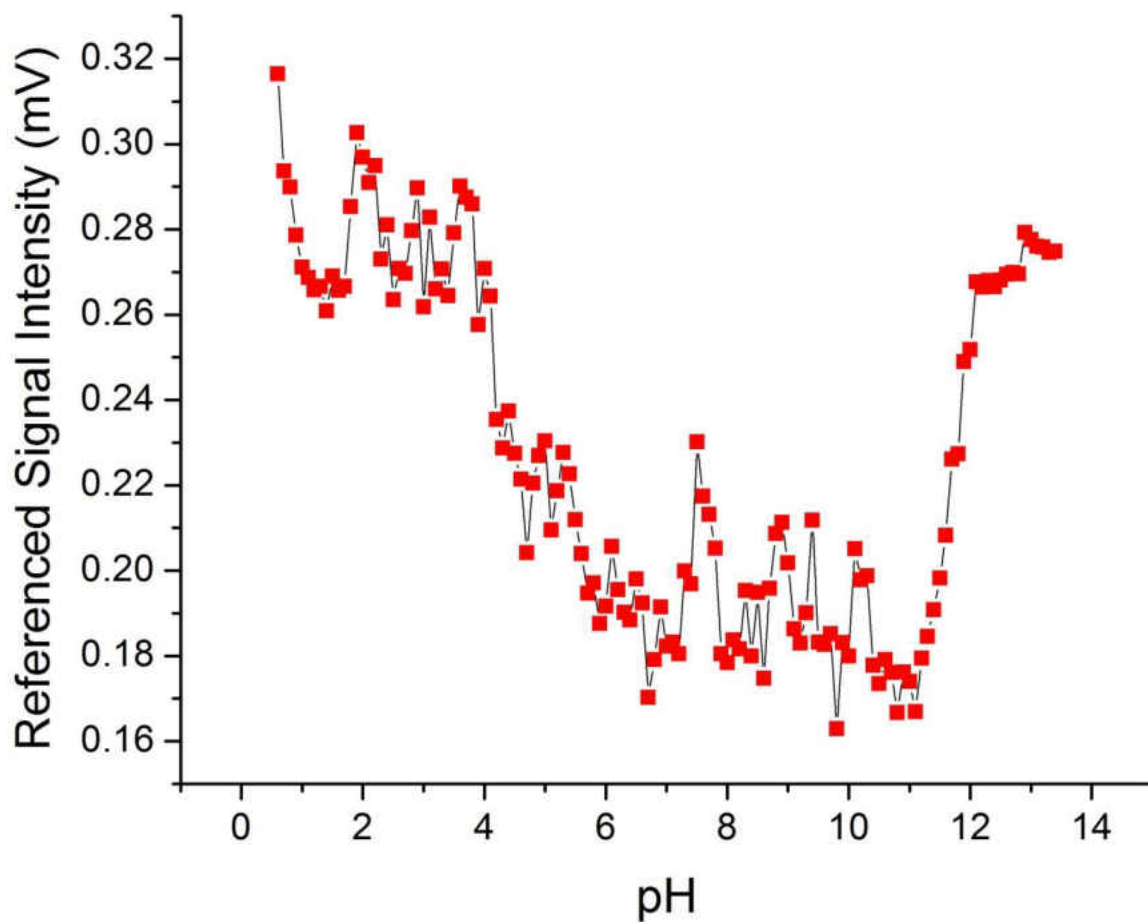
Figure 4.10 Studying the effects of pH on the PEG-DA polymer without the presence of fluorophore. The signals measured are showing the amount of light scattered within the polymer as the pH level is changed. The referenced signal refers to the ratio of pulse energies between the scattered excitation light and the pulse energy measured by the fast photodiode. Figure reprinted with permission from Ref. 12.
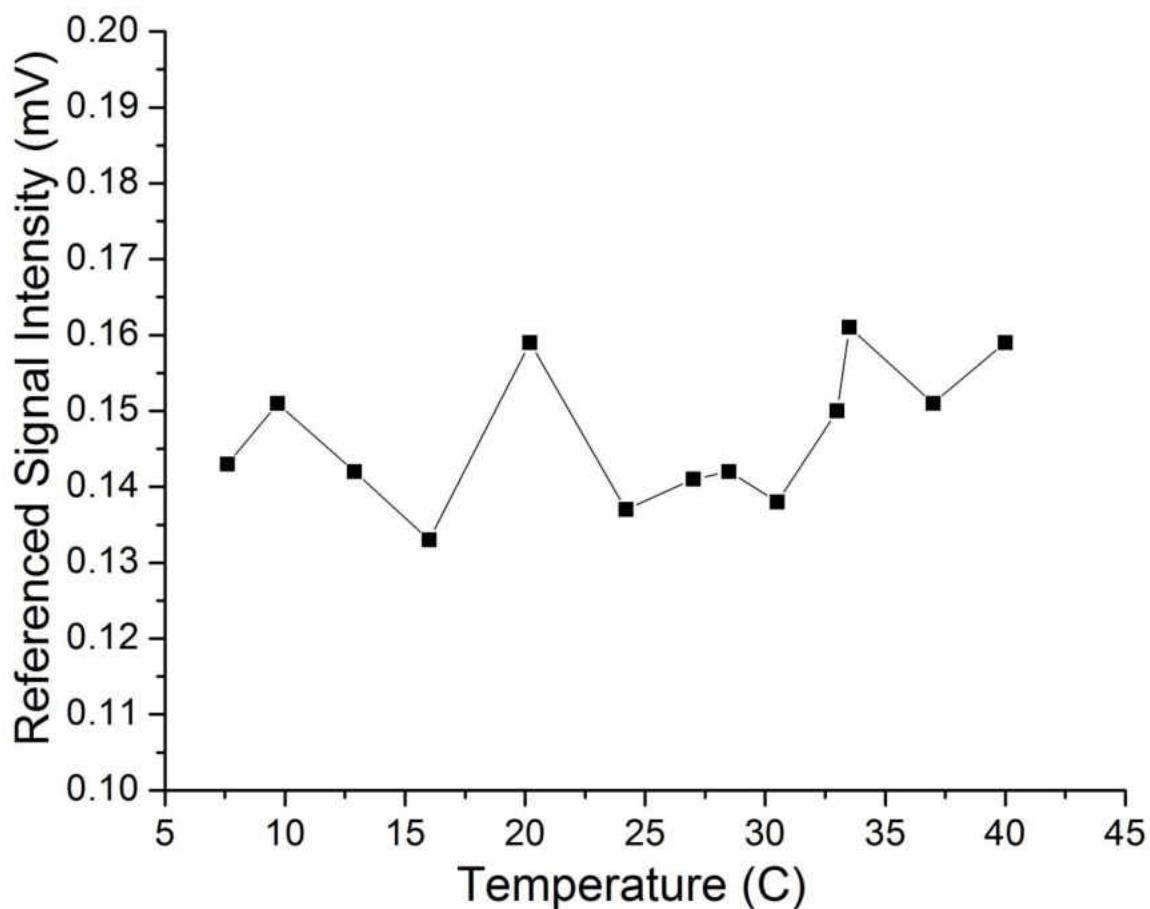
Figure 4.11 The fluorescence signal of DDETA within the optical fiber platform as the temperature is increased. PEG-DA was not included on this sensor due to a demonstrated temperature sensitivity of the polymer. One data point depicts the average of 200 individual data points, internally averaged by the oscilloscope during the data collection process. Each point plotted represents the ratio of integrated pulse energies observed for DDETA and the fast photodiode detector located near the laser.
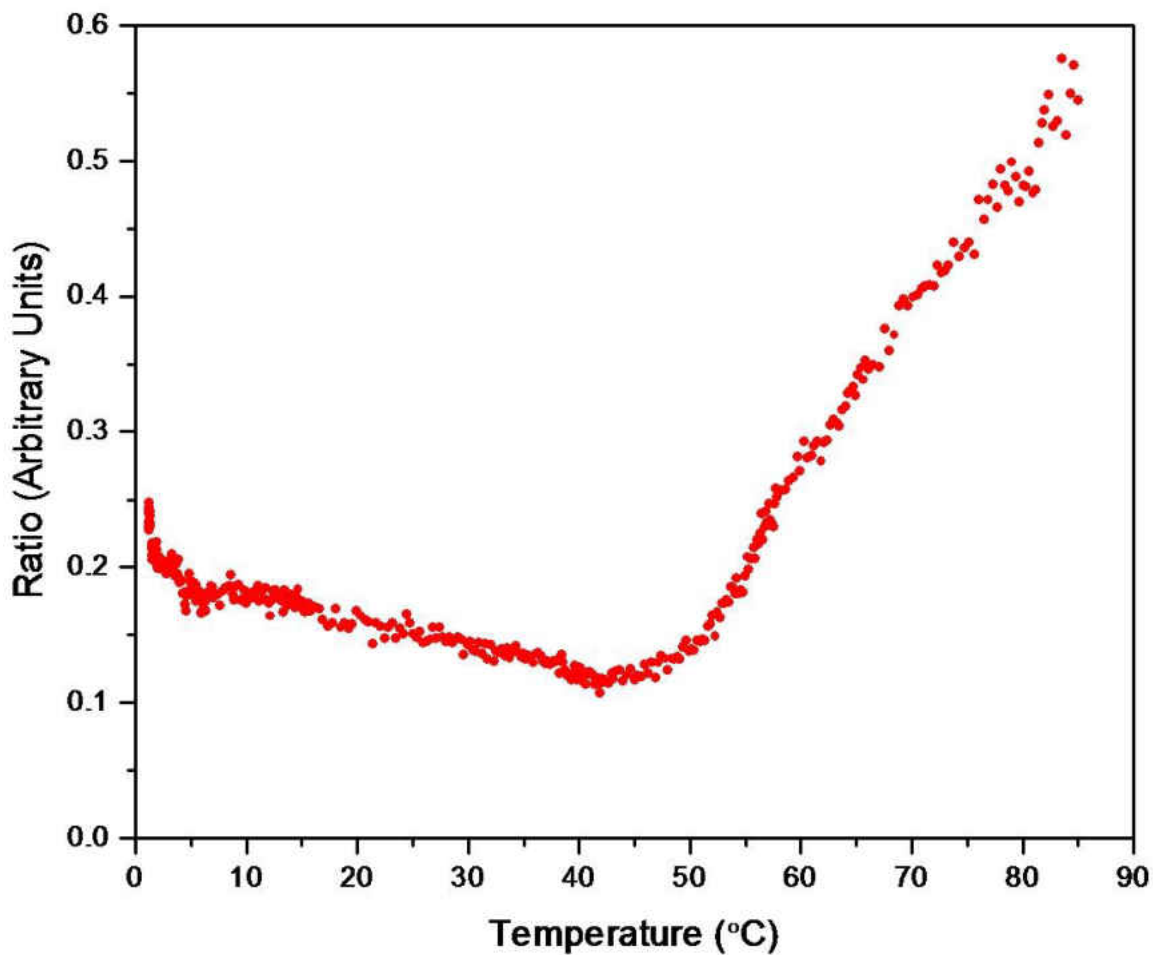
Figure 4.12 Studying the effects of temperature on the PEG-DA polymer without the presence of fluorophore. The signals measured are showing the amount of light scattered within the polymer as temperature is modulated. The ratio refers to the ratio of pulse energies between the scattered excitation light and the pulse energy measured by the fast photodiode. Figure reprinted with permission from Ref. 12.
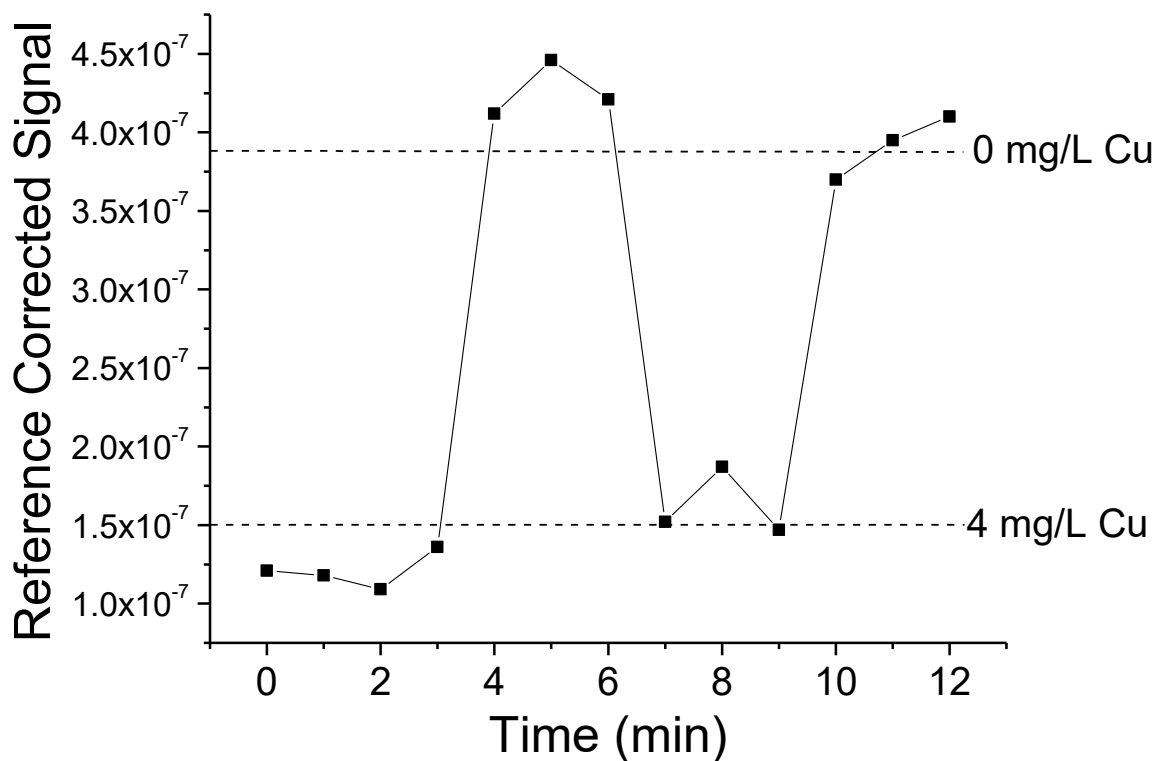
Figure 4.13 A depiction of the response time and reversibility of an optical fiber sensor containing DDETA. The reversibility was achieved by washing with a 0.05 M EDTA solution. Response times are estimated to be less than one minute, however the instrumental setup limited data collection to one point per minute. Because of this sampling rate, only one data point, representing the integrated average pulse energy, per minute was collected. Each data point represents 200 individual fluorescence pulses internally averaged by the oscilloscope during data collection.
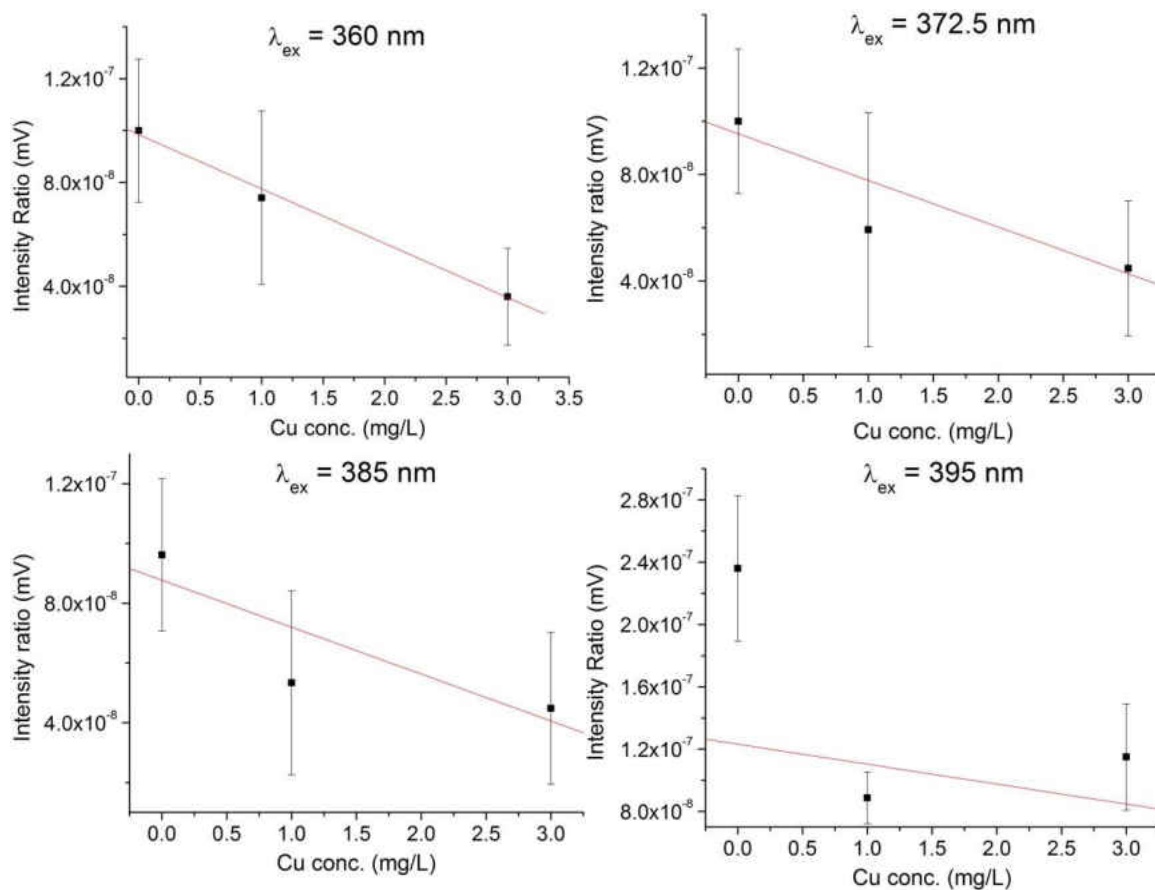
Figure 4.14 A crossed-fiber sensor containing DDETA analyzed copper-containing solutions at different excitation wavelengths. As seen, having a wavelength close to 365 provides the most linear response.
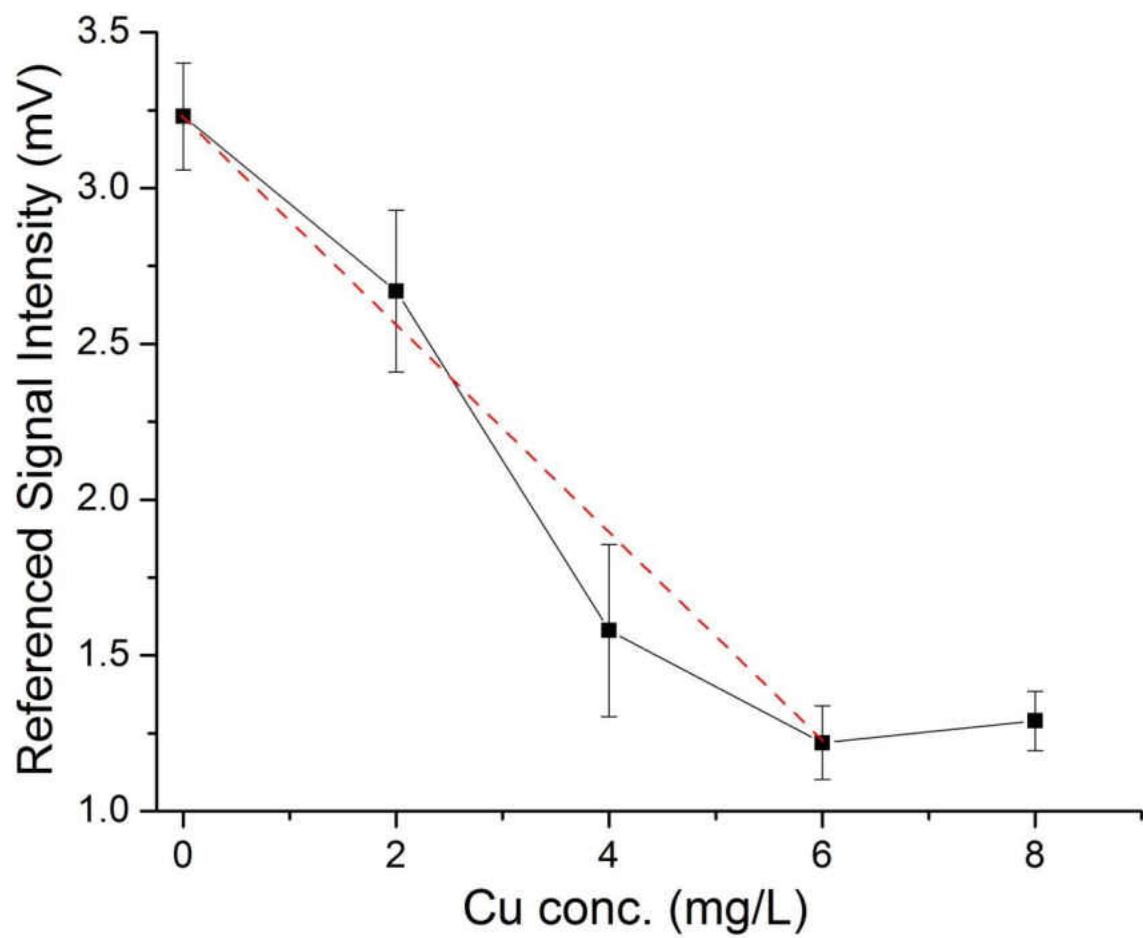
Figure 4.15 A calibration curve obtained for a copper sensor which did not utilize the PEG-DA polymer. Lack of the polymer yielded a larger linear dynamic range of 0-6 mg/L Cu.
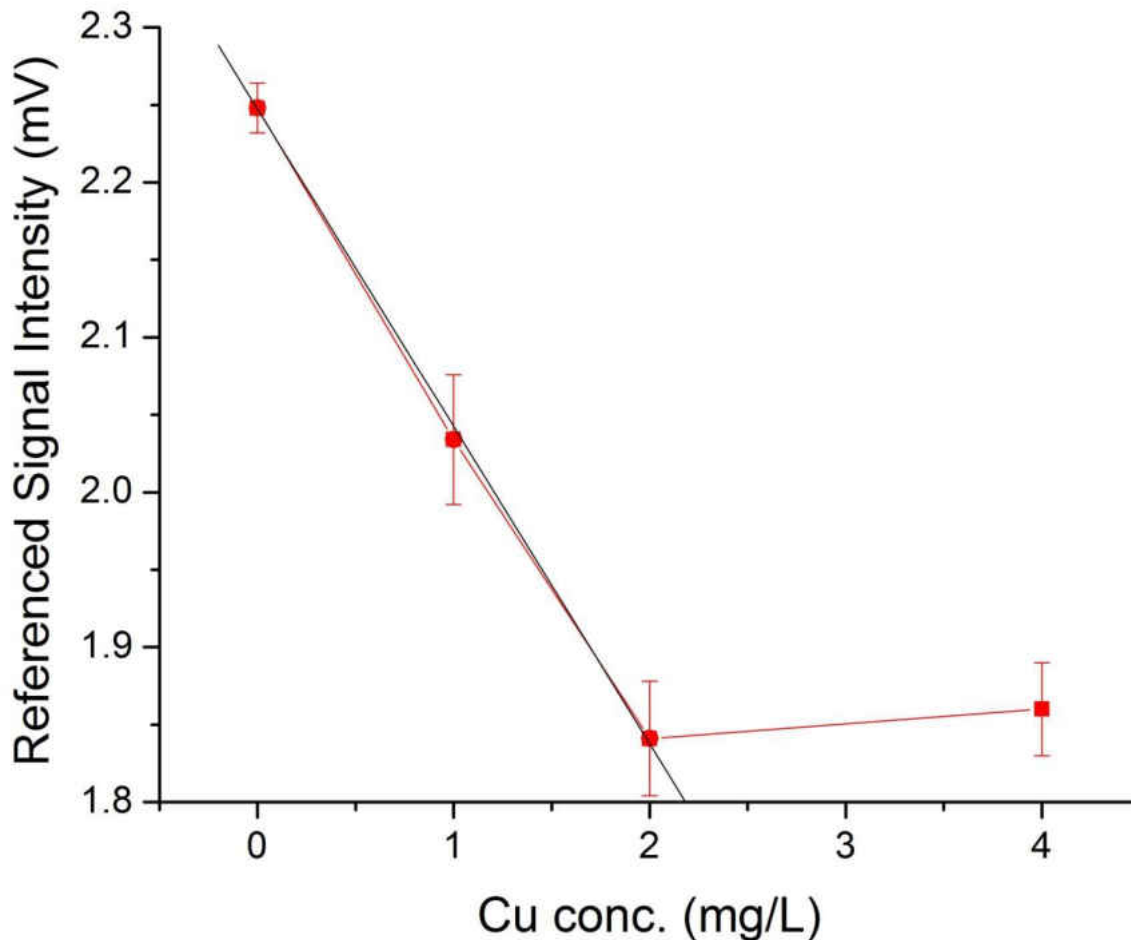
Figure 4.16 A calibration curve for a copper sensor with the PEG-DA polymer included. While the linear dynamic range is smaller, the precision of each data point is improved. The average percent relative standard deviation for the data shown here is 1.60% while the data collected for **Figure 4.16** has an average percent relative standard deviation of 9.91%. Both data sets used the average integrated pulse energy from 4 sets of 200 individual pulses to calculate each point on the plot.
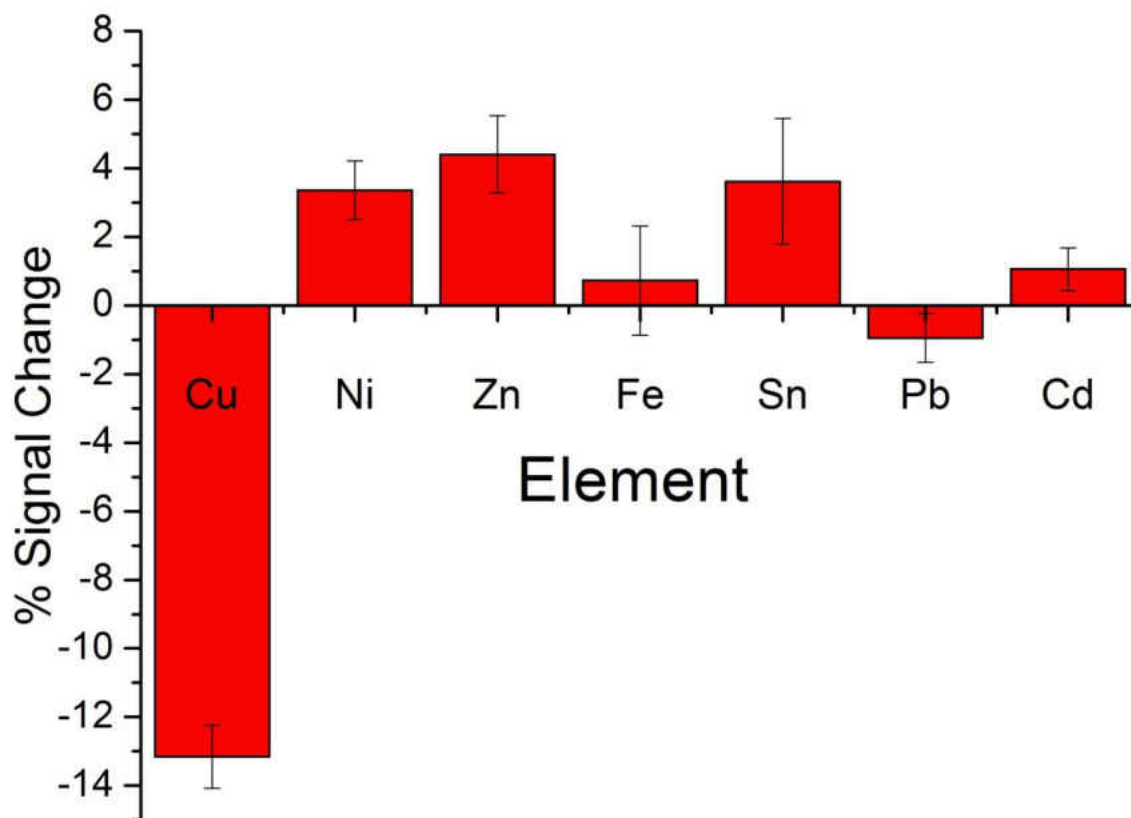
Figure 4.17 The % signal change of fluorescence that individual elements induce on the copper sensor, DDETA.
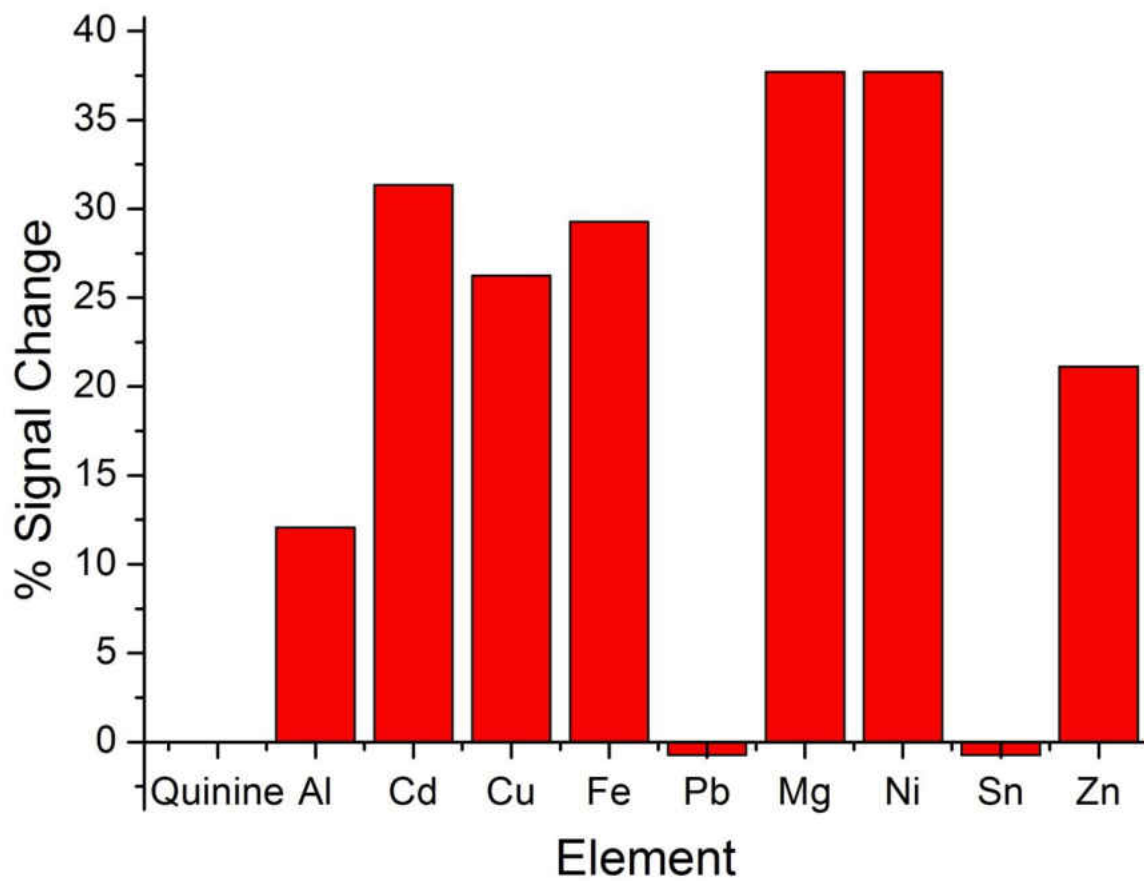
Figure 4.18 The fluorescence response of quinine sulfate, free in solution, to individual elements, each at a concentration of 1 mg/L in solution, demonstrating the need for PAN encapsulation.
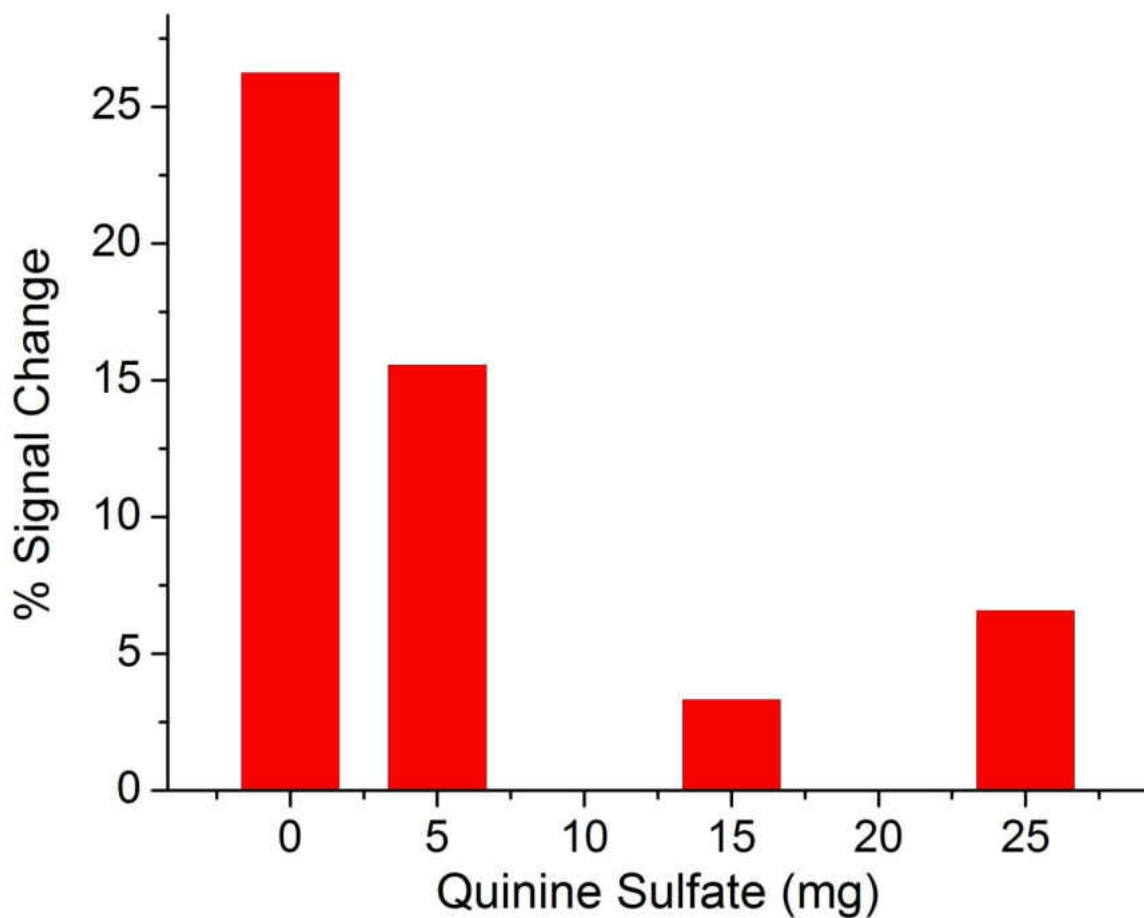
Figure 4.19 A comparison of PAN encapsulation methods. Different amounts of quinine sulfate were used during the PAN encapsulation process and these values (in mg) are displayed. The % signal change relates the change in fluorescence when the PAN encapsulated quinine was exposed to 0 or 1 mg/L of copper. The 0 mg quinine sulfate data point depicts the response noted by a non-encapsulated quinine solution.
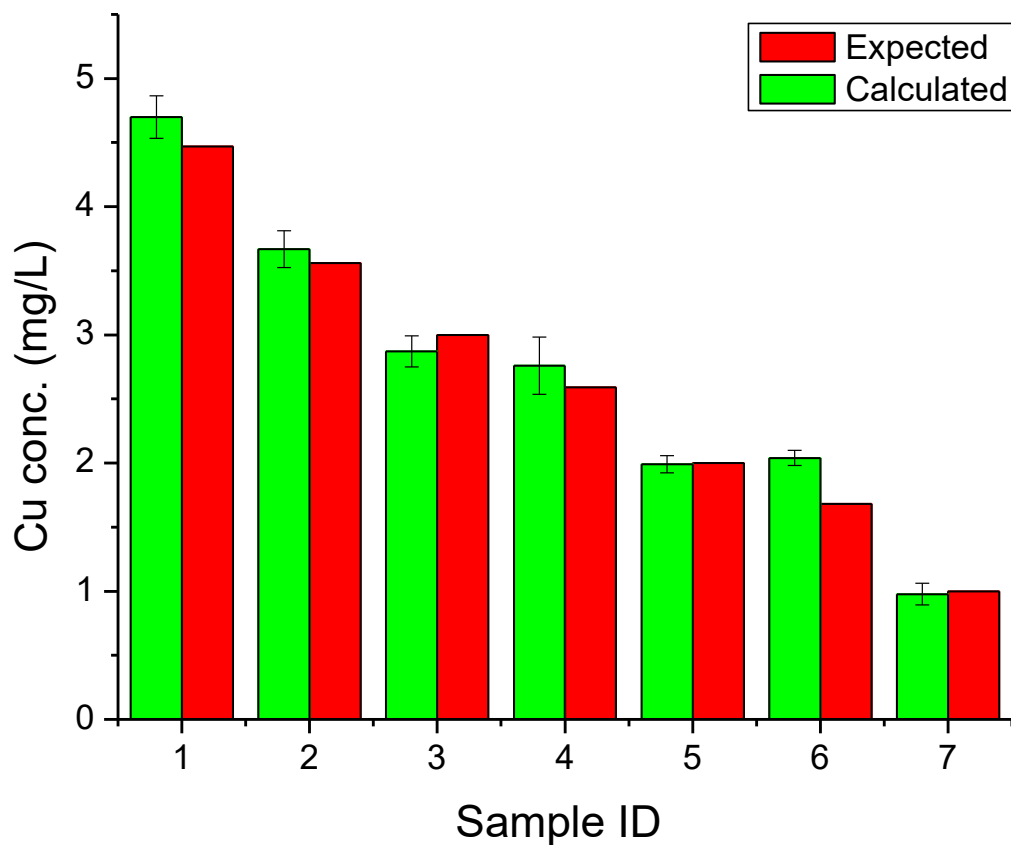
Figure 4.20 A graphical depiction comparing the copper concentration calculated using Eqn. 4.6 against the expected copper concentrations.

Expected Value (mg/L)	Calculated Conc. (mg/L)	% Error	Pass/Fail T-test
1	0.98 ± 0.09	2.3	pass
1.68	2.04 ± 0.28	21.4	fail
2	1.99 ± 0.07	0.5	pass
2.59	2.76 ± 0.20	6.56	pass
3	2.87 ± 0.12	4.33	pass
3.56	3.67 ± 0.20	3.09	pass
4.47	4.69 ± 0.16	5.15	fail

Table 4.1 A table detailing the values obtained for sample analysis by the copper sensor using Eqn. 4.6 to determine the concentrations of the samples. The pass/fail column in the table indicates if the two values (stated and derived) statistically different. A "pass" means that the two values are not statistically different indicating that use of the predictive equation to determine the concentration of copper was successful. The t-test is set at 95% confidence where N = 4.
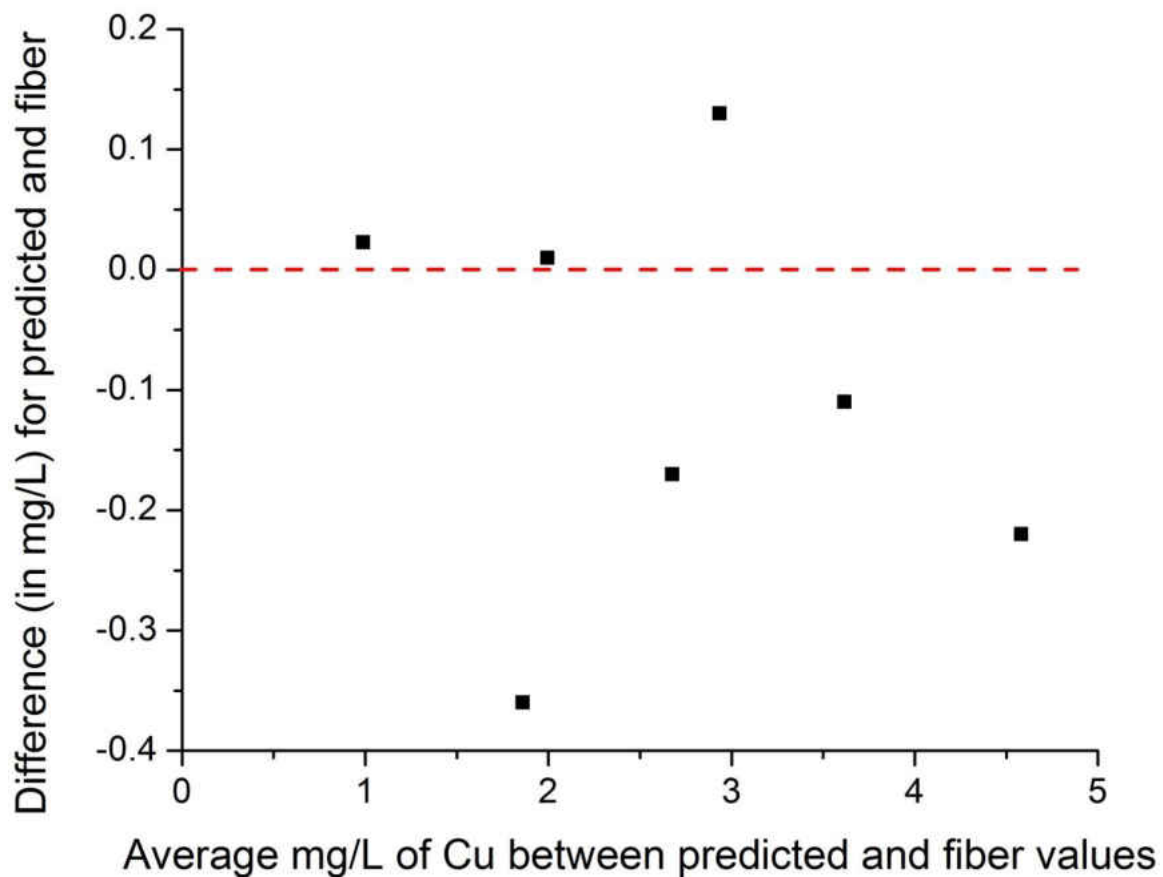
Figure 4.21 Using the Bland-Altman test revealed that there is a potential for bias when analyzing copper sensors due to the number and magnitude of samples occurring below the red line. The red line serves as a guide. If all points fell perfectly on the red line, there would be no difference in values between methods.

References

1. Ding, L., Cui, X., Han, Y., Lü, F., Fang, Y. Sensing Performance Enhancement via Chelating Effect: A Novel Fluorescent Film Chemosensor for Copper Ions. *J. Photochem. Photobiol., A*. **2007**, 1*86*, 143

2. ThorLabs. http://www.thorlabs.us/Thorcat/12200/BFH48-1000-SpecSheet.pdf (Accessed 2/23/13)

3. Hoytink, G. Intermolecular electron exchange. *Acc. Chem. Res.***1969**, *2(4)*, 114

4. Yoon, J., Ohler, N., Vance, D., Aumiller, W., Czarnik, A. A Fluorescent Chemosensor Signalling only Hg(II) and Cu(II) in Water. *Tetrahedron Lett.* **1997**, *38(22)*, 3845

5. Anaspec. http://anaspec.redwhale.com/products/product.asp?id=28807 (Accessed 2/18/13)

6. Valuer, B., *Molecular Fluorescence Principles and Applications*. Wiley-VCH: New York, 2002

7. Bartzatt, R. Fluorescent labeling of drugs and simple organic compounds containing amine functional groups, utilizing dansyl chloride in Na_2CO_3 buffer. *J. Pharmacol. Toxicol. Methods*. **2001**, *45*, 247

8. Weber, G., Borris, D. The use of a Cholinergic Fluorescent Probe for the Study of the Receptor Proteolipid. *Mol. Pharmacol.* **1971**, *7*, 530-537

9. Nakayama, K., Endo, M., Fujitsuka, M., Majima, T. Detection of the Local Structural Changes in the Dimer Interface of BamHI Initiated by DNA Binding and Dissociation Using a Solvatochromic Fluorophore. *J. Phys. Chem. B*. **2006**, *110(42)*, 21311

10. IUPAC. Compendium of Chemical Terminology, 2nd ed. (the "Gold Book"). Compiled by A. D. McNaught and A. Wilkinson. Blackwell Scientific Publications, Oxford (1997)

11. Lakowicz, J. *Principles of Fluorescence Spectroscopy*. 3rd ed. Springer: New York, 2006

12. Messica, A., Greenstein, A., Katzir, A. Theory of fiber-optic, evanescent-wave spectroscopy and sensor. *Appl. Opt.*, **1996**, *35(13)*, 2274

13. Henning, P. University of Wisconsin-Milwaukee, Milwaukee WI. Unpublished work, 2012

14. U.S. Environmental Protection Agency. Electroplating and Metal Finishing Point Source Categories; Effluent Limitation Guidelines, Pretreatment Standard and New Source Performance Standards. *Federal Register*. **1983**. *48*(137), 32462-32488

15. *A Fluorescence Reference Material*; National Measurement Laboratory, U.S. Dept. of Commerce; Washington DC, 1980

Chapter 5

Four Sensor Array Development and
Characterization

5.1 Introduction

The ability to analyze for more the one compound simultaneously or the same compound at several points with a multi-sensor array has several advantages. Multi-component analysis can shorten total analysis time significantly, reduce reagent consumption and reduce the cost required for analysis. A multi-sensor array, either by determining one analyte at several points or providing multi-analyte capability, also has the ability to provide longitudinal data. This type of data collection can be used to provide the spatial distribution of an analyte. This has potential applications in several areas, ranging from monitoring industrial processes at various locations to monitoring natural waterways at set intervals. Over the past ten years, several different multi-analyte sensors have been developed.[1] For example, sensors capable of analyzing temperature, oxygen, pH and carbon dioxide have been combined in a variety of ways, allowing for the simultaneous measurement of two, three, or even four analytes.[2-5] Another area of interest is to develop sensors capable of sensing biological materials. Along the same lines a nine-analyte system has been developed to test for the presence of various types of bacteria on a solid waveguide structure.[6] However, research to develop a functional optical-fiber-based dual-analyte array for transition metal species has not yet been described. However, in this research, a four-sensor array has been developed that is capable of monitoring both zinc and copper simultaneously. These sensors are paired with another crossed-fiber junction serving as an intensity reference, using the compounds developed in earlier chapters.

5.2 Sensor construction and platform integration

Due to the increase in the number of sensors regions required for the four-sensor array, it was deemed impractical to continue using the polypropylene blocks previously employed to house the optical fibers. The space between each sensor region needed to accommodate the polymer blocks made the fibers more susceptible to breaking while other cladding sections were being removed or during the block assembly process. A flat plastic slab with the dimensions of 9" × 9" × 0.5" with drilled 0.5" diameter holes was therefore employed instead. The holes were drilled to create a 5×5 array, yielding a platform capable of housing 25 sensor regions. (This slab was created by Dr. Paul Henning during an earlier research project and was repurposed for this research.) The stripped optical fibers were placed on the platform and then secured down with segments of cellophane tape between each sensor region. This prevented bending or slipping of the sensor regions, effectively replacing the individual block design. Each bare fiber section was positioned over a hole in the plastic slab to allow solution and analyte access. The optical fiber sensors on the slab were immersed in a 9"×13" Pyrex® baking dish. Even after immersion in water, the cellophane tape provided sufficient adhesion to keep the fiber immobilized. The tight fit between the plastic slab and baking dish also served to eliminate the possibility of the slab from twisting, turning or sliding in solution. Because the emission fibers were of differing lengths (1, 15, 25 and 35 m), the excess fibers were looped around a ring stand to keep them from becoming entangled with each other. The four emission fibers had the cladding removed at the distal end of the fiber with a fiber stripping tool, exposing about two inches of fiber cores. This reduced the diameter of each fiber and allowed all four fibers to be bundled into one temporary SMA connector

with coupling to the PMT. While this was sufficient for a four-sensor array, any further increase in the number of sensors will require a new coupling process, as the SMA connector will have too small of a diameter to accommodate the additional fibers.

Before construction of the array is undertaken, the order in which the sensors will be placed on the array requires attention. There are two issues that must be considered when determining sensor order. The first is the question of which sensors should be placed closest to the source of the excitation pulses. This consideration needs to be dictated by the transmission capability of the fiber. The excitation wavelength which suffers the most attenuation losses within a fiber should be required to transit the smallest length of fiber in order to reach the sensor regions. This will minimize the decrease in the excitation pulse energy, thus providing more energy for the excitation of the fluorophores located at the sensor and reference regions. Literature from the manufacturer states that the fiber used to connect the excitation source to the sensor regions has an attenuation of approximately 150 dB/km for radiation emitted at 365 nm.[7] Pulses generated at 495 nm have an attenuation of only 10 db/km, which represents a significant improvement in the transmission capability of the fiber. Coupled with the energy loss due to attenuation, some of the energy will be absorbed by fluorophores located at a sensor region as an excitation pulse passes through, even if this is not a region of interest. This absorption will occur at each sensor region, creating a cumulative effect for sensors at the end of the array. Since pulses at 495 nm experience lower levels of attenuation, these pulses will be able to better accommodate these losses and still provide sufficient energy for excitation of the desired sensor regions.

The second issues concerns which sensor requires the shortest (or longest) emission fibers. This decision is closely related to the rationale for determining which regions will be located closest to the excitation source. Because the copper-specific and reference fluorophores will experience weaker excitation pulse energy than FZ-1 and Dragon Green, the amount of fluorescence generated will also be less. Another factor that will influence the fluorescence intensity generated by each fluorophore is the fluorescence quantum yield. Although literature values do not exist for three of the four compounds studied here, a comparison may still be made. Quinine sulfate, a commonly used quantum yield standard, has a quantum yield of 0.54.[8] This is much less than 2',7'-difluorofluorescein, the fluorophore analogous to FZ-1 from Chapter 3, which has a quantum yield of 0.92.[9] The difference in quantum yield shows that quinine sulfate will probably produce lower fluorescence energies for equal pulse energies, when compared to FZ-1.

After taking both of these design elements into consideration, the optimal order for the four-sensor array will consist of having the copper-specific sensor and respective reference located first and second with respect to the excitation source. This sensor and reference pair will also have the shortest emission fibers in order to maximize the amount of fluorescence reaching the detector.

Although the overall order of the sensors is important, the order between the reference and analyte-specific sensor must also be considered. To provide an accurate account of the changes in excitation energy, the reference sensor should precede the metal-sensitive sensor. If the metal-specific sensor were to be excited first, absorption losses by the fluorophore and light scattering by the polymer will occur. These factors

may obscure small shifts in the pulse energy that the reference sensor is designed to measure. For the zinc-specific and reference pair, this arrangement is possible. However, this arrangement was not possible for the copper-specific and its reference sensor regions. As stated earlier, the copper sensor requires significant bending of the fibers to undergo the synthesis process. This required that the copper sensor be created first. The cladding for the other three sensor or reference regions were not removed until after the copper sensor was created. Because of this fact, the copper sensor was separated from the other sensor regions by approximately twelve inches to prevent the Bunsen burner from thermally decomposing the copper sensor region. Several unsuccessful alternatives involving the quinine sulfate reference sensor placement were investigated before placing the copper sensor first in the array arrangement. To avoid the thermal decomposition of the copper-specific sensor, the distance between the reference and sensor regions was increased to approximately 1 foot instead of the 2 inches between normal sensor regions. The zinc sensor was still located after the copper-specific sensor but with a similar separation length from the copper-specific sensor. The increase of the distance between the sensor regions induced a much higher incident rate of fibers breaking during the cladding removal process. The metal template used to expose the fiber core would cause the fibers to bend or bow and often resulted in a breakage of one of the already exposed regions. As the copper sensor required a minimum of four days to synthesize, this method for fiber arrangement was discarded as an inefficient use of time. Longer excitation fibers may have addressed the breakage issue; however, with the degree of fiber attenuation occurring at 365 nm, increasing the length of the excitation fiber would have an adverse effect on the pulse intensity. These two factors led to the

reversal of the order for the sensor pair whereby the copper-specific sensor was excited first followed by the reference sensor. The results of this approach will be discussed shortly.

5.3 Four sensor development

One of the major concerns with developing a four-sensor array is minimizing the amount of scattered radiation as a pulse travels through each sensor region. This issue is controlled principally by altering the composition of the PEG-DA polymer. Initial sensor work involved using a polymer that contained 25 % TPT. Although this is an effective tool to reduce the rate of dye leaching, the amount of light scattering due to the higher refractive index of the polymer is significant and could reduce the excitation intensity to a point where the third or fourth sensor may not be sufficiently excited. As such, the amount of TPT was reduced to 5% and ultrapure water was added to make up the difference.

A four-sensor array was developed with each sensor containing 10% of FZ-1. There were several reasons why FZ-1 was chosen for all four sensors regions during the first design. First, FZ-1 was the only fluorophore which could be completely dissolved within the polymer while the polymer was still a liquid. Both Dragon Green and the PAN-encapsulated quinine sulfate are comprised of insoluble polymer beads, which prevented the integration of identical amounts of either compound into multiple sensor regions. In a liquid polymer stock solution, both of these compounds tend to aggregate eventually yielding un-equal amounts of fluorophore in different sensor regions. Allowing for complete dissolution yielded four sensor regions, which would have equal

amounts of fluorophore located within. This would remove differences in fluorophore concentration as a source of changes in fluorescence intensity of any of the sensor regions. Secondly, FZ-1 is excited at 495 nm, which has already been established as the excitation wavelength that suffers from smaller attenuation losses over the same distances than excitation pulses generated at 365 nm. The increase in excitation pulse strength reaching the sensor regions would provide the best chance of exciting all of the sensor regions. Lastly, of all the fluorophores used in this research, FZ-1 demonstrated the strongest fluorescence on the crossed-fiber sensor platform.

The setup consisted of one excitation fiber that was used to connect the four sensor regions. Four individual fibers with lengths of 1, 15, 25, and 35 m were used to collect the fluorescence signals. These four fibers had all cladding and buffer materials physically removed from the tips of the fibers, exposing the silica cores and all four were then bundled together within a temporary SMA connecter. This prevented the fluorescence from one sensor region from traveling through another sensor region. This is desired because the fluorescence signal will scatter or possibly be re-absorbed as it passes through other sensor regions when only one fiber is used to collect the fluorescence emission of all the sensor regions. As the interest of this initial study was to develop four sensors in one array in which all four sensor regions had fluorescence signals perceived by the detector, no reference sensors were included in the design. The fast photodiode detector was only employed to provide to mark the time at which the laser fired.

Two different methods of excitation were investigated. The first coupled the excitation light into the sensor array so that the sensor with the shortest emission fiber

was excited first. The second coupled the excitation source to the sensor array so that the sensor connected to the longest emission fiber was excited first. As shown in Figures 5.1 and 5.2, exciting the sensor with the shortest emission fiber does not provide enough excitation power for the fluorescence of the last sensor to be collected by the PMT. However by having the strongest excitation pulses interact with the sensor having the longest emission fiber first, the fluorescence for all sensors are recognized by the detector. The length of the emission fiber required that these be looped around a support system. These loops induce transmission losses within the fiber, and confirm that coupling the source to the sensor where the fluorescence must travel the longest distance is the proper approach. Previous data from the development of two- sensor arrays had shown that sensors excited later in the array would generate weaker signals. However, this was not observed for the four-sensor array when the excitation order was reversed (longest to shortest emission fiber). Instead, the variance in signal was attributed to the coupling efficiency and the variability within different sensor regions.

After confirming that a four-sensor array was feasible with one metal-sensing fluorophore, a new sensor array was created. This new array contained all of the fluorophores – both the analyte-specific and reference compounds – investigated during the course of this research. The order of the sensors, starting with the sensor located closest to source, was as follows: the copper-specific sensor (DDETA), copper reference sensor (QS), zinc reference sensor (Dragon Green) and ending with the zinc-specific sensor region (FZ-1). To ensure maximum fluorescence signal, the excitation source was coupled to the end of the array closest to the sensor regions of interest. The sensors were placed in a pH-5.5-buffered solution to maximize the zinc sensor signal. Figure 5.3

shows that all four of the sensor regions demonstrated measureable amounts of fluorescence that were successfully resolved in time. There are a few points to discuss regarding this figure. First, the data points displayed in Figure 5.3 are a combination of two data sets. Because two different excitation wavelengths were required, the data had to be collected in two halves. The first two data points, corresponding to the copper-specific sensor and reference with excitation occurring at 365 nm, were collected first. The second half, corresponding to the zinc-specific sensor and reference with excitation occurring at 495 nm, was collected immediately following the conclusion of the copper analysis. The order of data collection was chosen arbitrarily but was kept constant during all further investigations. The two portions of the data were then combined to yield Figure 5.3. It should be noted that no settings were changed on the oscilloscope when changing the excitation wavelength. When looking at Figure 5.1, it is observed that the first peak detected is truncated, indicating that the measurement scale for that particular peak was too small and required adjustment. This is a correctable feature, but it is possible that a weak fluorescence signal will be obscured and left unrecorded during this process. However, for Figure 5.3 all of the fluorescence signals were generated at similar intensity levels, requiring no scale adjustment.

There are two ways to corroborate that the peaks from the oscilloscope trace were fluorescence signals generated by the sensor regions. By placing an optical filter in the path between the fiber and detector, any scattered excitation light should be removed. Secondly, the relationship of a peak to the neighboring peaks on the oscilloscope trace in time can be used to calculate the length of optical fiber between adjacent sensor regions. While the discussion below may appear to indicate the presence of only one emission

fiber connecting all of the sensors, each of the peaks analyzed to produce Table 5.1 were collected from sensors with an individual, dedicated emission fiber. To perform these calculations, the speed of light within the fiber must be estimated. Knowing the speed of light in a vacuum (c) and the refractive index of the core of the fiber (1.46) provides the means to determine the speed of light (v) in an optical fiber via Eqn. 5.1.[10]

$$\frac{c}{\eta_{core}} = v \qquad \text{(Eqn 5.1)}$$

After determining the speed of the light in the fiber (2.03×10^8 m/s), the difference in time (Δt) between sensor regions is calculated from the Figure 5.3 by measuring the point of the peak with respect to time for the sensors and taking the difference between two sensor regions. Using the relationship between speed and time yields the difference in length of the emission fiber between adjacent sensor regions. To calculate the total length of a certain emission fiber, the difference in time between when the first sensor's fluorescence signal is recorded and the response of the sensor of interest will be calculated. This difference in time is used to calculate the difference in length of the two emission fibers. As the first emission fiber is less than one meter long, the difference in length will provide a direct estimate of the overall length of the emission fiber attached to the sensor of interest.

A summary of this information is provided in Table 5.1. While these values are an approximation, the difference between the measured distance and the calculated distance only differ by 3% at most. This is not definitive proof of sensor fluorescence, but when combined with the features designed to prevent scattered excitation light from reaching

the detector (i.e., crossed-fiber sensor, optical filter) it provides a strong argument that the data observed is the fluorescence signal from the fluorophores.

The last step for verification of the four-sensor array was to perform measurements of zinc and copper within the same solution in a quasi-simultaneous manner. Zinc and copper were added at the same time to three liter, pH-5.5-buffered solutions. Once again, the choice was arbitrarily made to determine copper first, followed by zinc determination. Transitioning between detection of the analytes involved changing the excitation wavelength of the nitrogen-pumped dye laser and relocation of the excitation fiber coupling to the end of the excitation fiber closest to the zinc sensor pair while leaving the sensor array immersed in the same solution. After immersion of the sensor array into solution, 5 minutes for sensor equilibration was allowed before beginning analysis for copper. Figure 5.4 shows that having both of the sensors immersed in the same solution allowed for measurement of both zinc and copper with a single optical-fiber-sensor array. All values determined during the analysis process were calculated by taking the pulse-energy ratio of the sensor and the respective reference. The data plot was generated by analyzing samples starting with the lowest concentration, in this case 0 mg/L, and progressing through higher concentrations. This had proven the most effective method during the individual sensor development so this practice was consistently followed. While the sensors are resettable, higher levels of either copper or zinc required longer amounts of time to completely remove the metal from the sensor regions. At concentration levels that were near the upper limit of the linear dynamic range, some sensors would also require multiple washings in order to clean the sensor regions. Due to the size and weight of the sensor array and Pyrex® dish full of solution,

removing the sensor array from the baking dish for emptying and refilling was kept to a minimum in order to prevent spilling or other accidents. A method in which the order of concentrations was selected randomly was not investigated here, but based on individual sensor observations, this approach is expected to be feasible.

Figure 5.4 also depicts the linear relationship that exists between the concentration of both copper and zinc and the respective change in fluorescence intensity. Examination of the data reveals very similar behavior to that observed for single-analyte sensor arrays. In Chapter 3, it was shown that when FZ-1 was exposed to solutions containing copper, the copper induced a small amount (approximately 4%) of fluorescence quenching when compared to the approximately 500% signal increase noted in the presence of zinc (Figure 3.5). When studying the copper-specific fluorophore, the presence of zinc induced a fluorescence enhancement (Figure 4.18), the incorrect type of signal change for how the copper sensor will behave in the presence of copper. The linear relationship between the fluorescence intensity and metal concentration observed for both sensors points to each of the sensor's ability to recognize the metal of choice while showing a resistance to being affected by the competing metal species. While this is promising data, the copper-sensor responses do demonstrate a deviation from perfect linearity. This may be due to errors associated with the measurements (insufficient equilibration time, incomplete regeneration of sensor before analysis) or solution preparation, but more data points are needed before conclusively stating that the copper sensor is not affected by zinc in solution.

While the design of the four-sensor array has been validated, there are technical issues which must be solved before the sensor array may be considered for sample

analysis, either in the lab or *in situ*. The overall size of the sensor array is dominated by the support structure designed to protect the fibers from breaking. This size requires that large volumes of solution (3 or more liters) be used for sample analysis, an impractical amount for most applications. Decreasing the size of the platform will help to address the issue, but the portability of the sensors between samples is still restricted, due to the rigid nature of the platform. A sample cell, designed in a manner similar to the one for single sensors described in Chapter 2, would compensate for the lack of sensor portability by allowing sample introduction and removal without disturbing the sample region.

A second technical issue focuses on the inability of the components of the sensor array to function as independent units. That is, if one sensor should prove to be inadequate or becomes un-usable prematurely, primarily due to dye leaching, the entire array must be discarded and remade. This is a very time consuming process, as each copper sensor requires four days for synthesis and there is a high risk of fiber breakage during the subsequent cladding removal process for the other sensor regions. An improvement to the sensor design would allow for individual sensors to be replaced without having to replace the entire array. Sodium hydroxide pellets have been used during this research to dissolve the polymer from the fiber for single optical fiber sensors, but treating one sensor in the array was not possible. As NaOH dissolves in solution, the increase in pH would cause unwanted degradation of all the polymers in solution. It should also be noted that the removal scheme for a polymer-based sensor does not apply to the copper sensor. In this case, if the copper sensor was inefficient or incapable of monitoring copper, the array would still require replacement. To have a sensor array

capable of monitoring solutions with comparable results to current technology, these two issues must be addressed.

5.4 Conclusion

A working four-sensor array has been built and validated during the course of this research. By developing each of the analyte-specific sensors individually, the combination into a four-sensor array was greatly simplified. The use of the crossed-fiber array allows for the application of sensors with different excitation wavelengths, providing a more versatile platform for analyte detection. This is made possible by the design of the array, which separates the fluorescence signals from each sensor region in time, relative to when the excitation pulse was created. Both sensors are capable of operating independently in the presence of the other analyte, a key factor in multi-elemental analysis. The research described herein provides promising results, but there are still hurdles to overcome in order to develop a robust sensor platform capable of analysis on the same level as current technology.
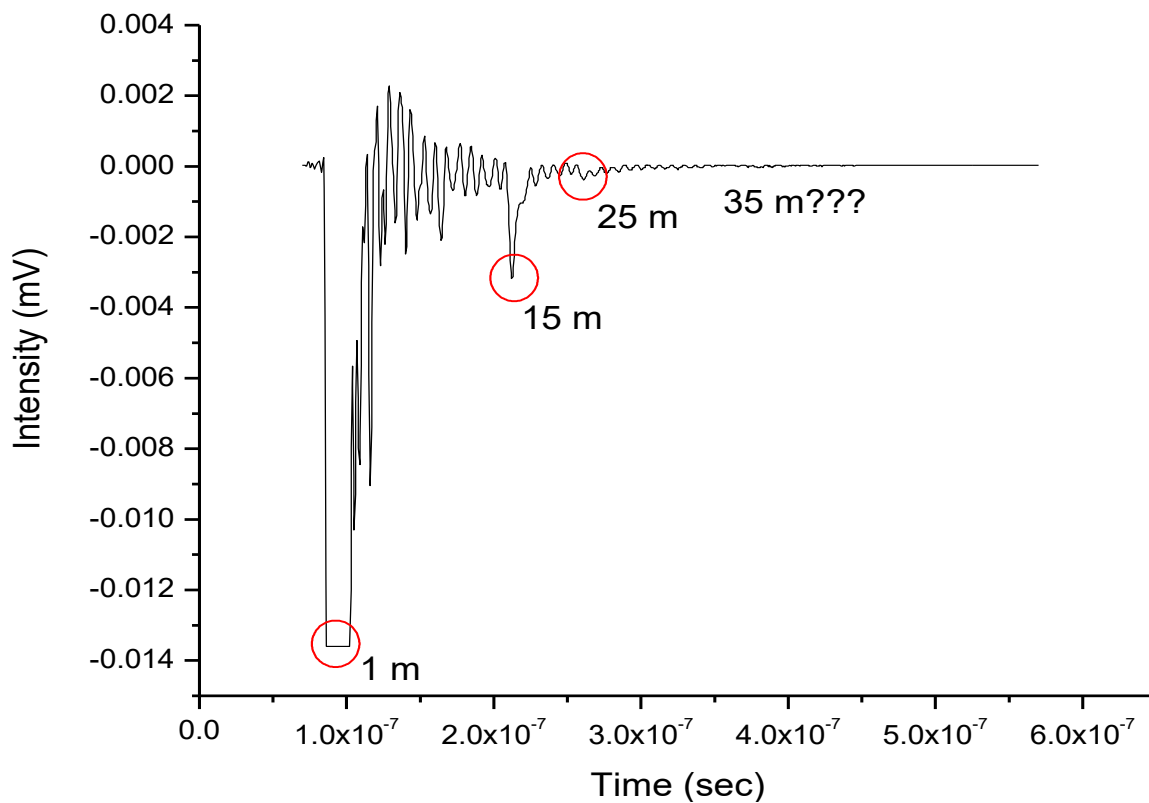
Figure 5.1 When the excitation pulse interacted first with the sensor attached to the shortest emission fiber it was observed that the third sensor region generated very weak signals while the last sensor region showed no fluorescence. The distances listed in the figure indicate the length of the emission fiber. FZ-1 was used in each of the sensor regions.
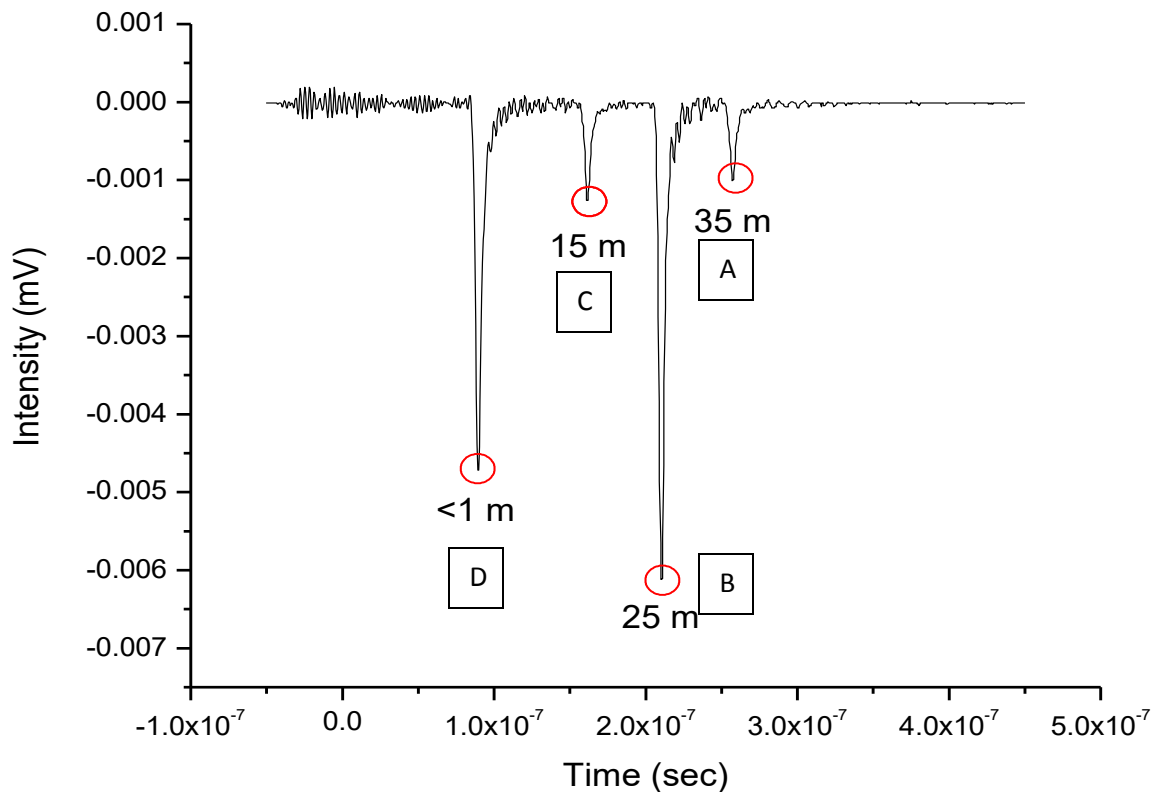
Figure 5.2 When the excitation pulse is directed to interact with the sensor region having the longer emission fiber, all of the sensor regions generated sufficient fluorescence to be measured by the detector. The distances once again describe the length of the emission fiber and FZ-1 was used as the fluorophore in each of the sensor regions. The labels located under or next to each peak alphabetically describe the order in which the sensor regions were excited starting with the longest fiber.
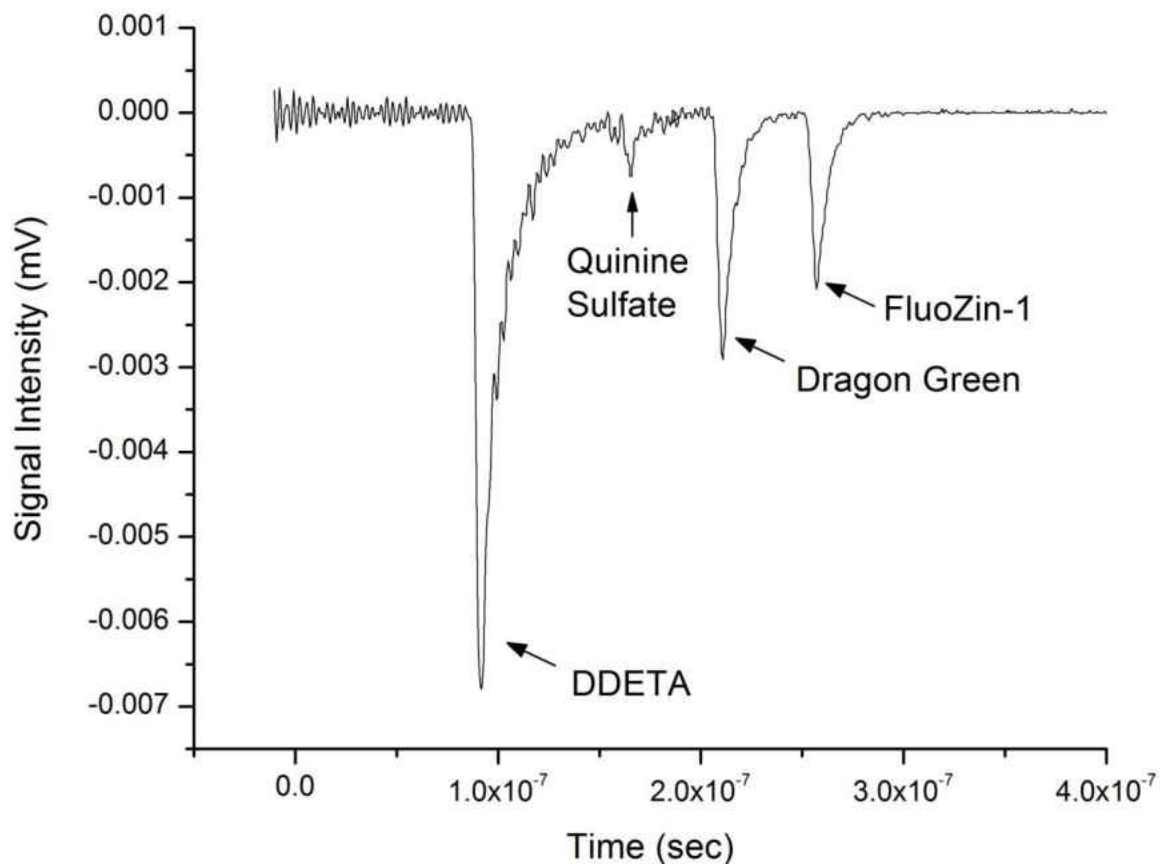
Figure 5.3 An oscilloscope trace confirming the fluorescence generated by each sensor region. The distances for the four emission fibers were 1, 15, 25 and 35 m. While all four sensors did generate fluorescence, the figure seen here is a combination of two sets of data, due to the change in the excitation wavelength. The data shown here is unaltered. That is no change in the scale of any of the peaks was made.

Sensor ID	Measured Fiber length (m)	Location of peak in time (sec)	Calculated fiber length (m)
DDETA	0.5 m	9.18E-08	
QS	15 m	1.65E-07	14.93
Dragon Green	25 m	2.11E-07	24.31
FZ-1	35 m	2.57E-07	33.69

Table 5.1 Measuring the fluorescence signal as a function of time allows for the estimated distance between different sensor regions. This provides support that peaks observed on the oscilloscope are fluorescence signals from the sensor regions.
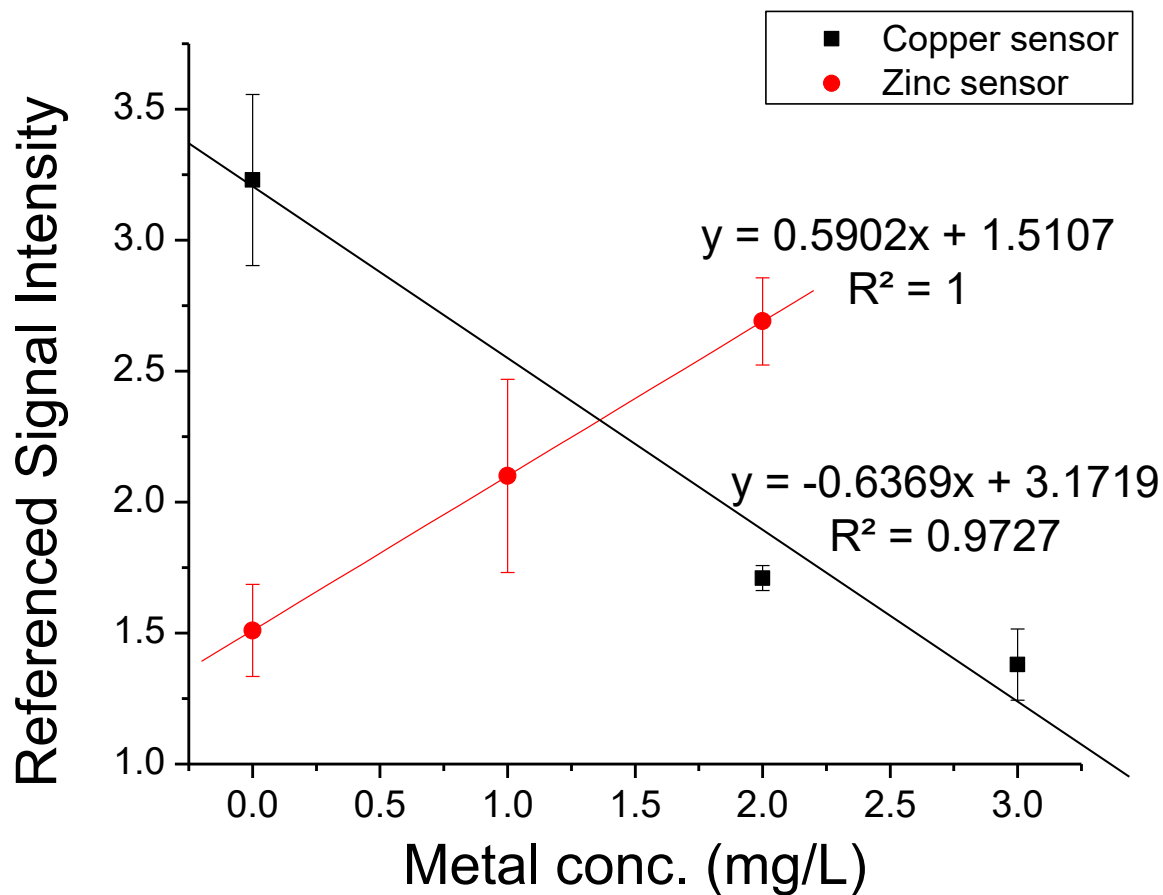
Figure 5.4 Using the four-sensor array provided a means of successfully measuring zinc and copper simultaneously in the same solution. The fluorescence signals of the analyte-specific fluorophore were collected separately due to the excitation wavelength. The sensors were never removed from the solution until analysis for both zinc and copper was complete for a particular solution. Four sets of 200 individual excitation pulses were collected to provide each data point with error bars indicating the 95% confidence interval.

References

1. Stich, M., Fischer, L., Wolfbeis, O. Multiple fluorescent chemical sensing and imaging. *Chem. Soc. Rev.* **2010**, *39*, 3102-3114

2. Kose, M., Omar, A., Virgin, C., Carroll, B., Schanze, K. Principal Component Analysis Calibration Method for Dual-Luminophore Oxygen and Temperature Sensor Films: Application to Luminescence Imaging. *Langmuir*, **2005**, *21(20)*, 9110-9120.

3. Stich, M., Borisov, S., Henne, U., Schaferling, M. Read-out of multiple optical chemical sensors by means of digital color cameras. *Sens. Actuators, B*, **2009**, *139(1)*, 204-207.

4. Wolfbeis, O., Weis, L., Leiner, M., Ziegler, W. Fiber-optic fluorosensor for oxygen and carbon dioxide. *Anal. Chem.*, **1988**, *60(19)*, 2028-2030.

5. Borisov, S., Seifner, R., Klimant, I. A novel planar optical sensor for simultaneous monitoring of oxygen, carbon dioxide, pH and temperature. *Anal. Bioanal. Chem.* **2011**, *400*, 2463-2474.

6. Taitt, C., Anderson, G., Lingerfelt, B., Feldstein, M., Ligler, F. Nine-Analyte Detection Using an Array-Based Biosensor. *Anal. Chem.* **2002**, *74(23)*, 6114-6120.

7. ThorLabs. http://www.thorlabs.us/thorProduct.cfm?partNumber=FT1000UMT (Accessed 4/3/13)

8. Lakowicz, J. *Principles of Fluorescence Spectroscopy*. 3rd ed. Springer: New York, 2006

9. Sun.W., Gee, K., Klaubert, D., Haugland, R. Synthesis of Fluorinated Fluoresceins *J. Org. Chem.* **1997**, *62*, 6469-6475

10. The Physics Classroom. http://www.physicsclassroom.com/Class/refrn/u14l1d.cfm (Accessed 4/3/13)

Chapter 6

Concluding Remarks and Future Directions

6.1 Summary of results

During the course of this research, the goal was to develop zinc- and copper-specific fluorescent sensors focusing on several key points. First the sensors must be able to reliably measure zinc and copper at environmentally relvant concentration levels. Next, sensors capable of rapidly recognizing changes in concentration, while also being reversible, are essential for a long-term or remote deployment. Also, a means of effectively correcting for variations in excitation intensity over hundreds of pulses is required for accurate measurements. In addition, both sensors, with reference correction must be able to accurately perform sample analysis. Finally, full utilization of the capability of the sensors requires that the two-sensor systems be combined into a sensor array. At the end of this summary, a critical analysis of the technology is presented to highlight the strengths and weaknesses of this research.

One possible application for the sensor involves in-situ monitoring of wastewater treatment streams within industrial facilities. As such, it is necessary that all sensors be able to monitor analytes of interest at concentration levels prescribed by regulatory authorities. For zinc, the EPA has stated that an average concentration of 1.48 mg/L of zinc may be discharged per day over a 30-day period. For copper, a concentration of 2.07 mg/L was set as the corresponding per-day limit for a 30-day period. Both the zinc sensor and the copper sensor demonstrated the capability to reliably monitor the respective elements at the mandated concentration levels. The zinc sensor has the potential to have multiple linear dynamic ranges based on the concentration of the zinc-specific dye in solution. However, the linear dynamic range determined most efficient for the zinc sensor was 0.05-1.50 mg/L. For the copper sensor, two different linear

dynamic ranges were determined. When the sensor was not encapsulated within the PEG-DA polymer a linear dynamic range of 0-6 mg/L was obtained. Encapsulation of the sensor yielded a linear dynamic range of 0-2 mg/L. However, encapsulation of the sensor also yielded a lower LOD & LOQ than a non-encapsulated sensor.

A second requirement for on-line waste monitoring is that the sensor demonstrates a rapid response to changes in concentration. Both sensors exhibited response times of less than three minutes and are easily regenerated using common reagents. The response times are determined mainly by the structure of the polymer. By using the microtemplating technique, a highly porous polymer is created, allowing for rapid analyte diffusion.

A benefit to using optical-fiber-based sensors is that analysis in remote locations is possible. Remote analysis may involve deployment within industrial pipelines or natural waterways that have limited access. However, optical fibers do experience transmission losses, and these losses mount as the distance between the excitation source and sensor region increases. These losses must be compensated for to obtain a measurable signal. The successful characterization of fluorophores capable of serving as reference materials was achieved. The fluorescence signal for both of these references remained unchanged, even after spiking the solutions with interfering species. Utilizing these newly developed fluorophores as a reference material greatly improved the accuracy and stability of the metal-sensing platform.

The ability to accurately measure samples is the hallmark of any established technology. As such, both sensors, with respective reference sensors, were used to

analyze several blind samples. The zinc sensor, after calibration, provided analysis with an average percent error of 8.18% or .08 mg/L of absolute error. The copper sensor presented a different approach to sample analysis. By creating a predictive equation based on multiple calibration curves, analysis of samples could be achieved without the need for daily calibration. This method provided an average percent error of only 6.36%. Both of these methods have demonstrated the ability to accurately measure samples over the course of 3 weeks.

To realize the full potential of an an optical fiber-based sensor array, all of the sensors, metal specific and reference, were combined to form one four- sensor array comprising two metal-specific sensors and two reference sensors. This combination allowes for the simultaneous measurement of both copper and zinc, while maintaining the accuracy and precision of each sensor determined during individual sensor development.

The results described above show that applicable zinc and copper sensors now exist that are capable of measuring both zinc and copper in aqueous environments. The linear dynamic range for both sensors include and encompass regulatory limits, as set down by the EPA, a vital requirement for waste water analysis. There are some factors that require addressing before the sensor may be deployed *in situ*, however. Waste streams are far from the clean, controlled conditions observed in a lab and as such, several issues regarding waste stream properties must be addressed. First, the pH of a waste steam is often very low (<pH 2.5) in order dissolve any solid metal in the waste stream and make waste treatment possible. During the development of these sensors, it was determined that both FZ-1 and PEG-DA are susceptible to changes in pH. For FZ-1, in order to achieve maximum fluorescence, the sensors must be in a pH-5.5-buffered

solution. The variability in pH must be minimized as the fluorescence intensity of FZ-1 will quickly drop off if the pH is not kept within a range of 5.5-6. For PEG-DA the pH must also be kept constant, as changes in the pH will affect the amount of excitation or emission radiation scattered within the polymer.

The issue of sensor reversibility must also be addressed. Although the sensors are reversible when exposed to cleaning solutions (ultrapure water or 0.05 M EDTA) the ability to respond to changes in concentration of either zinc or copper is limited in the absence of these cleaning agents. Both fluorophores (DDETA and FZ-1), in order to achieve selectivity for zinc and copper, bind with their respective metal. This attachment process does not reverse without the presence of the cleaning solution. Therefore, if left in a waste stream with no addition of cleaning reagents, the sensor will only be able to record increases in the level of each metal. This could still be applicable as it would serve to alert the user that a treatment process has failed, and allowing for elevated levels of metals discharged. However, it is currently not able to provide measurements, which can account for both increasing or decreasing levels of zinc or copper.

Another factor that will limit not only the lifetime of the sensors but also the reliability is dye leaching. While this is not an issue for DDETA, as it is covalently bound to the optical fiber surfaces, the other three fluorophores (FZ-1, Dragon Green, quinine sulfate) do leach from the PEG-DA polymer. This issue is exacerbated when the micro-templating process is utilized. While the micro-templating does allow for a more rapid diffusion of the analyte to the sensor region, it also allows for a more rapid diffusion of the fluorophore out of the polymer. This feature will be enhanced as moving streams of water will most likely induce a higher rate of dye leaching. As a result of this,

periodic calibration will be required to ensure the accuracy of the measurements provided. The exact length of time required between calibrations is not known at this time; it is possible that multiple calibrations during the same day will be required.

6.2 Future Developments

When discussing the course of future research related to crossed-fiber sensor arrays for the determination of metals in solution, one must first state the goal that is to be achieved at the culmination of the research. The final product for this research is the deployment of optical fiber sensors, either *in situ* or on a lab bench, capable of providing accurate, real-time metal analysis, focusing on industrial waste management. Because many of the properties already researched in this body of work have focused on characteristics pertaining to a laboratory-based system, areas of research required to develop remote sensors will be discussed. These areas of research break down into two groups: sample pre-treatment before analysis and issues pertaining to sensor deployment.

The first category is to assess means of sample treatment prior to an analysis by the crossed-fiber array for zinc or copper. To successfully treat the samples potential interferents must be identified. For the current sensor design, the sources of interference will be dominated by the following: turbidity, pH, and other metal species present in the sample, especially lead, cadmium and nickel. Before any chemical modification is completed, it is important that the sample undergo a filtration process. Most waste treatment systems use precipitating agents to remove metals from solution. The precipitates are allowed to settle to the bottom of the treatment chamber. However, it is possible that some of the precipitate will reach the sensor's location. This precipitate

may cause fouling of the micro-templated regions, slowing response times or blocking access of the metal to the fluorophore. A filter will act as simple and effective tool to remove the precipitates suspended in solution. Secondly, the need for pH adjustment is critical, especially when performing zinc analysis. After filtration, a pH-5.5-buffer must be introduced in order to maximize the efficiency of the zinc sensors. A correction for the interfering metals present in solution can be accomplished in one of two ways. The first involves the use of complexing agents to selectively remove interfering compounds. An example of this would be to dope the sample solution with sodium sulfate, causing lead to precipitate as lead sulfate, removing lead as an interferent. A second method would involve the development of metal-specific sensors, capable of monitoring for nickel, cadmium or lead. In a manner similar to FZ-1, there are fluorophores commercially available which are marked to be nickel, cadmium, or lead specific. These new sensors, coupled with the sensor already developed by the Geissinger group to measure pH, would facilitate an analysis method capable of providing information not only about the metals of interest, but also on the factors that have been shown to influence the analysis.

The second issue confronting remote monitoring capability involves the deployment of the sensor array within a sample environment. In-stream measurements within waste treatment processes are unlikely to succeed due to the pre-treatment requirements of the sensor array as well as the predicted increase of dye leaching when exposed to moving solutions. To accommodate for this, an alternative arrangement would be to divert a small amount of the waste stream to a holding tank where the sensors are located. This solution could undergo filtration and pH adjustment along with

any metal complexation required before performing the analysis. While this design is technically not remote as it still requires the user to perform tasks related to every analysis, the benefits of having on-site analysis capability still provides an analysis method not yet exploited for zinc and copper.

When examining the physical layout of the current sensor array scheme two things are apparent. The size of the sensor array was large (8.5" × 8.5") and as a result, three liters of solution was required for sample analysis. The majority of this size was due to the solid substrate used to support the optical fibers in solution. A reduction in this platform would significantly reduce the volume of solution required. Secondly, as stated earlier, when one of the sensor regions fails the entire array requires replacement. A means of selective replacement for certain sensor regions would provide a more versatile platform, maximizing the useful lifetime for each sensor region.

To this point, the discussion has focused on improving the sensor array for multi-analyte capabilities. However, there are other multi-sensor applications which could be exploited. As stated in Chapter 3, a change in the concentration of FZ-1 will result in a change of the linear dynamic range for zinc analysis. This relationship could be exploited, allowing for the deployment of a zinc sensor array capable of monitoring a larger range of zinc concentrations. By varying the concentration of FZ-1 at each sensor site, the range of measurable zinc concentrations would increase. A second application of an array would be to perform metal analysis as part of a longitudinal study. This type of analysis could be used for depth profiling in environmental waterways or in a wastewater holding tank to ensure the waste treatment processes was successful. The

crossed-fiber design allows for the depth profile to be dictated by the needs of the user rather than limitations experienced by a single fiber doped with multiple sensor regions.

To conclude, the applications of the crossed-fiber array design are still in the beginning stages. Fluorescent compounds already identified as potential analyte-specific compounds are coupled with the knowledge that new fluorescent sensors for a variety of compounds are developed every year. This will allow for the continued expansion and development of analyte-specific sensors contained within the crossed-fiber array platform.

CURRICULUM VITAE
NAME: Steven P. Kopitzke
D.O.B: April 9th, 1984

<u>EDUCATION</u>

University of Wisconsin-Milwaukee, Milwaukee, WI **2007-2013**
Ph.D. in Chemistry
Focus: Physical Chemistry
Dissertation: *An optical-fiber based sensor array for the simultaneous analysis of zinc and copper in aqueous environments*
Advisor: Dr. Peter Geissinger

University of Wisconsin-Parkside, Kenosha, WI **2002-2007**
B.S. in Chemistry
Minor: Economics
Senior Thesis: *The Determination of Indoor Atmospheric Mercury Levels Using Plants*

<u>AWARDS</u>

Teaching Lab Service Award **Spring 2013**
Louise Arndt Fellowship **Summer 2012**
Moczynski Outstanding Teaching Assistant Award **May 2011**

<u>TEACHING EXPERIENCE</u>

<u>University of Wisconsin-Milwaukee, Milwaukee WI</u>

Teaching Assistant for CHEM 221
Fall 2008; Fall 2009-Spring 2013
Taught 1st year analytical chemistry, focusing on analytical laboratory techniques
Guest lectured for Prof. Mark Dietz

Teaching Assistant for CHEM 105
Fall 2007, Spring 2011
Taught 1st year chemistry for engineers

Teaching Assistant for CHEM 102
Summer 2008, 2009, 2010, 2011
Taught 1st year general chemistry

Teaching Assistant for CHEM 584
Spring 2008
Taught senior-level analytical/physical chemistry focusing on instrumental techniques
Successfully developed and implemented a new experiment in class curricula

<u>University of Wisconsin-Parkside</u>

Senior Group Mentor for Chem 100, 101
Fall 2006, Spring 2007
Provided supplemental instruction for two groups of 6 students per semester taking introductory chemistry courses

<u>RELATED EXPERIENCE</u>

University of Wisconsin-Milwaukee, Milwaukee, WI
Project Leader – Chemical Inventory Conversion
June 2012 – August 2012
Trained and coordinated 25 graduate students to build an electronic database of chemicals contained within the UW-Milwaukee Chemistry Dept.
Trained and assisted 7 research groups with inventory conversion process

University of Wisconsin-Milwaukee, Milwaukee, WI
Officer of UW-Milwaukee Student chapter of the Society
for Applied Spectroscopy
March 2010 – May 2013
Served as Secretary, President & Vice-President.
Secured approximately $8,000 for various project from university grants.
Co-developed, coordinated and participated in university-recognized high school outreach projects

University of Wisconsin-Milwaukee, Milwaukee WI
Chemical Inventory Conversion
June 2011 - December 2011
Worked as part of a team to enter all chemicals and containers within the UW-Chemistry Dept. educational labs into a new electronic database

<u>SKILLS</u>
- Spectroscopy
- Optical fibers
- Trace metal analysis
- Lasers systems
- Scanning electron microscopy

<u>PUBLICATIONS AND PATENTS</u>

- Henning, P., Geissinger, P., Kopitzke, S., Frost, J. (2013). Fiber-optic sensors for real-time monitoring. U.S. Patent app. 20130092846

<u>PRESENTATIONS AND POSTERS</u>

ORAL PRESENTATIONS

- *An optical-fiber based sensor array for the simultaneous analysis of zinc and copper in aqueous environments*
  April 19th, 2013, Presented at UW-Milwaukee Chemistry Recruitment Weekend

- *Multi-Elemental Optical Fiber-Based Sensors for Aqueous Environments,*
  October 3rd, 2012, Presented at SciX 2012, Kansas City, MO

- *Multi-Elemental Optical Fiber-Based Sensors for Aqueous Environments*
  March 1st, 2012, Presented at AWRA-WI Chapter, Wisconsin Dells, WI

POSTER PRESENTATIONS

- *Multi-Elemental Optical Fiber-Based Sensors for Aqueous Environments*
  Sept. 30th, 2013 Presented at SciX 2012, Kansas City, MO
  Authors: Steven Kopitzke, Peter Geissinger

- *Multi-Elemental Optical Fiber-Based Sensors for Aqueous Environments*
  May 19th, 2012 Presented at UWM Awards Day
  Authors: Steven Kopitzke, Peter Geissinger

- *Optical Fiber-Based Tools For a Multi-Element Sensor in Aqueous Environments*
  October 7th, 2011 Presented at Younger Chemists Comittee, Milwaukee WI
  Authors: Steven Kopitzke, Peter Geissinger

- *Optical Fiber-Based Tools For a Multi-Element Sensor in Aqueous Environments*
  October 4th, 2011 Presented at FACSS 2011, Reno NV
  Authors: Steven Kopitzke, Peter Geissinger

- *Real-Time Optical Fiber Sensors for Metals in Aqueous Environments*
  June 2011 2011 SBIR National Conference, Washington DC
  Authors: Paul Henning Steven Kopitzke, Peter Geissinger

- *Optical Fiber-Based Tools for a the Analysis of Zinc in Aqueous Environments*
  May 10th, 2011 Presented at UWM 2011 Student Awards Day, Milwaukee WI
  Authors: Steven Kopitzke, Peter Geissinger

- *Optical Fiber-Based Tools for a the Measurements of Zinc Concentrations in Aqueous Environments*
  March 3rd, 2011 Presented at AWRA-WI Chapter, Appleton, WI
  Authors: Steven Kopitzke, Peter Geissinger

- *Optical fiber-based tools for the analysis of zinc in aqueous environments*
  December 16, 2010 Presented at Pacifichem 2010, Honolulu HI
  Authors: Steven Kopitzke, Peter Geissinger

- *Optical fiber-based tools for the analysis of zinc in aqueous environments*
  October 21st, 2010 Presented at Younger Chemist Committee, Milwaukee, WI
  Authors: Steven Kopitzke, Peter Geissinger

- *Optical fiber-based tools for the analysis of zinc in aqueous environments*
  October 19th, 2010 Presented at FACSS 2010, Raleigh, NC
  Authors: Steven Kopitzke, Peter Geissinger

- *Fiber optic based sensor for remote temperature measurement*
  October, 2009 Second Author, FACSS 2009 Louisville, KY
  Authors: John Frost, Steven Kopitzke, Veronica Rigo, Peter Geissinger

- *Sample Preparation Strategies for Trace Metal Analysis by Atomic Spectroscopic Technologies*
  May 2007, Presented at UW Undergraduate Research Symposium, Madison, WI
  Authors: Steven Kopitzke, Adam Barsamian, Joe Topczewski, Lori B. Allen

- *Flow Injection Donnan Dialysis: Determination of Mercury in Water Samples*
  March, 2006 Third Author, Pittcon 2006 Orlando, FL
  Authors: Lori B Allen, Adam Barsamian, Steven Kopitzke, Edward Manteufel, Christine Evans

PROFESSIONAL ASSOCIATIONS

American Chemical Society – Analytical Division
American Water Resource Association – Wisconsin Chapter
Society for Applied Spectroscopy